LOW TEMPERATURE SYNTHESIS AND PROPERTIES OF LEAD FERRONIOBATE $Pb(Fe_{0.5}Nb_{0.5})O_3$

by

Chienchia Chiu

Thesis Submitted to the Faculty of the
Virginia Polytechnic Institute and State University
in partial fulfillment of the requirement for the degree of

MASTER OF SCIENCE

in

Materials Engineering

APPROVED:

S. B. Desu, Chairman

C. W. Spencer

W. T. Reynolds

November, 1990
Blacksburg, Virginia

LOW TEMPERATURE SYNTHESIS AND PROPERTIES OF LEAD FERRONIOBATE $Pb(Fe_{0.5}Nb_{0.5})O_3$

by

Chienchia Chiu

Committee Chairman: Seshu B. Desu

Materials Engineering

(ABSTRACT)

Pure, single phase stoichiometric $Pb(Fe_{0.5}Nb_{0.5})O_3$ (PFN) powders were successfully formed by molten salt synthesis using mixture of NaCl and KCl salts. Lower temperatures and shorter times (0.5 hour at 800°C) were needed for single phase PFN formation from molten salts relative to those required for solid–state methods (4 hours at 1000°C). A systematic study indicating the effects of process parameters, such as temperature, time, and amount of flux with respect to starting oxides, on the PFN formation mechanism and its resulting powder characteristics is reported. The particle size increased with increasing synthesis temperature, the rate of increase is greatest above 900°C which is close to the melting point of lead oxide. PFN powders formed by molten salt synthesis were cuboidal, and were free from agglomerates.

The sinterability, microstructure, and dielectric properties of these powders have been studied for the pure form and with the presence of lead oxide or lithium carbonate. The dielectric properties were sensitive to as–sintered density, the type of additive and the amount of additive. For pure PFN, the highest valve of

dielectric constant is 12,270 at 1MHz, which is sintered at 1100^{0}C for 13 hours. Ceramics sintered with lead oxide additive exhibited inferior dielectric properties although lead oxide served as a sintering aid to increase the as–sintered density. The dielectric properties of PFN with lithium carbonate sintered at 1000^{0}C were attractive: the dielectric constant was increased to 14,000 at 1MHz and the D.C. conductivity was reduced. This reduction in the D.C. conductivity was interpreted in terms of the substitution of lithium for iron.

ACKNOWLEDGEMENT

I would like to express my greatest appreciation to Dr. Seshu B. Desu for his guidance and patience. Appreciation is also expressed to Dr. Chester W. Spencer and Dr. William T. Reynolds for their reviewing this thesis and suggestions. Special thanks to the all members of the thin film laboratory in the Department of Materials Engineering, especially Mr. Chen–Chung Gene Li. Finally, I would like express my deepest sense of thanks to my family and friends for their helping and encouraging.

Table of Contents

Chapter 1: Introduction.....1

Chapter 2: Literature Review.....10

2.1 Synthesis of $Pb(Fe_{0.5}Nb_{0.5})O_3$.....10

2.1.1 Synthesis of Single Crystal.....10

2.1.2 Powder Synthesis.....11

2.1.2.1 Solid–State Reaction Synthesis.....11

2.1.2.2 Molten Salt Synthesis.....15

2.2 Stability of Perovskite.....19

2.3 Dielectric Properties of $Pb(B'_xB''_{1-x})O_3$ Perovskite.....21

2.3.1 Polarization in Dielectrics.....21

2.3.2 Dielectric Loss.....24

2.3.3 Ferroelectrics.....25

Chapter 3: Experimental Procedure.....31

3.1 Molten Salt Synthesis of PFN Ceramic Powders.....31

3.2 Sintering and Microstructure Characterization of Pure PFN powders and PFN Powders with PbO or Li_2CO_3 Additions.....34

3.3 The Dielectric Properties of Pure PFN Powders and PFN Powders with PbO or Li_2CO_3 Additions.....35

Chapter 4: Results and Discussion.....37

4.1 Synthesis and Reaction Mechanisms of PFN in Molten Salt.....37

4.1.1 Formation Process.....37

4.1.2 The Effect of Flux Composition and Flux/Oxide Weight Ratio.....46

4.1.3 Morphology.....49
4.2 Sintering and Microstructure Characterization of the PFN Powders.....64
4.2.1 Sinterability of Pure PFN Powders.....64
4.2.2 PFN Powders with Lead Oxide Additives.....66
4.2.3 PFN Powders with Li_2CO_3 Additives.....71
4.3 Dielectric Properties.....81
4.3.1 Dielectric Properties of Pure PFN Powders.....81
4.3.2 Dielectric Properties of PFN with PbO Additives.....89
4.3.3 Dielectric Properties of PFN with Li_2CO_3 Additive.....91
Chapter 5: Summery.....100
Chapter 6: References.....102

Chapter 1: INTRODUCTION

Multilayer ceramic capacitors consist of alternating layers (>200) of dielectric material (most often $BaTiO_3$) and metal electrodes. Because of their unique design they show very high capacitance values. In terms of annual production rate, multilayer capacitors, with greater than 12 billion units per annum, outnumber any other electronic device currently in production. One of the most important applications of the multilayer ceramic capacitors is as decoupling capacitors, suppressing voltage transients in integrated circuits. Continued efforts towards miniaturization of integrated circuits are placing significant demands on maximizing volumetric efficiency of multilayer capacitors. The capacitance per unit volume of a single dielectric layer (C/V) is proportional to the dielectric constant (K) and inversely proportional to the square of the thickness of the dielectric according to the following equation:

$$\frac{C}{V} = \frac{\epsilon_0 K}{t^2} \tag{1.1}$$

where ϵ_0 (= 8.854×10^{-12} F/m) is permittivity of vacuum, and t is thickness of the dielectric layer. Thus to increase the capacitance volumetric efficiency of the multilayer ceramic capacitors, there are two alternatives: reduce the thickness of the active dielectric and/or utilize a ceramic material with a high dielectric constant.

Presently the thickness of an active dielectric is in the range of 15 to 35 μm, which appears to be the lower limit for current processing techniques [1]. Since there are certain limitations on the dielectric thickness extensive research has been

carried out on the dielectric materials having high dielectric constants. Lead ferroniobate, $Pb(Fe_{0.5}Nb_{0.5})O_3$, abbreviated as PFN, is the most promising dielectric with reported dielectric constant values close to 26,000, which is 4 to 5 times higher than that of the conventional capacitor dielectric $BaTiO_3$.

Lead ferroniobate was one of the first ferroelectrics discovered in which magnetic ordering was found. Ferroelectric Curie point of PFN is around 105^0C, and it is antiferromagnetic. It is also a relaxor ferroelectric of disordered perovskite type, in which two kinds of ions (e.g., Fe^{3+} and Nb^{5+}) are randomly distributed in the B position of ABO_3. Because of its disordered cation arrangement, solid solutions based on PFN show diffuse phase transitions (DPT) which are characterized by a broad maximum for the temperature dependence of the permittivity and a large deviation from Curie–Weiss law in a wide temperature range around the transition point. Diffused phase transitions are not only of fundamental interest but also are of practical importance in the development of ferroelectric materials for capacitor applications [2].

PFN system offers several advantages over the traditional $BaTiO_3$ based compositions regarding multilayer ceramic capacitor technology. Due to its high capacitance per unit volume, more miniature multilayer capacitors than possible previously can be fabricated using PFN based compositions. Table 1.1 presents lead–based solid solutions that are reported recently for the use in multilayer capacitors. The other advantage is the ease in controlling the Curie temperature, at which the dielectric constant has a maximum value, within a range of operating temperatures. This allows the preparation of capacitors with a low temperature

Table 1.1 Relaxor Composition Families* for Capacitors

Composition	Manufacturer
PFN–PNN[3]	T.R. Shrout et al.
PMN–PT[4,5]	W.Y. Pan et al./A. Morell
PFN–PFT[6]	M. Halmi et al.
PZN–PT[7]	S.R. Winzer et al.
PMN–PZN[8]	M. Lejeune et al.
PFW–PMT, PMW–PFT[9]	K. Uchino et al.
PFN–PMW[10]	A. Tawfik et al.
PZN–PT–BT[11]	S.L. Baumler et al.

*Composition Designations:

PFN–$Pb(Fe_{0.5}Nb_{0.5})O_3$, PNN–$Pb(Ni_{0.33}Nb_{0.67})O_3$, PMN–$Pb(Mg_{0.33}Nb_{0.67})O_3$

PT–$PbTiO_3$, PFT–$Pb(Fe_{0.5}Ta_{0.5})O_3$, PZN–$Pb(Zn_{0.33}Nb_{0.67})O_3$,

PFW–$Pb(Fe_{0.67}W_{0.33})O_3$, PMT–$Pb(Mg_{0.33}Ta_{0.67})O_3$, PMW–$Pb(Mg_{0.5}W_{0.5})O_3$,

PFT–$Pb(Fe_{0.5}Ta_{0.5})O_3$, BT–$BaTiO_3$

coefficient by laminating many ceramic layers with different Curie temperatures.

Due to the possibility of low firing temperature (<950^{0}C) for PFN based compositions, inexpensive electrodes such as silver, or even Ni or Cu can be used, thus providing significant savings. In contrast, high sintering temperatures ($\geq$ 1300^{0}C) are needed for most compositions based on $BaTiO_3$, which in turn require the use of noble metals such as Pd (m.p. 1552^{0}C), Pt (m.p. 1769^{0}C), or their alloys for internal electrodes which can make up to 50% to 60% of the selling price of capacitor. Yonezawa [12] has reported PFN based dielectric composition that fires at <900^{0}C, low enough for the use of 100% silver electrodes. Since then, several studies have appeared on PFN based capacitor compositions [3,13–18]. Utilizing PFN based compositions (and using 85% Ag and 15% Pd electrodes), a multilayer capacitor has been developed and is currently being manufactured by Nippon Electric Co. (NEC) in Japan [13].

In addition to their use in ceramic capacitors, PFN based solid solutions have also been used for the fabrication of piezoelectric transformers and magnetoelectric transformers [19]. The presence of Fe, whose oxidation state is sensitive to oxygen partial pressure, makes them a very good candidates for ferroelectric–semiconductor materials [20]. Nimura and Doi [21], in their one page short note, have first reported the positive temperature coefficient of resistivity (PTCR) in PFN.

Due to its wide applicability, several reports on PFN appeared in the literature. But majority of these reports basically concentrated on PFN based solid solutions (capacitor compositions) prepared by solid state methods. Very few

reports dealt with the pure PFN compound and furthermore, due to poor control of process parameters and/or the use of solid–phase synthesis methods, the reported properties of this compound are often inconsistent.

PFN was first synthesized in late 50's by Smolenskii et al [22] using traditional solid–state methods and established its ferroelectric behavior. Bokov et al were the first to indicate that this material is antiferroelectric below -130^0C [23]. There is a considerable discrepancy regarding the measurements of its Neel point [24,25]. Astrov et al [24] reported a Neel point of -246^0C, whereas, Neel point at -118^0C was observed by Pietrzak et al [25]. Platonov et al [26], using electron diffraction, determined the crystal structure of PFN. At room temperature, the symmetry of PFN is rhombohedral which is ferroelectric and antiferromagnetic. The valves of the lattice parameters for the rhombohedral are [27]:

$$a_r = 4.0127 \pm 0.0005 \text{Å}$$

$$\alpha_r = 89.91 \pm 0.03^0$$

A phase transition occurs at the range from 96^0C to 120^0C from rhombohedral to cubic (paraelectric) state, viz $F_R(R3m) \longrightarrow$ Cubic (m3m). However, the deviation of PFN from cubic structure at room temperatures is too small and thus the crystal structure can be considered as pesudocubic [28]. The typical structure of this perovskite is shown in Figure 1.1 with Fe^{+3} and Nb^{+5} randomly distributed in octahedral sites. The unit cell of this perovskite–structured oxide may also be presented as the octahedra of $(Fe_{0.5}Nb_{0.5})O_3$ units centered on the corners of a cube, which are linked to each other by the sharing of oxygen ions. The lead ion is

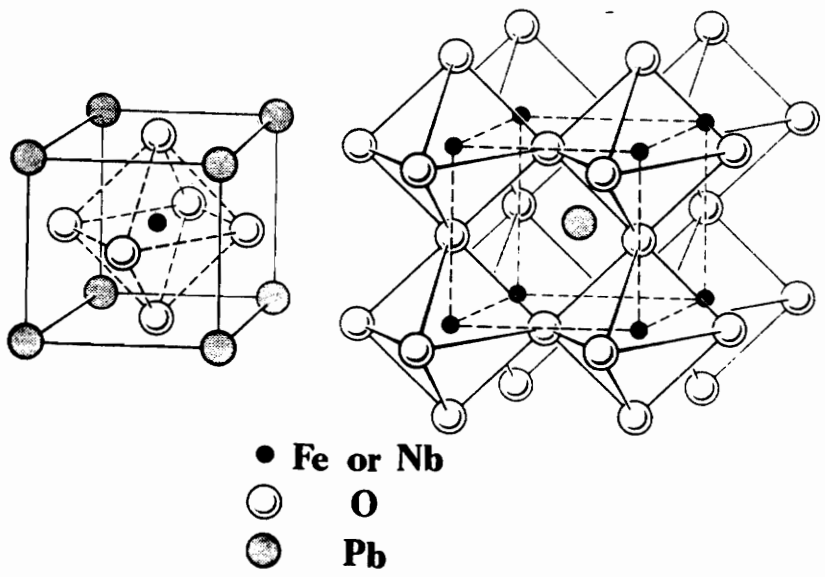

Figure 1.1 Perovskite structure (Idealized)

located at the center of the cage formed by the octahedra. The cations in PFN are displaced along pseudocubic direction.

Data on the ferroelectric properties of PFN are, however, fragmentary and often inconsistent. In particular, the experimentally determined spontaneous polarization of PFN, $P_s = 5 \times 10^{-2}$ C/m^2 [29] is much lower than predicted value based on atomic displacements $P_s = 0.12$–0.4 C/m^2 [26] as well as the value $P_s = 0.4$ C/m^2 for isomorphous compound $Pb(Fe_{0.5}Nb_{0.5})O_3$, PFN. Furthermore, recent optical and X–ray diffraction studies of PFN crystals indicated an additional phase transition at 80^{0}C besides the well known transition to cubic phase [30]. The X–ray analysis performed on a polycrystalline sample did not show unequivocally the existence of a such a transition at 80^{0}C [27].

The observed discrepancies may be ascribed to the poor control of the process parameters, and/or to the use of traditional solid–phase methods. In solid–state method, the PFN powders are prepared by mixing and reacting appropriate amounts of PbO, Fe_2O_3, and Nb_2O_5 at around 900^{0}C. This simple procedure always yielded a multi–phase product, possibly due to the occurrence of several reaction intermediates. Several improvements to this simple process were later suggested for improving the purity of the product [1,3]. Although, these modifications increased the probability of obtaining the single phase PFN, but these disadvantages of solid–phase synthesis such as, powders of nonuniform size, and variations of stoichiometry due to nonuniform mixing of the reagents and evaporation of the part of lead oxide at high reaction temperatures, will still remain.

Development of reproducible synthesis technique and a better understanding of process, structure, and property interrelationships of PFN material and its solid solutions can have significant impact on electronic industry, especially the billion dollar ceramic capacitor industry. It is also becoming increasingly clear that the dielectric properties of PFN are very sensitive to ceramic processing and thermal history, but no systematic studies have been published so far which relate process parameters to PFN properties.

Molten salt synthesis has been reported to be one of the simplest techniques to prepare pure, stoichiometric ceramic powders of multicomponent oxides [31–33]. Since the diffusivities of components are much higher in comparison to those of solid–state reactions, significantly lower powder formation temperatures and times were needed by using the molten salt method. Furthermore, control of powder morphology was found to be much easier by using this technique [34]. Recently, lead niobate powders formed from both molten salt and solid–state methods were systematically analyzed, and the effects of molten salts on the phase stability, on stabilization of high temperature polymorphs, on impurity incorporation, as well as on powder morphology were documented [35]. The molten salt method had also been extensively utilized to prepare $PbNb_2O_6$ [31], ferrites [36], and $Bi_4Ti_3O_{12}$ [37].

Preliminary studies, based on the recent work of Lopatin et al [38], showed that using molten salt method stoichiometric single phase PFN powders can be made at temperatures as low as 200^0C than those needed for solid–phase methods. It was also observed that the room temperature properties are very sensitive to the changes in process parameters. Encouraged by the preliminary results, this research

was directed toward developing an understanding of interrelations between process parameters, structure and properties of PFN synthesized by molten salt technique which is optimized by way of understanding kinetics and mechanism of formation.

The main objectives of the research are: (1) to develop a synthesis technique for reproducibly making PFN powders by way of understanding kinetics and mechanism of formation, and (2) to develop a model to interrelate process parameters to structure and properties of PFN. The kinetics and mechanism of formation were investigated by studying the reaction rate as a function of process parameters such as reaction temperature, reaction time, amount of molten salts, and amount of excess lead oxide in the starting composition. To interrelate process parameters, structure and properties, microstructure and electrical and dielectric properties were studied as a function of sintering temperature, anneal, and controlled addition of dopants. Emphasis will also be given to the sinterability of molten salt derived powders.

Chapter 2: LITERATURE REVIEW

2.1 Synthesis of $Pb(Fe_{0.5}Nb_{0.5})O_3$

2.1.1 Synthesis of single crystal

The single crystals of PFN were first synthesized by Galasso et al [39] in 1965 by using lead oxide flux. The perovskite samples were prepared as powders and fired for several hours at 800^{0}C, mixed with the flux, and then packed into platinum crucibles. In order to prevent excess vaporization of the flux, crucibles were covered firmly. For growing crystals of PFN, 64wt% of lead oxide was mixed, and the samples were cooled at 5^{0}C/hr from 1230^{0}C to 800^{0}C.

In 1969, Astrov et al [24] used PbO–$PbCl_2$ flux to synthesize PFN single crystals. The composition of the flux was: one part of PbO to four parts of $PbCl_2$. The PFN single crystals were synthesized at 850^{0}C in a stream of oxygen. Crystals were grown at the temperature of 1100^{0}C. The rate for cooling of PFN was 15^{0}C/hr in this flux.

However, the single crystals grown from the above methods were of the order of 1mm. Brunskill et al [40] proposed a procedure to grow high quality single crystals of PFN of the order of 10mm by using accelerated crucible rotation technique (ACRT) in PbO flux. The composition of PbO in this method is from 55wt% to 70 wt% with the soaking temperatures from 1100^{0}C to 1260^{0}C. The cooling rate is stepwise with 0.4^{0}C/hr in the first series and 0.25^{0}C/hr in the second

series to around 900^{0}C. Then the flux was cooled naturally to room temperature.

2.1.2 Powder Synthesis

2.1.2.1 Solid–state reaction synthesis

Solid–state reactions, which have been applied to most of the ceramic powders, have also been applied to the fabrication of PFN ceramic powders since the first synthesis by Smolenskii [22]. The formation mechanisms of these conventional processes were studied by Lejeune et al [18] and Kassarjian et al [16].

In the study of Lejeune et al [18], the formation of PFN was classified into three regions. The reaction sequences for the first temperature region, 560^{0}C to 640^{0}C, correspond to the following reactions:

$$PbO + Nb_2O_5 \longrightarrow Pb_3Nb_2O_8\ (P_3N) \tag{2.1}$$

$$PbO + Nb_2O_5 \longrightarrow Pb_2Nb_2O_7\ (P_2N) \tag{2.2}$$

$$PbO + Fe_2O_3 \longrightarrow Pb_2Fe_2O_5\ (P_2F) \tag{2.3}$$

$$PbO + Fe_2O_3 + Nb_2O_5 \longrightarrow Pb(Fe_{0.5}Nb_{0.5})O_3\ (PFN) \tag{2.4}$$

The main product is P_3N in this temperature region. Reactions 2.1 and 2.2 also correspond to an endothermic peak in DTA curve.

The second region is from 640^{0}C to 730^{0}C. In this region, P_2N decomposed and the amounts of P_3N, P_2F, and PFN were increased. The reactions were

described below:

$$Pb_2Nb_2O_7\ (P_2N) \longrightarrow Nb_2O_5 + PbO \tag{2.5}$$

$$PbO + Fe_2O_3 \longrightarrow Pb_2Fe_2O_5\ (P_2F) \tag{2.6}$$

$$Nb_2O_5 + PbO \longrightarrow Pb_3Nb_2O_8\ (P_3N) \tag{2.7}$$

$$PbO + Fe_2O_3 + Nb_2O_5 \longrightarrow Pb(Fe_{0.5}Nb_{0.5})O_3\ (PFN) \tag{2.8}$$

The decomposition Reaction 2.5 was also included in the endothermic peak of the first temperature region; whereas this peak in the DTA curve spread over a large temperature range (~ 100^{0}C).

In the third higher temperature region of 730^{0}C to 950^{0}C, P_3N and P_2F were decomposed, and consequently the PFN phase was increased. The reactions were:

$$Pb_3Nb_2O_8\ (P_3N) \longrightarrow Nb_2O_5 + PbO \tag{2.9}$$

$$Pb_2Fe_2O_5\ (P_2F) \longrightarrow Fe_2O_3 + PbO \tag{2.10}$$

$$PbO + Fe_2O_3 + Nb_2O_5 \longrightarrow Pb(Fe_{0.5}Nb_{0.5})O_3 + \text{traces of } P_3N \tag{2.11}$$

where the decomposition of P_3N phase, Reaction 2.9, was connected to an exothermic peak corresponding to a liquid phase appearance.

Although PFN was formed at temperatures as low as 560^{0}C, the amount of PFN was increased with increasing temperature up to 950^{0}C. It should also be noted that exposures to high temperatures (>950^{0}C) and longer times results in the

decomposition of the PFN phase, and leads to the increase of pyrochlore phase content (P_3N). This may be attributed to the volatilization of lead oxide, which also causes difficulties in producing other lead based perovskite relaxors [1].

Kassarjian et al [16] investigated the sequence of reactions for the stoichiometric mixture of $PbO/Fe_2O_3/Nb_2O_5$ through temperatures ranging from room temperature to 800^{0}C. The sequence of reactions are presented below:

$$PbO + Nb_2O_5 + Fe_2O_3 \xrightarrow{600^0C} Pb_3Nb_4O_{13}\ (P_3N_4) + Pb_2Nb_2O_7\ (P_2N) + (PbO{+}Fe_2O_3) \tag{2.12}$$

$$PbO + Fe_2O_3 + Pb_3Nb_4O_{13}\ (P_3N_4) + Pb_2Nb_2O_7\ (P_2N) \xrightarrow{700^0C} Pb_3Nb_2O_8\ (P_3N) + Pb_2Fe_2O_5\ (P_2F) + \text{pyrochlore} + Pb(Fe_{0.5}Nb_{0.5})O_3 + (PbO) \tag{2.13}$$

where "pyrochlore" denotes the cubic pyrochlore structure of lead–iron–niobate, probably $Pb_3(Fe,Nb)_4O_{13}$.

From the two reaction sequences described above, it is noted that the intermediate lead niobates of both sequences do not quite agree with each other. Below 700^{0}C, Lejeune et al [18] report $Pb_3Nb_2O_8$ (P_3N) being the major phase, whereas, $Pb_3Nb_4O_{13}(P_3N_4)$ or $Pb_2Nb_2O_7$ (P_2N) were reported by Kassarjian et al [16]. The similarities in diffraction patterns of the lead–niobate phases may partly account for the reported differences. Nevertheless, it is obvious that high temperatures (*e.g.* 900^{0}C–1000^{0}C) lead to the increase of the amount of PFN, but the presence of the second phase $Pb_3Nb_2O_8$ (P_3N) cannot be avoided by this route.

Thus, it is obvious that the pure phase of PFN can not be obtained by using the conventional solid–state synthesis due to the formation of stable lead–niobate phases at lower temperatures (*e.g.* 500°C–600°C). A double–calcination was proposed by Fu et al [41] to eliminate these lead–niobate pyrochlore phases. They reported that nearly pure perovskite PFN phase could be obtained by doubly calcining the mixture of $4PbO/Fe_2O_3/Nb_2O_5$ at the temperature of 700°C and then 900°C for 2 hours, each. The reaction sequence is presented below:

$$\begin{aligned} PbO + Fe_2O_3 + Nb_2O_5 \xrightarrow{700^0C} & Pb_3Nb_4O_{13}\ (P_3N_2) + Pb_2Nb_2O_7\ (P_2N) \\ + Pb_2Fe_2O_5\ (P_2F) + PbO + Pb(Fe_{0.5}Nb_{0.5})O_3 & \xrightarrow{900^0C} \\ & Pb(Fe_{0.5}Nb_{0.5})O_3 \end{aligned} \tag{2.14}$$

It is believed that the effect of double calcination on obtaining PFN is based on the nucleation of PFN accelerated by the appearance of $Pb_2Fe_2O_5$.

Swartz et al [3] reported that single phase PFN can be obtained by first prereacting the B site refractory oxides of $Pb(B'_{0.5}B''_{0.5})O_3$ perovskite to form the appropriate wolframite $B'B''O_4$ compounds and subsequently reacting with PbO. The purpose of this prereaction is to bypass the formation of the intermediate pyrochlore phases. Thus, the amount of pyrochlore phases could be significantly reduced. The following reactions were proposed as the possible solution:

$$Fe_2O_3 + Nb_2O_5 \xrightarrow{1000^0C} FeNbO_4 \tag{2.15}$$

$$FeNbO_4 + PbO \xrightarrow{800^0C} Pb(Fe_{0.5}Nb_{0.5})O_3 \tag{2.16}$$

The reaction times are 4 hours for both reactions 2.15 and 2.16. Fe_2O_3 is prereacted with Nb_2O_5 to form $FeNbO_4$. This compound is attractive for two reasons [42]:

(1) In order for PbO to react with $FeNbO_4$ to form pyrochlore phase, it would first have to liberate Fe_2O_3 from $FeNbO_4$. The kinetics of this process must be slow enough to prevent the formation of pyrochlore phases.

(2) The wolframite structure of $FeNbO_4$ is an oxygen octahedral structure, and should be a good starting point from which the perovskite structure can be formed.

2.1.2.2 Molten salt synthesis

For solid–state synthesis, the formation of the PFN compound is controlled by the solid–state diffusion across inter–particle contacts. In general, great care has to be taken to obtain an intimate mixture of the starting oxides. It is very difficult to obtain a completely homogeneous product from a single solid–state reaction because the diffusional process involved requires long periods of time to be completed. In practice, the product from the first solid–state reaction is milled, and then reacted again at high temperatures. This process may be repeated several times to attain relatively great homogeneity but entails the penalties of milling cost and contamination due to the wear of the milling media.

A technique for PFN powder synthesis, that avoids most of the difficulties mentioned above, is molten salt synthesis. The process is based on the use of a molten salt solvent to act as the medium of reaction among the constituent oxides.

The desired compound will be formed if it is thermodynamically more stable than the constituent oxides, and this stability is based on more than simple entropy of mixing [32]. The stability of the product causes a smaller solubility in molten salt than any one of the constituent oxides. Solubilities of oxides in molten salt vary from less than 1×10^{-10} mole fraction to more than 0.5 mole fraction, typically 1×10^{-3} to 1×10^{-7} mole fraction [32]. However, the complete reaction can be accomplished in a relatively short period of time because of the small distances for diffusion in an intimate mixture of the constituent oxides in molten salt, and the relatively high mobility of species in molten salt. Typically, mobilities of oxides in molten salts vary from 1×10^{-5} to $1\times10^{-8}cm^2sec^{-1}$ and are much higher than those in the solid–state reaction ($1\times10^{-18}cm^2sec^{-1}$) [32]. The reaction proceeds by supersaturation of the molten salt solvent by the product compound, which in turn precipitates from the solution. The reactants are continuously consumed during this process until the residual concentration remains in solution commensurate with the intrinsic solubility in the melt. Alternatively, some reactants may be introduced in excess to drive all other reactant concentrations to effectively zero level, if these reactants are more soluble under acidic or basic conditions than is the product. These excess reactants are then removed by acidic or basic washing from the product.

In selecting the molten salt solvent, two requirements have to be met:

(1) The molten salt solvent should not enter into any undesirable side reactions with either the reactants or product compounds; *i.e.*, it is a true solvent.

(2) The salt solvent should also possess sufficient aqueous solubility so

that it can be removed by simple water washing.

In addition to the advantages of lower synthesis temperatures and shorter reaction times, the control of powder morphology is much easier in molten salt method. Hayashi et al [36,43] and Kimura et al [44] used this technique to develop different shapes of $(Ni_{0.5}Zn_{0.5})Fe_2O_4$ ferrite, rod–shaped $BaTiO_3$, and Bi_2WO_6 powders. The shape anisotropy of starting powder particles plays a dominant role and the selection of molten salt solvent is also important.

When constituent oxides were heated in molten salt solvent, the development of the complex oxide particle is followed by two stages [34]:

(1) the formation of complex oxide particles

(2) particle growth

In the formation stage, the size and shape of complex oxide powders are determined by the formation mechanisms, which depend on the relative dissolution rates of the reacting components into molten salt. The product is formed on the surface of the slower dissolving components, and the complex oxide with the same shape as those of the slower dissolving components is obtained when one component dissolves faster than the others. The dissolution rates of the reacting components depend on the particle sizes and the solubilities in the molten salt. On the other hand, when all the reactants have comparable dissolution rates in molten salt, the complex oxide formation takes place somewhere in the molten salt. If this mechanism is dominant during the formation process, the complex oxide powders with a lumpy shape will be formed, depending on the degree of interaction between the complex oxide and the salts.

In the particle growth stage, even lumpy particles can attain a characteristic shape because of the anisotropy in growth rate of different crystalline faces. The faster growing facets disappear and the slower growing facets develop. When the oxide has a large or moderate growth anisotropy, powder particles with a shape anisotropy, such as plate or needle, are obtained. Particle sizes are controlled by selections of heating temperatures and time periods. On the other hand, when the oxide has a small growth anisotropy, equiaxed particles are produced. Morphology of the particle is not only determined by the reactants, but also by the nature of the flux and the mole ratio of flux to oxides [34].

Although molten salt synthesis has been successfully utilized in synthesizing complex oxide powders, the synthesis of lead–based perovskite $\{Pb(B'_xB''_{1-x})O_3\}$ was not reported until the year of 1987. Lopatin et al [38] reported that PFN powders can be synthesized by this technique using molten sodium and potassium chlorides. In contrast to the conventional solid–state method, this method bypassed most of the intermediate compounds. The reaction mechanism was simplified by this molten salt method according to the following equations:

$$PbO + Nb_2O_5 \longrightarrow Pb_3Nb_4O_{13}\ (P_3N_2) \qquad (2.17)$$

$$Pb_3Nb_4O_{13} + Fe_2O_3 + PbO \longrightarrow Pb(Fe_{0.5}Nb_{0.5})O_3 \qquad (2.18)$$

Thus, The reaction occurs in two stages. Initially $Pb_3Nb_4O_{13}$ (P_3N_2) is formed and subsequently $Pb(Fe_{0.5}Nb_{0.5})O_3$. (P_3N_2), PbO, and Fe_2O_3 react to produce $Pb(Fe_{0.5}Nb_{0.5})O_3$ in the second stage, which is limited by the diffusion of lead oxide.

2.2 Stability of perovskite

There are two basic requirements for forming a stable perovskite structure: (1) the ionic radii of cations should be within certain limits and (2) the ionic contribution to cation–anion bonds should be high [45]. The first requirement relates to the perovskite unit cell size. Goldschmidt proposed the concept of a tolerance factor ",t," to describe the stability limits of a crystal structure in terms of the ionic radii. For perovskite structure (ABO_3), the tolerance factor is given by [45]:

$$t = (r_a + r_b)/\sqrt{2}\,(r_a + r_o) \qquad (2.19)$$

where r_a and r_b are the ionic radii of cations A and B, respectively, and r_o is the ionic radius of oxygen. Shrout et al [1] concluded that for the perovskite structure the ",t," value may be within the range from 0.88 to 1.09.

The second requirement relates to the ionic character of the chemical bonds in the compound. The amount of ionic character is proportional to the difference between the electronegativities of cations and anions. The tolerance factors and electronegativity differences for several known ABO_3–type perovskite compounds are shown in Figure 2.1. For compounds containing more than one B–site cation, as in the case of ferroelectric relaxors, the weighted average was used for the calculation of r_b. A weighted average was again used for determining the electronegativity difference, as expressed in the following equation:

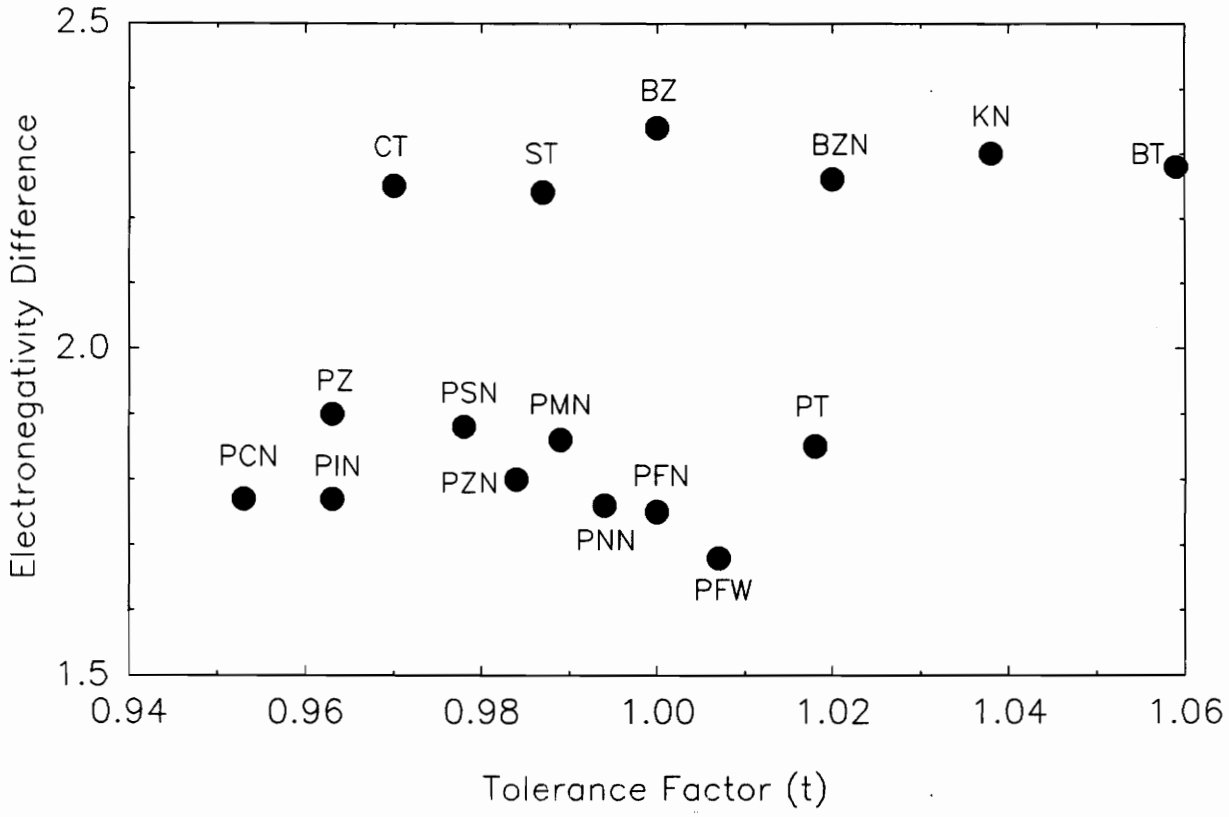

Figure 2.1 Plot of electronegativity difference vs tolerance factor for several perovskite compounds[1].

$$\frac{(X_{A\text{-}O}+X_{B\text{-}O})}{2} \qquad (2.20)$$

where $X_{A\text{-}O}$ is the electronegativity difference between the A–site cation and oxygen, and $X_{B\text{-}O}$ is the electronegativity difference between the B–site cations and oxygen. As shown in Figure 2.1, it is evident that ideal perovskite compounds have a tolerance factor t≈1 and a high electronegativity difference (strong ionic bonding), such as $SrTiO_3$. But for PbO–based $Pb(B'_xB''_{1-x})O_3$ perovskite compounds, the electronegativity differences are small; and for many of these compounds, the tolerance factor is considerably less than one, and therefore they may be less stable in perovskite structure. This prediction agrees with the experimental results with regard to the ease of preparation of these compounds with pure perovskite phase. Thus the addition of a small amount of stable perovskite compounds (*e.g.* $BaTiO_3$, $SrTiO_3$) was utilized to stabilize the PbO–based perovskites because of the increase of the tolerance factor and electronegativity difference [1,45]. This process was demonstrated in synthesizing $Pb(Zn_{0.33}Nb_{0.67})O_3$ (PZN) ,which is the most difficult relaxor perovskite to prepare in single–phase perovskite form, by adding 6 to 7 mole% $BaTiO_3$ [1].

2.3 Dielectric properties of $Pb(B'_xB''_{1-x})O_3$ perovskite

2.3.1 Polarization in dielectrics

First consider a homogeneous dielectric consisting of polarizable units which may be atoms, ions, molecules, unit cells, or macromolecular chains. The relationship between the polarization ",P," and the local electric field ",E'," is given

by [46]:

$$P = N\alpha E' \tag{2.21}$$

where N is the number of dipoles per unit volume and α is the polarizability.

There are various possible mechanisms for the polarization in a dielectric material. And the total polarizability of the dielectric can be represented as the sum of these contributions. For ferroelectric materials:

$$\alpha = \alpha_e + \alpha_i + \alpha_o + \alpha_s + \alpha_f \tag{2.22}$$

where:

α_e: electronic polarization, due to the shift of the center of gravity of the negative electron cloud in relation to the positive atom nucleus in an electric cloud.

α_i: ionic polarization, due to the displacement of ions in an electric field from the equilibrium positions, and the accompanying displacements of their electron clouds.

α_o: orientation polarization, associated with the presence of permanent electric dipoles which exist even in the absence of an electric field.

α_s: space charge polarization, the characteristic of polycrystalline materials which contain mobile charges. These mobile charges are present because they are impeded by surfaces, because they are not supplied at an electrode or discharged at an electrode, or because they

are trapped in the material. This kind of polarization is favored by grain boundaries or by the second phase, both of which act as barriers against the motion of charge carriers.

α_f: due to the co–operative change in direction of dipoles in the domain of ferroelectric materials [47].

α_e, α_i and α_o are the most important contributors to the permittivity (dielectric constant K) for ferroelectric ceramics. For high–K dielectric ceramics, another polarization contributor, charge hopping, should also be considered [48]. This makes a large contribution to dc conductivity and dielectric loss.

In an ideal capacitor the electric charge adjusts itself instantaneously to any change in applied voltage. However, there is an inertia–to–charge movement that shows up as a relaxation time for charge transportation. The phenomenon is analogous to the time required for elastic strain to follow an applied stress. Just like the relaxed and unrelaxed elastic modulus, the dielectric constant is dependent on frequency. The only process, which is rapid enough to follow alternative fields of any frequency is in the visible part of the spectrum, the electronic polarization [46]. Ionic polarization can follow an applied high–frequency field (in the infrared range). The frequency range of orientation and space charge polarization depended on the nature of the system but, in general, important only at low frequency.

The reported dielectric permittivity of PFN varies from 5000 to 26,000 depending on the frequency [3,6,10,21,22,27,49]. It is also that the dielectric permittivity is a sensitive function of heating rate, sintering temperature, sintering

time and atmosphere.

2.3.2 Dielectric loss

The time required for polarization shows up as a phase retardation of charging current in an alternating field. Instead of being 90^0 advanced, it is advanced by some angle $90-\phi$. The tangent of the angle ϕ ($\tan\phi$) is the dielectric loss The electric field and the current flux density are represented in complex notation:

$$E = E_o e^{iwt} \tag{2.23}$$

$$D = D_o e^{i(wt-\phi)} \tag{2.24}$$

thus
$$D = K^*E \tag{2.25}$$

and
$$K^* = K_s e^{-i\phi} = K_s(\cos\phi - i\sin\phi) \tag{2.26}$$

where $K_s = D_o/E_o$. In terms of a complex dielectric constant

$$K^* = K' - iK'' \tag{2.27}$$

therefore
$$K' = K_s\cos\phi \tag{2.28}$$

$$K'' = K_s\sin\phi \tag{2.29}$$

From equations 2.28 and 2.29 the loss tangent (dielectric loss) is given by

$$\tan\phi = K''/K' \tag{2.30}$$

This phase shift, corresponding to a time lag between an applied voltage and

induced current, causes loss currents and energy dissipation in AC circuit.

For the purpose of obtaining a high capacitance in the smallest physical space, such as multilayer capacitor, the material with high dielectric constant material need to be used. In addition to high dielectric constant, it is equally important to have a low value of the dielectric loss ",$\tan\phi$,".

The dielectric loss results from three primary processes [46]:

(1) Ion migration losses

a. DC conductivity losses

b. ion jump and dipole relaxation losses

(2) Ion vibration and deformation losses

(3) Electron polarization losses

The electron polarization losses give rise to absorption and color in the visible spectrum. The ion vibration and deformation losses are not a major concern for frequencies below 10^{10} Hz. By far the ion migration losses, which tend to increase at low frequencies and high temperatures, are the major factor affecting the use of ceramic materials. As shown in Figure 2.2, the total value for $\tan\phi$ is the sum of individual contributions. At lower frequencies conduction losses become important, at moderate frequencies ion jump and dipole losses are most significant, and at sufficiently high frequencies ion vibration effects becomes important.

2.3.3 Ferroelectricity

The ferroelectricity of cubic perovskites can be explained by barium titanate

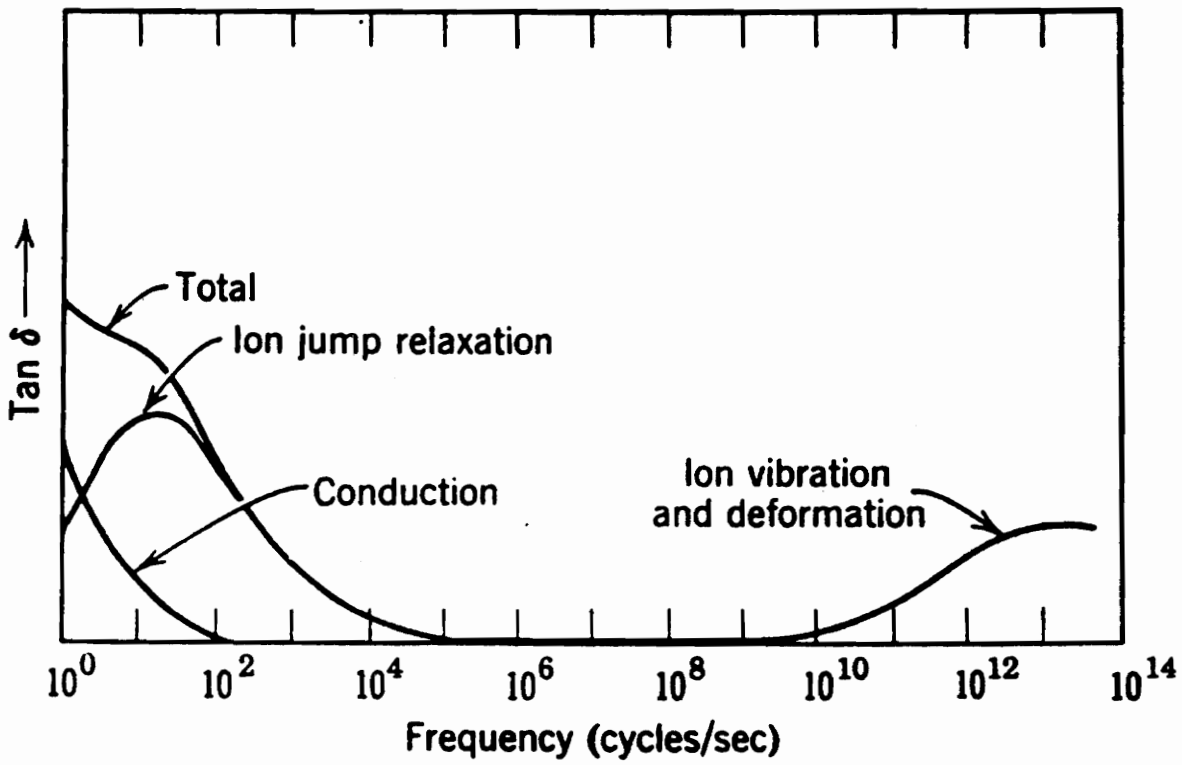

Figure 2.2 Effect of different dielectric loss mechanisms on $\tan\delta$[46].

at the temperatures above Curie temperature (120^{0}C) [46]. Since the titanium ion fits into the octahedral interstice of this structure, this titanium ion has no fixed unsymmetrical position. At high temperatures, the open octahedral site allows the titanium ion to develop a large dipole moment in an applied field. On cooling below the Curie temperature, the octahedral structure changes from cubic to tetragonal symmetry. For barium titanate, the titanium ion is in an off–center position corresponding to a permanent electrical dipole, as shown in Figure 2.3. As a consequence the dielectric constant falls from the high peak value and shows little dependence on temperature. However, the structure of PFN changes from cubic to rhombohedral when the temperature falls down to its Curie temperature [10,28,40]. Thus the dependence of the dielectric constant on temperature is different from the behavior of $BaTiO_3$ below 120^{0}C.

PFN shows the properties of relaxors which are a class of ferroelectric dielectric. For this material, the temperature of the peak of the dielectric constant is frequency–dependent and shows a great dependency of the dielectric constant on the frequency than normal ferroelectric materials do (*e.g.* $BaTiO_3$). Generally high–K dielectrics show a gradual fall in permittivity with increasing frequency, some 2 to 5% per decade, over the range 10^2 to 10^8 Hz. In addition, they show a broadening of the T_c (Curie temperature) peak which can be referred to as a Curie region. They are said to possess "diffuse phase transition."

All relaxors contain two or more species of ion on the same site, such as $Pb(Fe_{0.5}Nb_{0.5})O_3$ (PFN), $Pb(Mg_{0.33}Nb_{0.67})O_3$ (PMN), $Pb(Sc_{0.5}Ta_{0.5})O_3$ (PST), and $Pb(Mg_{0.5}W_{0.5})O_3$. In these relaxors, the A–site cation is lead. Because these

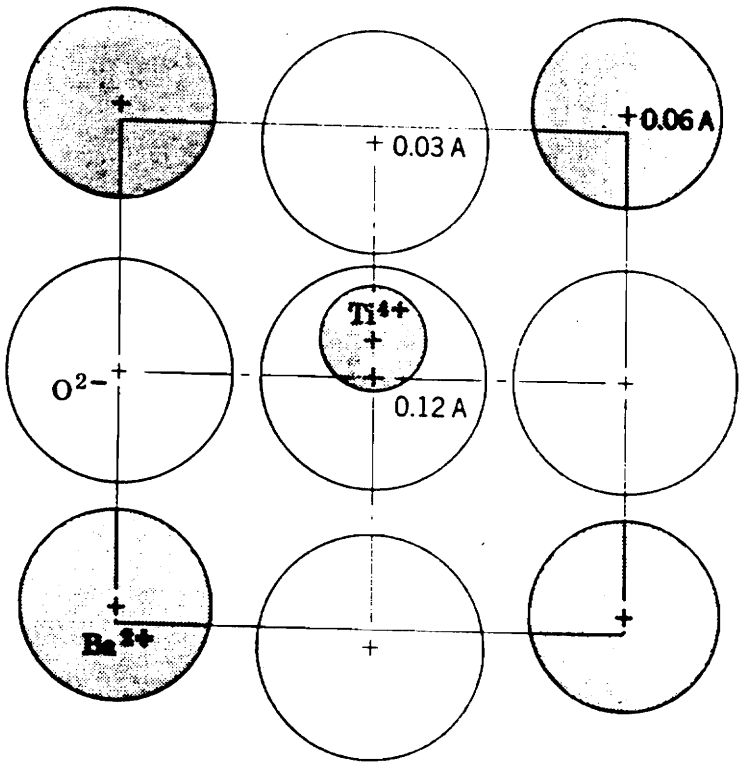

Figure 2.3 Ion position in tetragonal $BaTiO_3$ [46].

compounds can be found with more than one atomic species occupying the B–sites, there is the possibility of structural ordering or disordering for the B–site cations. The perovskite–structured relaxors are divided into two groups: those in which the B–site cations are always randomly distributed (*i.e.* they are disordered), and those in which the cations can achieve partial or complete order. It had been reported that the degree of ordering can be varied in certain relaxor materials, such as $Pb(Sc_{0.5}Ta_{0.5})O_3$ (PST), by thermal annealing [51,52]. The schematic results are shown in Figure 2.4. The origin of the diffuse phase transition is believed to be a distribution of Curie temperatures in the material due to compositional fluctuations, or microinhomogeneity (disorder) in the B–site cations [53]. From a dielectric engineering point of view, it is clear that ordering should be minimized in order to obtain the highest dielectric constant over the maximum temperature range.

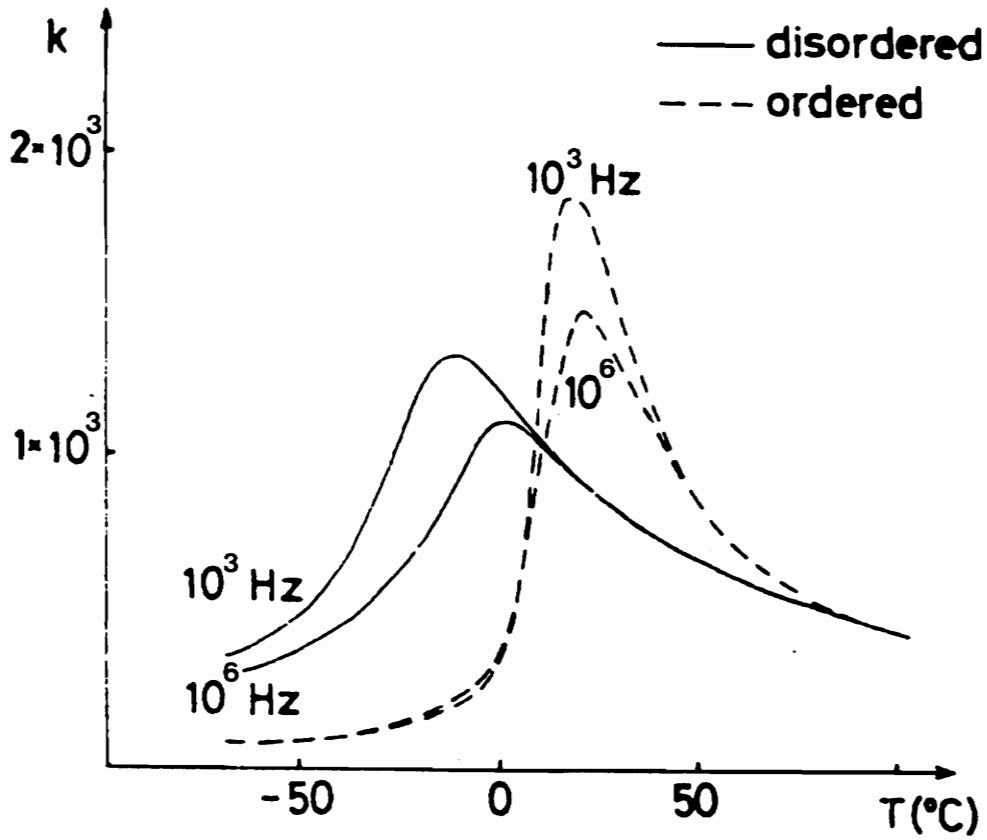

Figure 2.4 Typical dielectric behavior for "disordered" and "ordered". The example presented is for disordered and thermally annealed crystals of PST[68].

Chapter 3: EXPERIMENTAL PROCEDURE

3.1 Molten salt synthesis of PFN ceramic powders

The basic idea of this technique is to utilize the molten mixture of NaCl and KCl as a reaction medium. Figure 3.1 shows the continuous solid solution of NaCl–KCl system [54]. As seen in Figure 3.1, this binary system exhibits a minimum melting point at 670^{0}C with a composition of 50 mole% NaCl. The melting points of pure NaCl and KCl are 800^{0}C and 770^{0}C, respectively. The temperature of the reaction carried out in this study was higher than that of the liquidus in this binary phase diagram.

"Reagent grade" oxides (PbO, Fe_2O_3 and Nb_2O_5) and chlorides (NaCl and KCl) were used in this study. Appropriate amounts of these chlorides and oxides were ground by using a mortar and pestle with acetone for about an hour to obtain uniformly distributed mixtures. Because of the expected loss of PbO possibly due to the volatilization or due to the reaction with molten salts, variable amounts of excess PbO were added to the starting mixtures. The excess amount of PbO was varied from 0 mole% to 20 mole%. The mixed slurry was dried at 120^{0}C for 2 hours for the complete removal of acetone. The dried powders were placed in a covered alumina crucibles and then fired in a box furnace at temperatures ranging from 700^{0}C to 900^{0}C for 1 to 3 hours. After the firing, the chlorides were removed from the product by washing them in hot water several times until the filtrate showed no reaction with a silver nitrate solution. The residual excess PbO was removed by treating the powders with boiling acetic acid (5 wt%) solution for 20 minutes. The

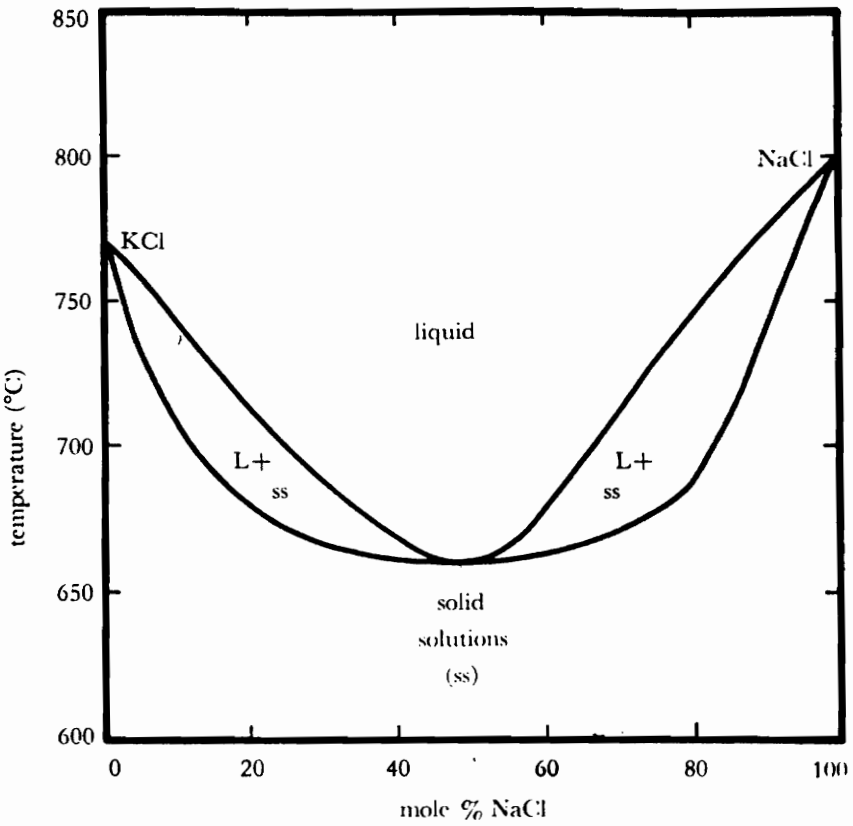

Figure 3.1 Phase diagram : KCl + NaCl system[54].

powders were finally dried at 150^{0}C for 2 hours.

The resulting phases in the powders were identified by standard X–ray diffraction (XRD) techniques, using a model PW–1792 diffractometer with CuKα radiation. In addition to identification of phases, this technique was also used to quantification of phase content of the powders. The relative amounts of perovskite (p) and pyrochlore (π) phases are directly proportional to the observed intensities of their respective peaks appearing in the X–ray diffraction patterns. The integrated intensity of the (hkl) peak of a phase " ,i," is given by the relation [55]:

$$I_i(hkl) = KV_i \frac{1}{v_i} |F_i|^2 e^{-2m_i} g_i \frac{1+\cos^2 2\theta_i}{\sin^2\theta_i \cos\theta_i} \frac{1}{2\mu_m} \qquad (3.1)$$

where $I_i(hkl)$ is the integrated intensity of the (hkl) peak; K is a constant dependent on the type of the radiation used and the beam size; V_i is volume fraction of phase i; v_i is volume of the unit cell; F_i is structure factor; e^{-2m_i} is Debye–Waller coefficient; g_i is multiplicity of the given reflection; μ_m is linear absorption coefficient of the mixture, and $(1+\cos^2 2\theta_i)/(\sin^2\theta_i \cos\theta_i)$ is Lorentz polarization factor.

Moreover, to take into account the volume fraction (Cα) of α phase in a mixture, the intensity of α in the mixture can be written as:

$$I\alpha = \frac{K_1 C\alpha}{\mu_m} \qquad (3.2)$$

where K_1 is a constant. Therefore, for the mixture of perovskite (p) and pyrochlore (π), the relationship between their concentrations and the intensities of their peaks

can be expressed as:

$$\frac{C_P}{C_\pi} = \frac{I_P}{I_\pi} \tag{3.3}$$

by using the direct comparison method [56].

The particle sizes and the morphology of the powders were studied by using scanning electron microscopy (SEM) with an energy–dispersive X–ray analyzer.

3.2 Sintering and microstructure characterization of pure PFN powders and PFN powders with PbO or Li_2CO_3 additions

For sintering and microstructure characterization, stoichiometric, single phase PFN powders were used. These powders were synthesized at 800^{0}C for 1 hour using 10 mole% excess PbO in the starting oxide powder mixture (Section 3.1).

The PFN powders were pressed into pellets by using 3 wt% of methocel as the binder. These pellets were sintered in closed alumina crucibles for periods ranging from 0.5 to 15 hours and at various temperatures following the binder burn–out at 400^{0}C. The sintered pellets were analyzed by X–ray diffraction to ensure that no pyrochlore phase was present. This is because longer sintering times and higher sintering temperatures might cause PbO loss which may lead to a conversion of the perovskite phase to pyrochlore phase.

For the effect of additions (PbO and Li_2CO_3), the excess amounts of the

additions added were varied from 0.5wt% to 2.0wt%. The sintering conditions for PFN with PbO addition were the same as those described for pure PFN powders. However, the sintering of PFN with Li_2CO_3 addition was carried out at sintering temperatures ranging from 900^{0}C to 1050^{0}C for 4 hours.

The fractured surfaces of the sintered pellets were observed using SEM with an energy–dispersive X–ray analyzer. The densities of the sintered pellets were determined by the ASTM immersion method using water as the immersion liquid [57].

3.3 The dielectric properties of pure PFN powders and PFN powders with PbO or Li_2CO_3 additions

For measuring dielectric properties, the powders preparation and sintering parameters are the same as those described in Section 3.2.

The sintered pellets were polished and coated with silver exopy on both sides, and then cured at 120^{0}C for 15 minutes. The dielectric property measurements were carried out using a HP 4192A LF impedance analyzer. The temperature dependence of dielectric properties was characterized during cooling cycle of the sample from temperatures close to 200^{0}C. The sample temperature was controlled using a (Thermodyne type 1300) furnace which is equipped with a (Omega CN 900) temperature controller. The capacitance ",C," contains both a geometrical as well as a material factor. For a large plate capacitor of area A and thickness d, the geometrical capacitance is given by [46]:

$$C_o = (A/d)\epsilon_o \tag{3.4}$$

where ϵ_o (= 8.854 × 10^{-12} F/m) is the permittivity (dielectric constant) of a vacuum. For a material having permittivity ϵ', the capacitance is expressed as:

$$C = C_o(\epsilon'/\epsilon_o) = C_oK' = K'\epsilon_o(A/d) \tag{3.5}$$

where K' is the relative permittivity or relative dielectric constant. K' is the material property which determines the capacitance and of principal concern for this study.

DC conductivity of PFN was measured at room temperature, 100^{0}C and 150^{0}C using (HP 4140B) a picoammeter. The σ (conductivity) was calculated from the following equation [58]:

$$V = IR = I(d/A)/\sigma \tag{3.6}$$

where V is the applied voltage, I is the current measured, d and A are thickness and area of the sample,respectively. Thus σ (conductivity) can be obtained from the slope of V vs I(d/A).

Chapter 4: RESULTS AND DISCUSSION

4.1 Synthesis and reaction mechanisms of PFN in molten salt

4.1.1 Formation process

XRD profiles of the PFN powders formed at various temperatures and times, and having different amounts of excess lead oxide in the starting mixture (flux to oxide weight ratio is one and flux is a mixture of equimolar NaCl and KCl) were determined. The X–ray diffraction patterns, as depicted in Figure 4.1(b), showed that for low formation temperatures ($\leq$ 700^{0}C) and short times ($\leq$ 1 hour), the powders are a two–phase mixture of the PFN phase and a significant amount of second phase [pyrochlore $Pb_3Nb_4O_{13}$ (P_3N_4)]. Increasing the formation temperature to about 800^{0}C led to powders having a single phase of PFN (Figure 4.1(a)). For reaction temperatures between 900^{0}C to 1000^{0}C, only the pure phase of PFN was obtained irrespective of the time and the amount excess lead oxide in the starting oxide mixture. The resulting percentage of the perovskite phase was determined by the following equation:

$$\%\text{Perov.} = 100 \times I_{perov}/(I_{perov}+I_{pyro}) \qquad (4.1)$$

where I_{perov} and I_{pyro} are intensities of major peaks [(110) and (222)] for perovskite and pyrochlore phases, respectively. The variations of %Perov. with formation temperature, time, and amount of excess lead oxide can be seen in Figure 4.2. For formation temperatures below 900^{0}C, the % Perov. increased with increasing

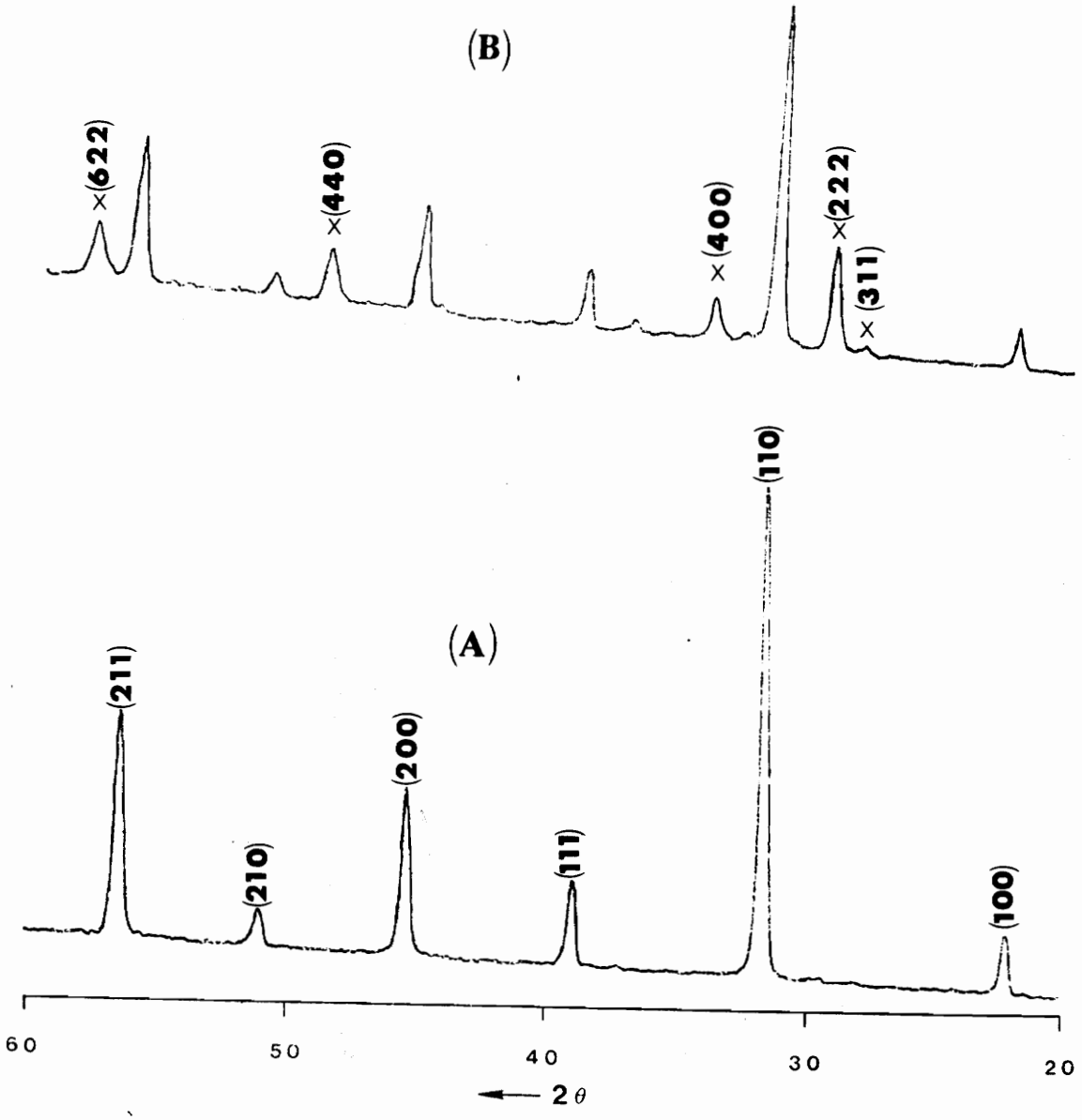

Figure 4.1 XRD profiles of PFN powders obtained at, (A) 800^{0}C for 1 hour with 10 ml.% of excess PbO showing pure phase of PFN, (B) 700^{0}C for 1 hour with 0 ml% of excess PbO showing PFN with pyrochlore phase (x: pyrochlore phase).

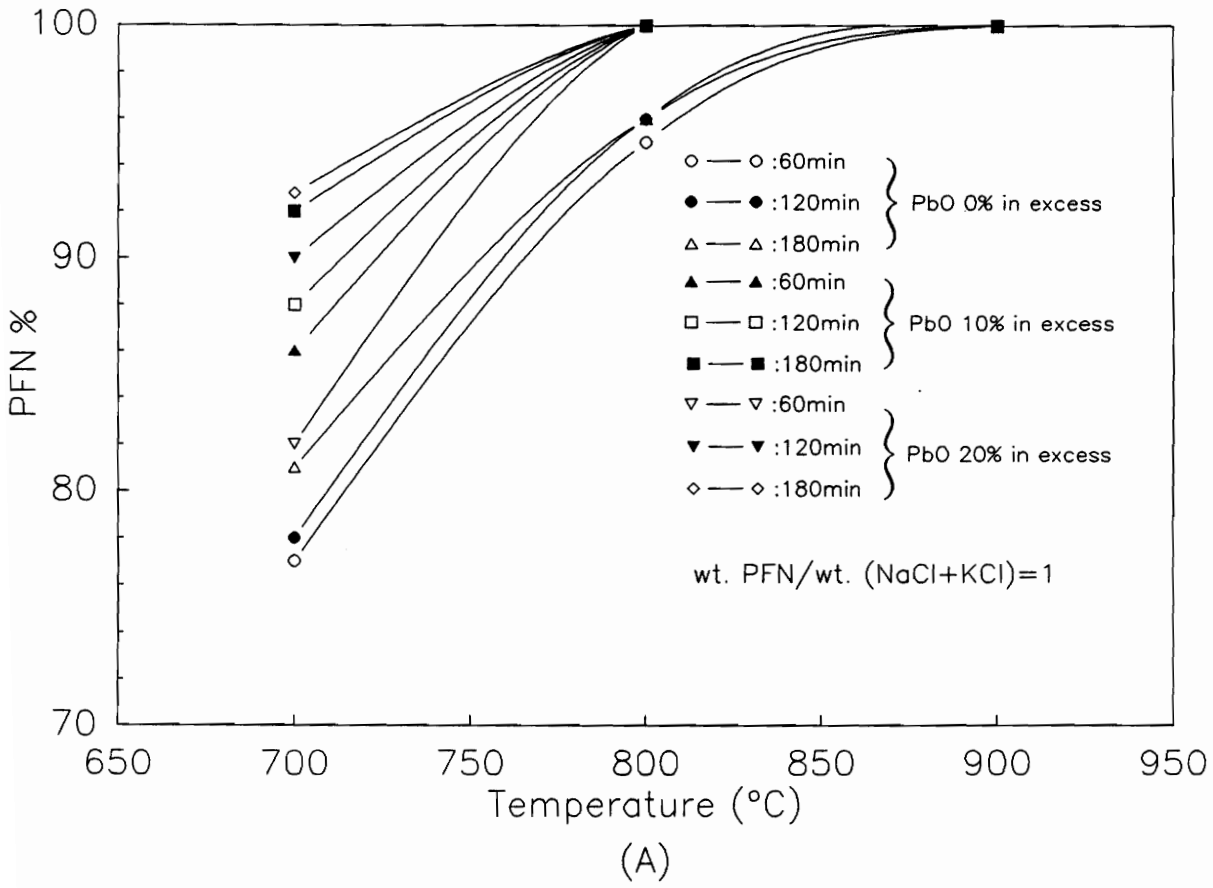

Figure 4.2 The variation of %Perov. with (A) formation temperature (B) time, and (C) amount of excess PbO.

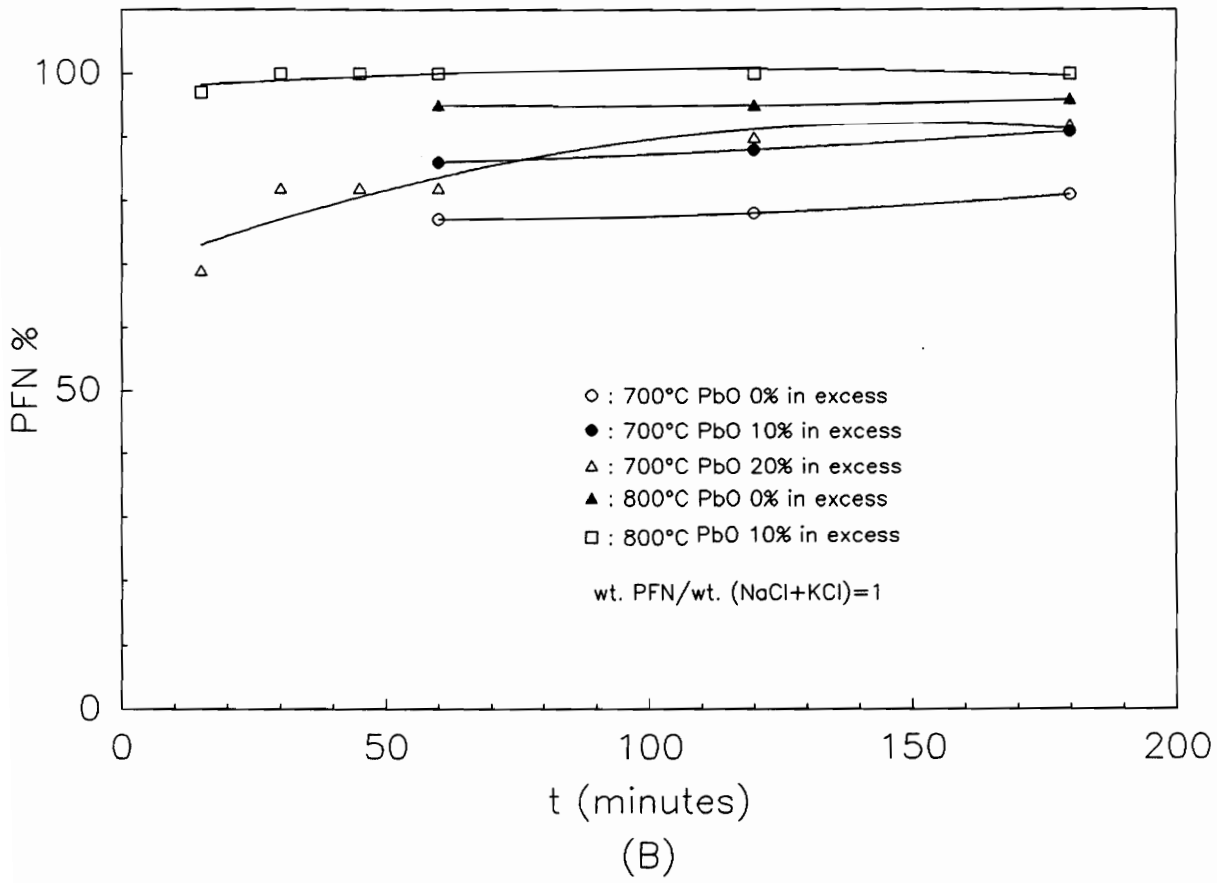

Figure 4.2 (Continued)

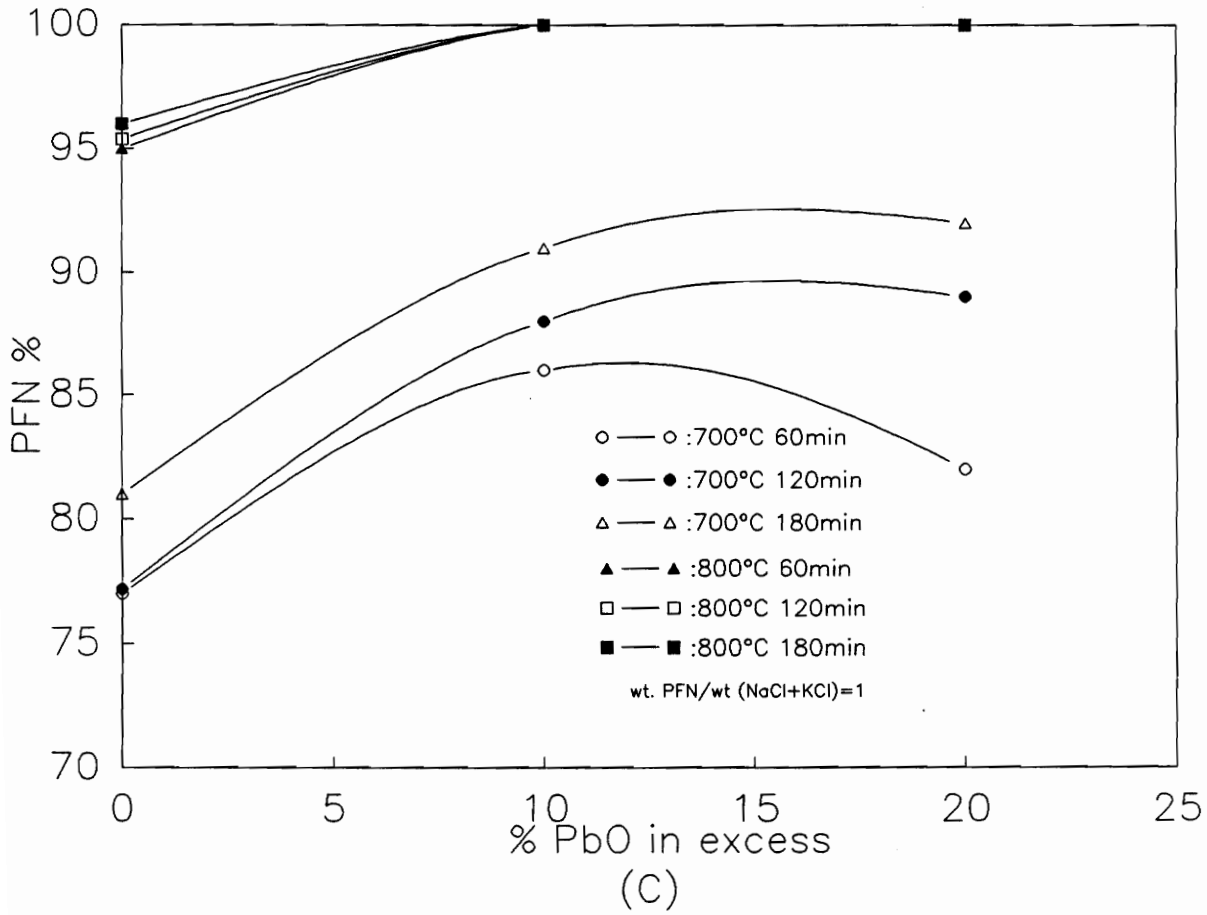

Figure 4.2 (Continued)

reaction temperature, time, and amount of excess lead oxide. It was also evident that the formation temperature had the most significant effect on the %Perov., as compared to the excess lead oxide concentration and the formation time. It should also be noted that a pure perovskite phase was not obtained at 700^{0}C for all the investigated times and compositions of the starting oxide mixture. However, pure single phase PFN could be easily obtained at 800^{0}C for 30 minutes with 10 mole% excess lead oxide.

Our results are different from those of Lopatin et al [38] who reported that (1) single phase PFN can be formed at 700^{0}C for 1 hour with 20 mole% excess of lead oxide and (2) at 800^{0}C, the amount of perovskite phase is always less than 100% and decreases significantly with increasing time. These discrepancies can be attributed to the differences in the purity and particle sizes of the starting oxide powders. Their observed decrease in %Perov. with increasing formation time at 800^{0}C can also be explained by considering secondary reactions. For the formation of PFN from molten salts (NaCl–KCl), there is only one second phase ($Pb_3Nb_4O_{13}$) formed in the product powders. The following formation reactions need to be considered:

$$3\,PbO + Nb_2O_5 \longrightarrow Pb_3Nb_4O_{13}\ (P_3N_2) \tag{4.2}$$

$$Pb^{+2} + Cl^- \longrightarrow PbCl_{2(g)}\uparrow \tag{4.3}$$

$$PbO_{(s)} \longrightarrow PbO_{(g)}\uparrow \tag{4.4}$$

$$Pb_3Nb_4O_{13} + PbO + Fe_2O_3 \longrightarrow Pb(Fe_{0.5}Nb_{0.5})O_3 \tag{4.5}$$

Since the boiling point of $PbCl_2$ is 950^0C, one can expect a significant loss of lead oxide due to Reaction 4.3. It follows from Reaction 4.5 that this loss of lead oxide obviously decreases the perovskite yield. The loss of lead oxide via the formation of $PbCl_2$ (Reaction 4.3) may also be the reason for the addition of excess lead oxide to the starting oxides to form stoichiometric PFN (Figure 4.2(C)). It is interesting to note that for the PbO, Fe_2O_3, and Nb_2O_5 powder mixture the number of possible reactions in molten salt is significantly smaller than the number of reactions possible in solid state (Chapter 2).

The lattice parameter of the PFN powders, prepared by molten salt synthesis, were calculated from the XRD peaks for 2θ values higher than 60^0, as they gave more accurate values. Irrespective of the preparatory conditions that were used in this study, the calculated lattice parameter was 4.011Å, which is close to the valves reported in literatures [27,59]. However, this calculation was based on the assumption that the structure of PFN is cubic perovskite at room temperatures. In fact, as stated in Chapter 1, PFN possesses a rhombohedral structure below curie temperature ($\approx 100^0$C) which in this case is very similar to the cubic structure. The splitting of the high angle diffraction lines, characteristic of the rhombohedral structure, were also observed in the diffraction pattern. Although the formed PFN powders were not chemically analyzed, we can indirectly conclude, from these observation, that the powders contained are of pure PFN phase.

In order to understand the formation mechanism of PFN from molten salts, sintered discs of the individual constituent oxides were analyzed for weight loss and by X–ray diffraction before and after heat treatment with molten salts. These

results were presented in Table 4.1. The solubility of Fe_2O_3 reported in the table is taken from the results of Haysshi et al [36]. It can be clearly seen from Table 4.1 that PbO and Fe_2O_3 are more soluble in molten salts than Nb_2O_5. This indicates that PbO and Fe_2O_3 species may be the transporting species during the reaction in molten salts. It should be noted that the interaction of Nb_2O_5 with molten salts at 800^0C to 900^0C for 2 hours results in the formation of a new phase in trace quantities which could not be identified. Further, analysis of products at various stages of reaction in molten salt, for the PbO, Fe_2O_3, and Nb_2O_5 mixture, did not yield any complex oxides containing either Pb and Fe or Fe and Nb.

The presence of significant quantities of pyrochlore phase (P_3N_2) for times as short as 5 minutes at 700^0C implied that Reaction 4.2 in the sequences of molten salt synthesis is the fastest reaction. At no stage of PFN formation in molten salts were compounds other than PFN, PbO, and $Pb_3Nb_4O_{13}$ (P_3N_2) observed. In contrast to molten salt synthesis, several intermediate compounds, such as $Pb_3Nb_4O_{13}$ (P_3N_2), $Pb_2Fe_2O_5$ (P_2F), $Pb_2Nb_2O_7$ (P_2N), and $Pb_3Nb_2O_8$ (P_3N), were identified at different stages in solid–state synthesis of PFN. Thus one can conclude that the reaction mechanism of PFN formation is much simpler in molten salt than that in solid–state. Therefore, when solid–state methods are used for the formation of PFN, it is not surprising to see secondary phases such as $Pb_3Nb_2O_8$ (P_3N) even for temperatures as high as 900^0C.

Table 4.1 Solubility of Oxides in Molten Salts

Oxide	T(°C)	Time(h)	Change in weight*	Product
Nb_2O_5	900	2	8.51×10^{-5}	Nb_2O_5+UP
Nb_2O_5	800	2	5.9×10^{-5}	Nb_2O_5+UP
PbO	900	2	-8.8×10^{-5}	PbO
PbO	800	2	-1.4×10^{-5}	PbO
Fe_2O_3[36]	900	–	-2.2×10^{-6}	–

*mole/g·salt

UP : Unknown Phase

4.1.2 The effects of flux composition and flux/oxide weight ratio

The effects of flux composition (NaCl/KCl ratio) and flux/oxide weight ratio on the formation of PFN were studied by fixing other parameters such as temperature, time, and amount of excess lead oxide at 800^{0}C, 60 minutes, and 10 mole%, respectively. The variation of either the flux composition or flux/oxide ratio did not have any effect on the ability to form single phase PFN. The only compositional difference seen was in the powders prior to the acetic acid wash. Figures 4.3 and 4.4 show the effects of flux/oxide ratio and the composition of flux, respectively, on the residual quantities of lead oxide before acetic acid wash. Figure 4.3 shows that no residual quantity of lead oxide could be detected when the flux/oxide ratio was smaller than unity. However, raising the flux/oxide ratio, increased the amount of residual lead oxide indicating that the conversion factor of lead oxide decreased with increasing amount of flux. This conversion rate decrease may be attributed to the increase in distance required for the lead oxide to diffuse with increasing flux/oxide ratio. Irrespective of the flux/oxide ratio, the excess amount of lead oxide observed was always smaller than 10 mole% indicative of some loss due to the formation of lead chloride (Reaction 4.3) and the evaporation of lead oxide (Reaction 4.4). In contrast to the flux/oxide ratio, the flux composition (NaCl/KCl ratio) had negligible effect on the amount of residual lead oxide (Figure 4.4)

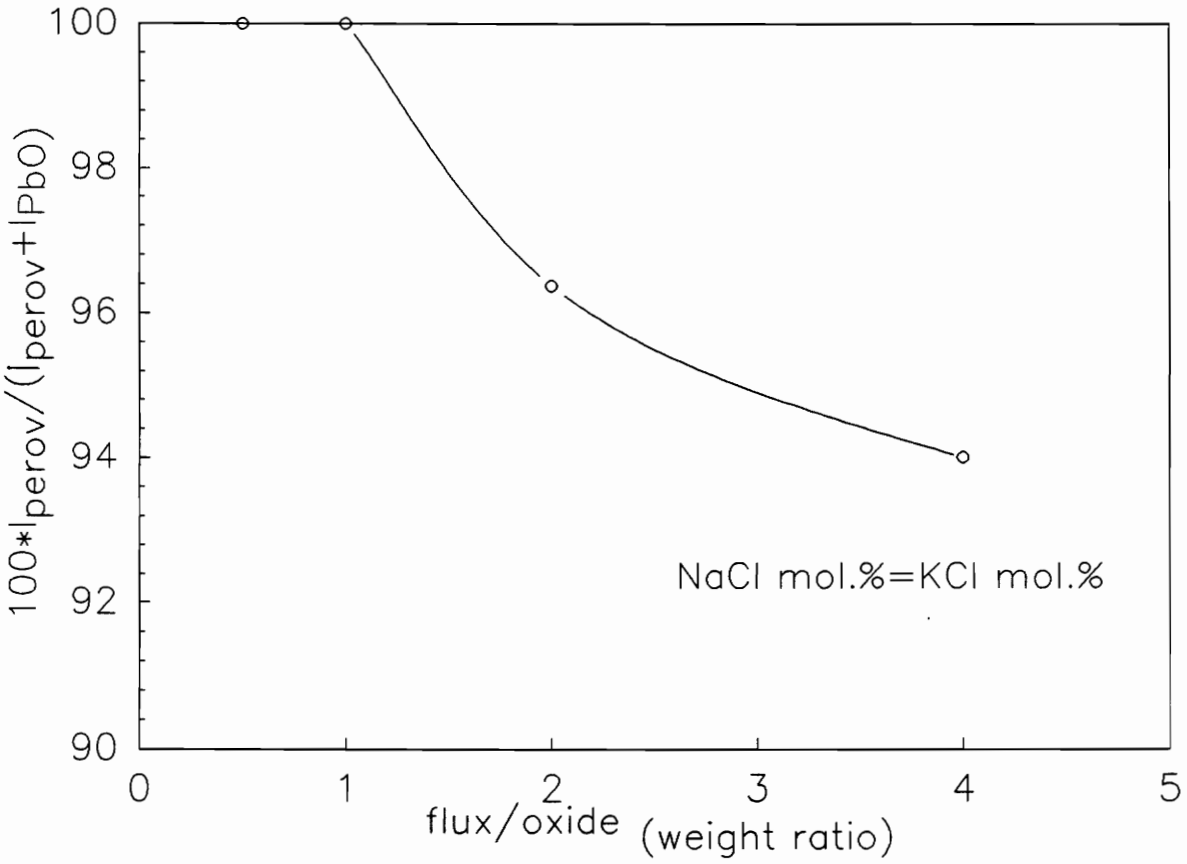

Figure 4.3 The effect of flux/oxide ratio on the amount of residual PbO.

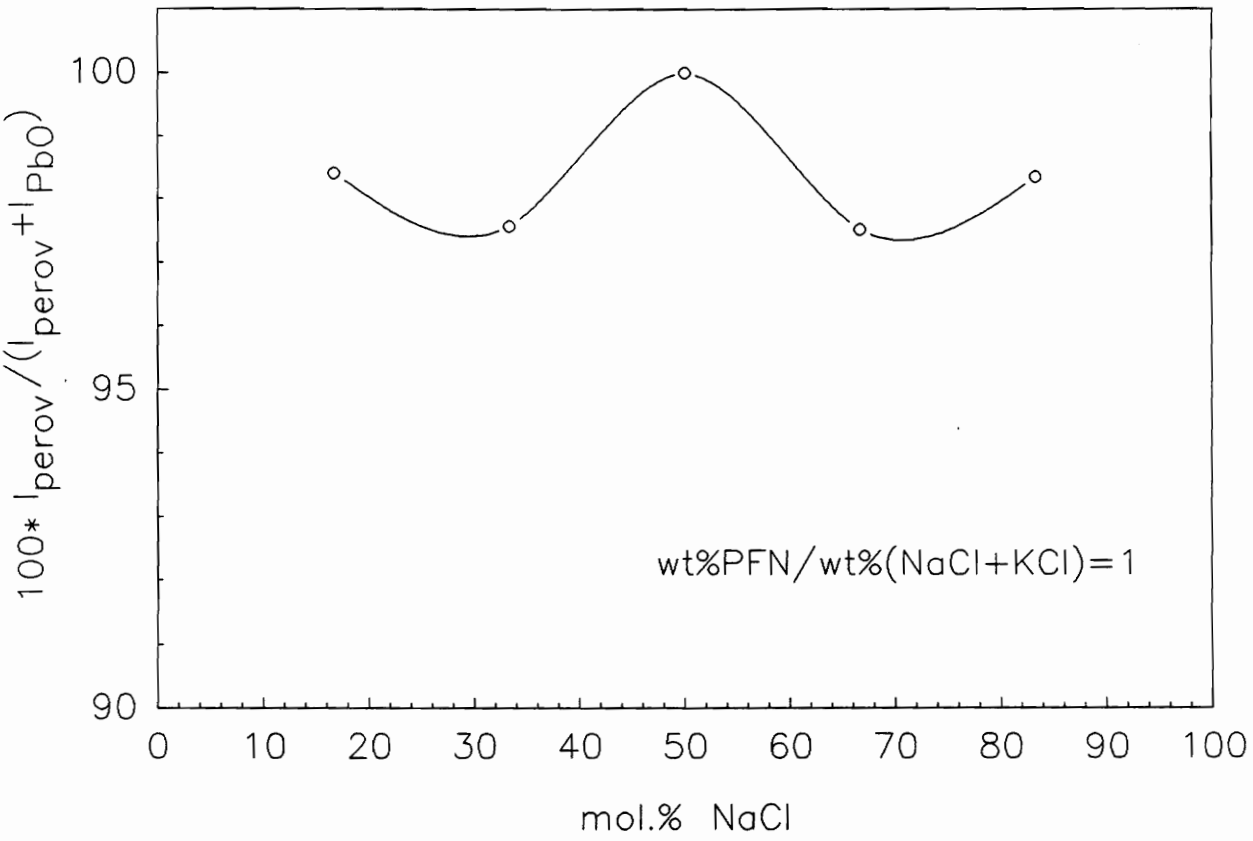

Figure 4.4 The effect of composition of flux on the amount of residual PbO.

4.1.3 Morphology

Scanning electron micrographs (SEM) of PFN crystallites, prepared at 800^{0}C and 900^{0}C for various formation times ranging from 30 minutes to 180 minutes, are shown in Figure 4.5. For comparison, SEM of the PFN powders prepared by solid–state method is also shown in Figure 4.5. It can be clearly seen from the pictures that in contrast to the highly agglomerated powders obtained by the solid–state method, no stable aggregates were observed for the molten salt synthesized PFN powders. Molten salt synthesized PFN crystallites were fairly rounded (cuboidal) and did not show any well defined facets. However, the crystallite size was governed by the formation conditions. In general, the resultant powder morphology is controlled mainly by the size and the shape of the slowly dissolving raw material (Nb_2O_5 in our case), and by the crystal growth process. Because PbO is the fastest dissolving component, and PFN is formed by the reaction of PbO and Fe_2O_3 with $Pb_3Nb_4O_{13}$, initially the morphology of PFN powder is controlled by the size and shape of $Pb_3Nb_4O_{13}$, which in turn is determined by the morphology of starting Nb_2O_5 (Figure 4.6). Therefore the development of the morphology of PFN powder is first controlled by the diffusion of PbO to the surface of Nb_2O_5 particle to form $Pb_3Nb_4O_{13}$. Further the species of PbO and Fe_2O_3 diffuse to $Pb_3Nb_4O_{13}$ to form PFN. Although it is expected that the shape of PFN crystallites are initially controlled by size and shape of Nb_2O_5, the final PFN morphology is determined by the anisotropy of the particle growth process. Lack of faceting at almost all sizes indicates that the growth anisotropy of PFN crystallite is very small. In other words, the interfacial energies of various faces of PFN in molten salt may have approximately the same values.

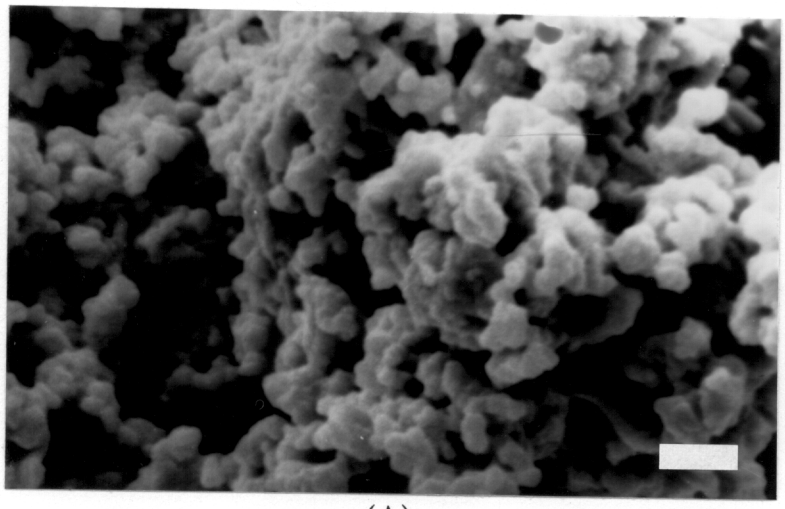

(A)

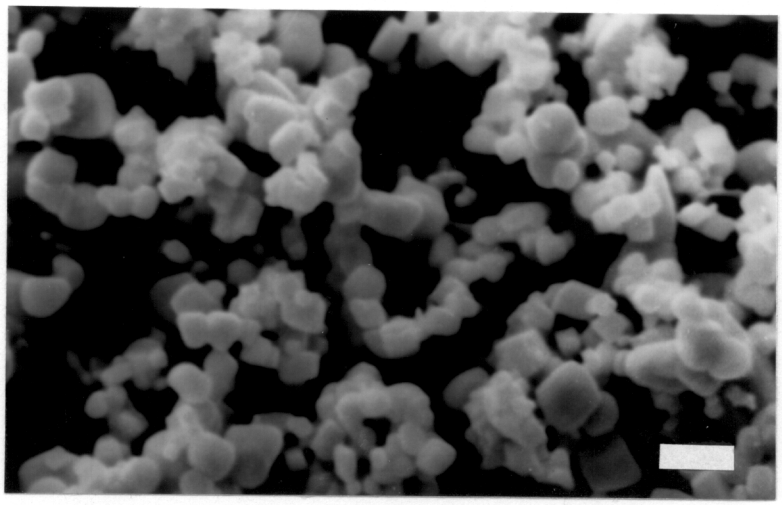

(B)

Figure 4.5 SEM photographs of PFN powders made by (A) solid–state reaction, (B) molten salt synthesis at 800^{0}C from 0.5 hr. with 10 ml.% PbO in excess.(Bar = 1μm)

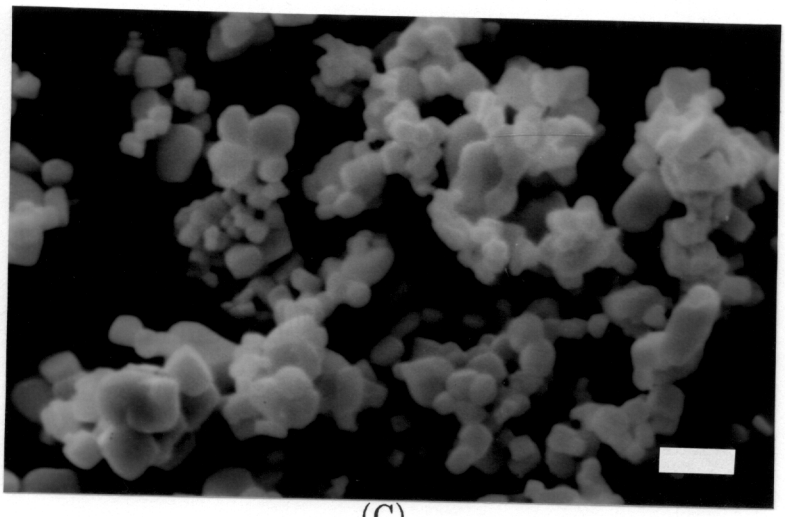

(C)

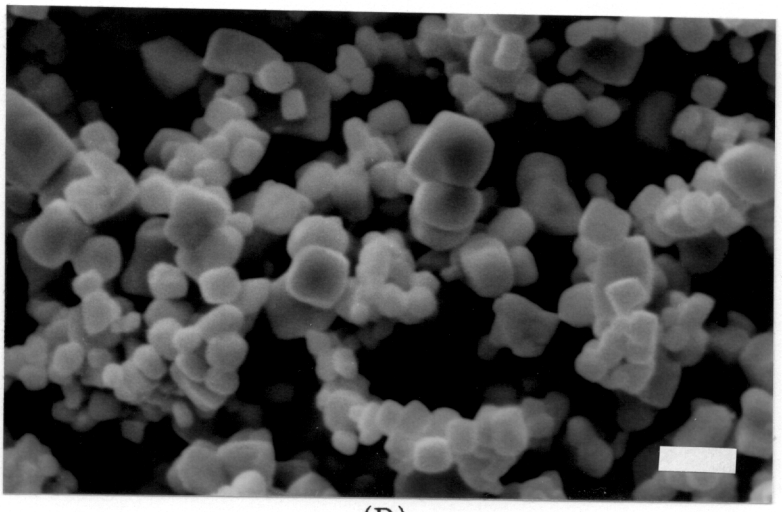

(D)

Figure 4.5 SEM photographs of PFN powders made by molten salt synthesis (C) at 800^{0}C for 1 hr with 10 ml.% PbO in excess, (D) at 800^{0}C for 2 hrs with 10 ml.% PbO in excess. (Bar = 1μm)

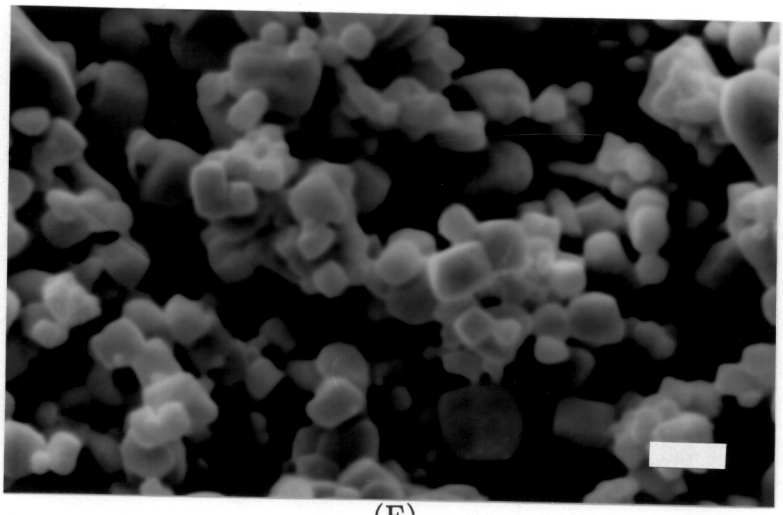

(E)

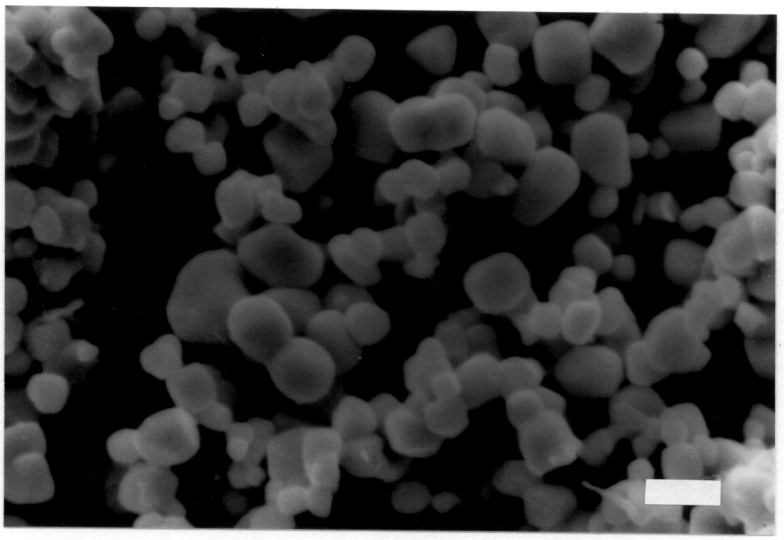

(F)

Figure 4.5 SEM photographs of PFN powders made by molten salt synthesis (E) at 800^{0}C for 3 hrs with 10 ml.% PbO in excess, (F) at 900^{0}C for 0.5 hr with 10 ml.% PbO in excess. (Bar = 1μm)

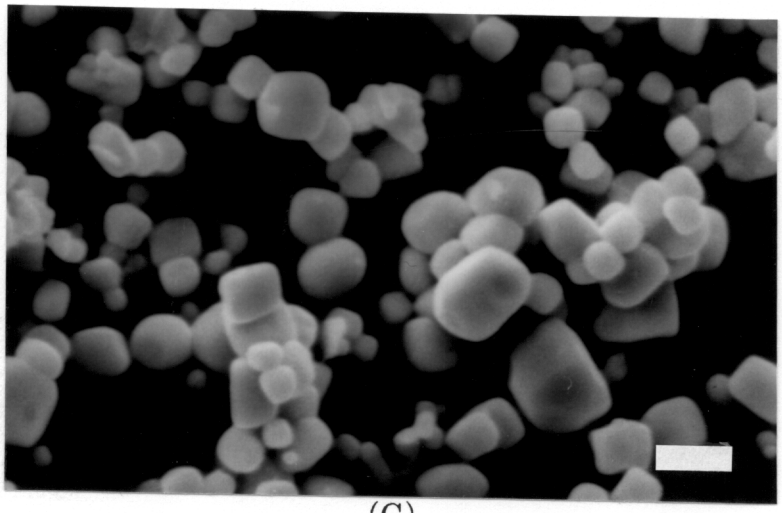

(G)

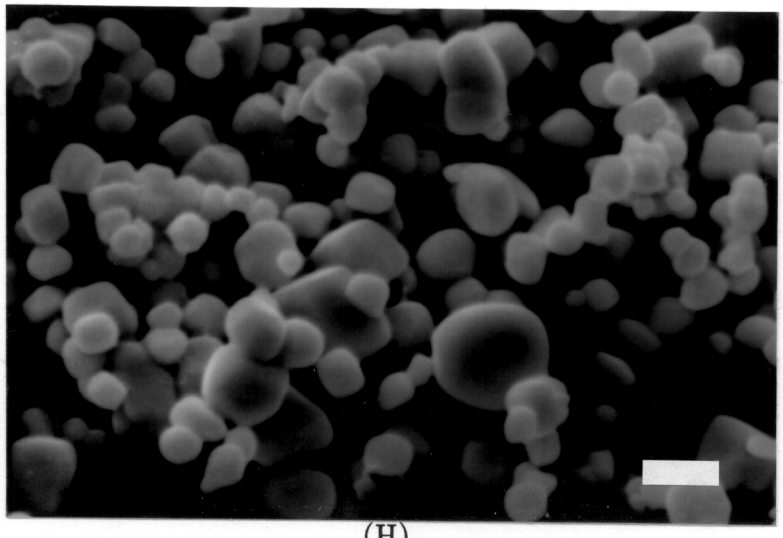

(H)

Figure 4.5 SEM photographs of PFN powders made by molten salt synthesis (G) at 900^{0}C for 1 hr with 10 ml.% PbO in excess, (H) at 900^{0}C for 2 hrs with 10 ml.% PbO in excess. (Bar = 1μm)

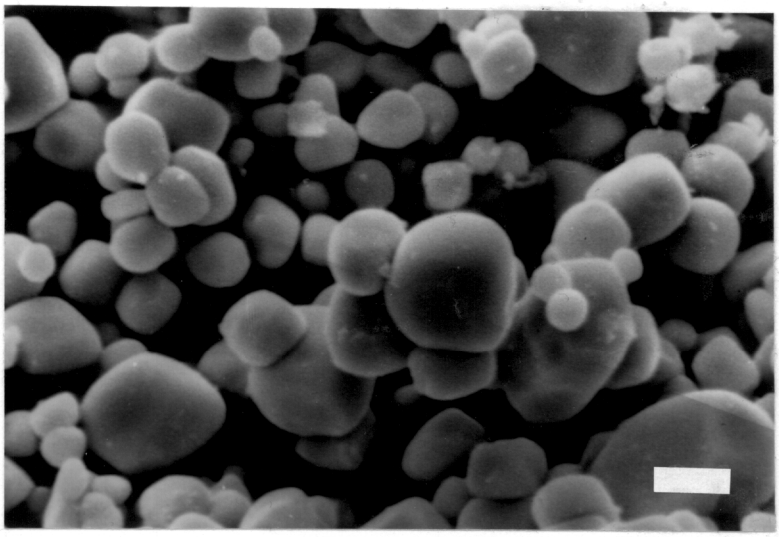

(I)

Figure 4.5 SEM photograph of PFN powders made by molten salt synthesis (I) at 900^{0}C for 3 hrs with 10 ml.% PbO in excess. (Bar = 1μm)

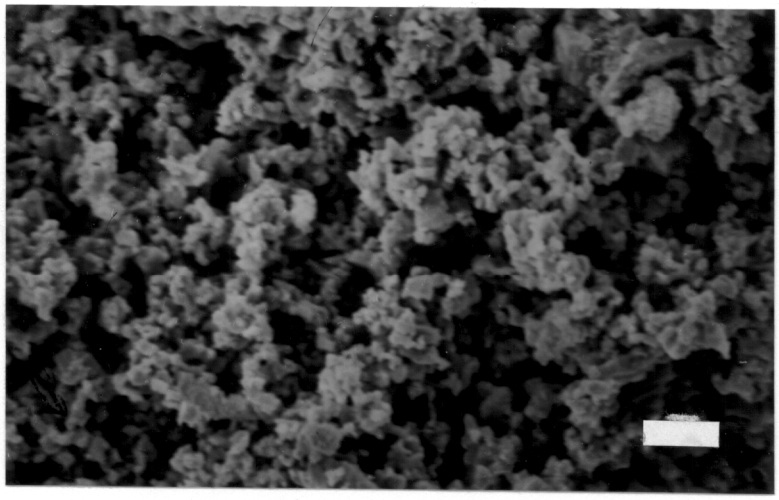

Figure 4.6 The morphology of starting Nb_2O_5 powders. (Bar = 4μm)

Figure 4.7 depicts the relation between the average particle size (APS) of PFN powders and the formation time (t) at different formation temperatures (T). Although there are some deviations, the particle size appears to increase with increasing formation time for a fixed temperature (for example at 800^{0}C, increase of formation time from 30 minutes to 3 hours increased the average particle size from 1.11μm to 1.58μm). The relationship between the average particle size (APS) and formation times (t) can be expressed as:

$$APS \propto t^n \tag{4.6}$$

where n is a constant having a value of 0.2 calculated using the slopes in Figure 4.7.

The APS had an Arrhenius dependence on the formation temperatures which is evident in Figure 4.8. The two distinct regions seen in Figure 4.8 indicate two different growth mechanisms. The apparent activation energies for particle growth, calculated using the data presented in Figure 4.8 and the empirical equation:

$$APS = t^n \exp(-\Delta Q/RT) \tag{4.7}$$

are 18.83 and 209.2 KJ/mole for the formation temperatures in the range 800^{0}C to 900^{0}C and 900^{0}C to 1000^{0}C, respectively. The increase in the activation energy above 900^{0}C (above the melting point of PbO) may be attributed to the changes either in melt viscosity or in the solubility of PFN in the melt.

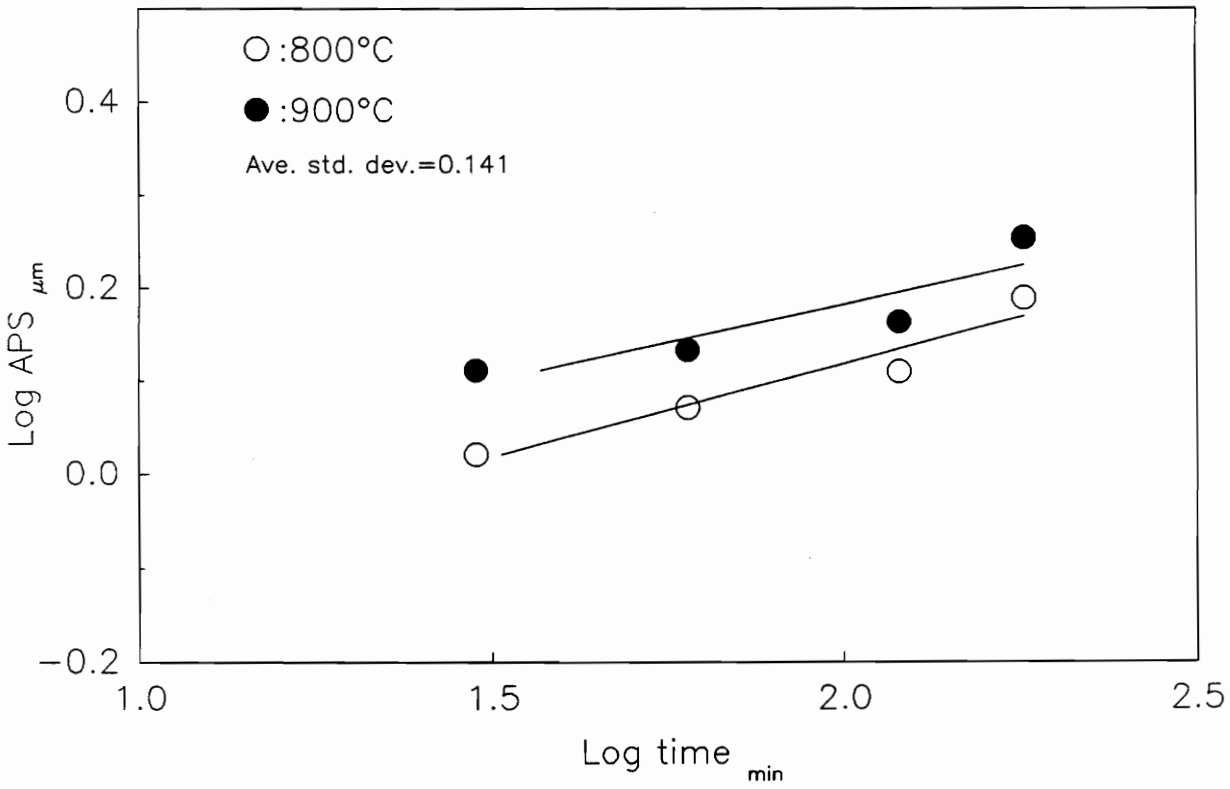

Figure 4.7 The relation between average particle size (APS) and formation time at different temperatures.

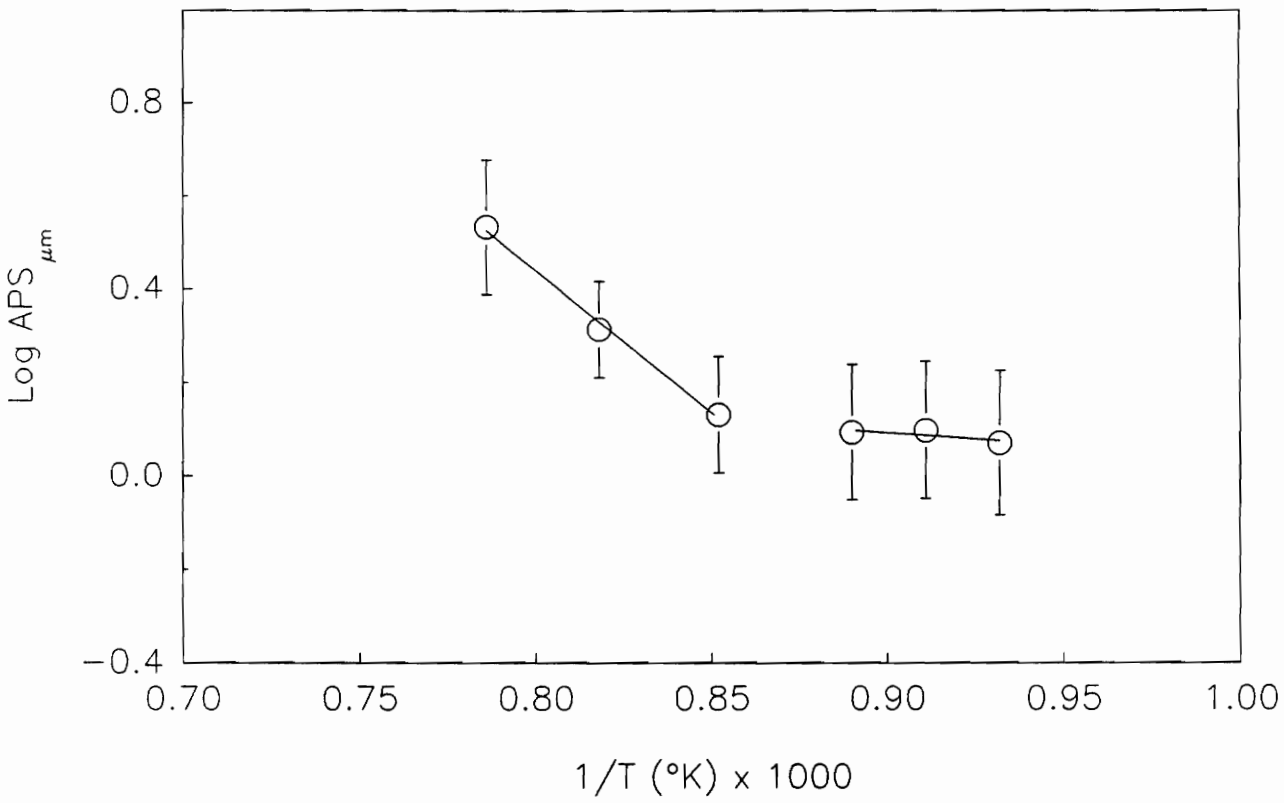

Figure 4.8 The relation between average particle size (APS) and formation temperature for 1hour of reaction and with 10 ml.% excess PbO in the starting oxide mixture.

The effects of flux/oxide ratio and the composition of the flux (NaCl/KCl) on the morphology of PFN powders in molten salt system are shown in Figures 4.9 and 4.10. It is evident that the particle sizes decreased with increasing flux/oxide ratio (Figure 4.9). This can be attributed to the increased distances for the constituent oxides (Fe_2O_3 and PbO) to diffuse to the surfaces of $Pb_3Nb_4O_{13}$ particles due to the increasing amount of flux. The growth rate of PFN particles also decreased by increasing this ratio. However, the particle sizes of PFN were insensitive to the composition of flux as compared to the flux/oxide ratio (Figure 4.10).

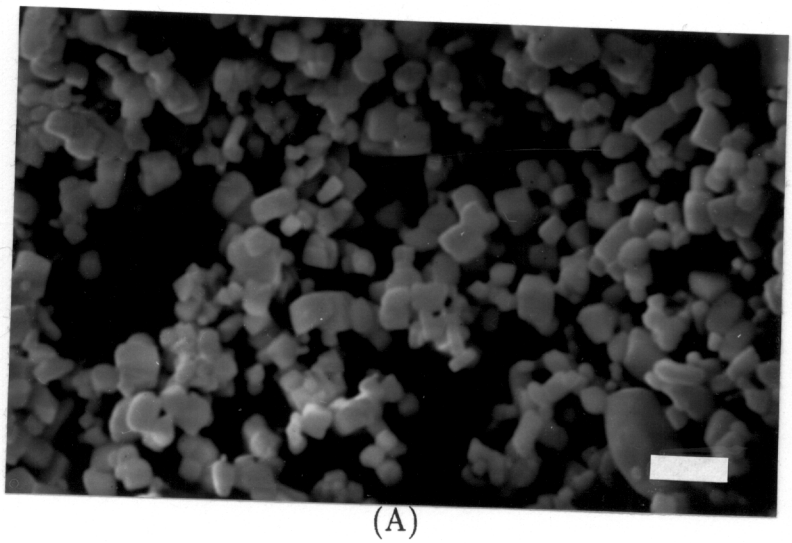

(A)

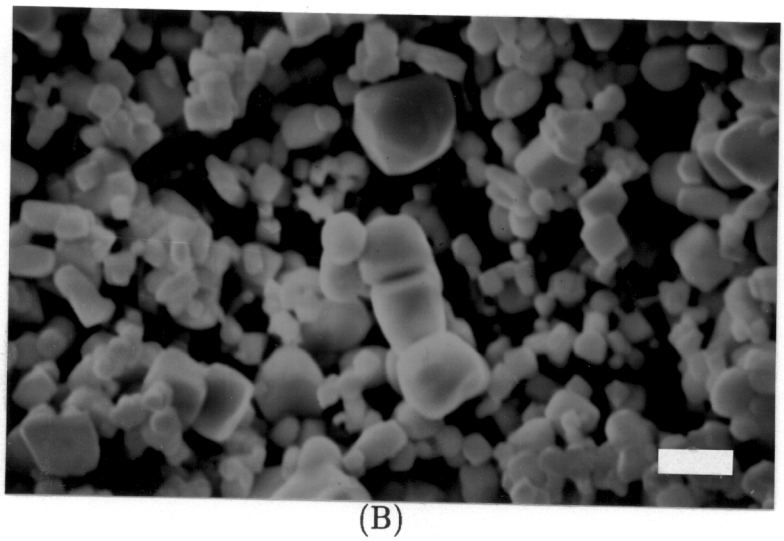

(B)

Figure 4.9 The SEM micrographs of PFN powders with different flux/oxides ratio; flux/oxides (A)= 4 (B)= 2 (C)= 0.5. The fabrication condition is 800^{0}C for 1 hour with 10 mol.% excess PbO. (Bar = 2μm)

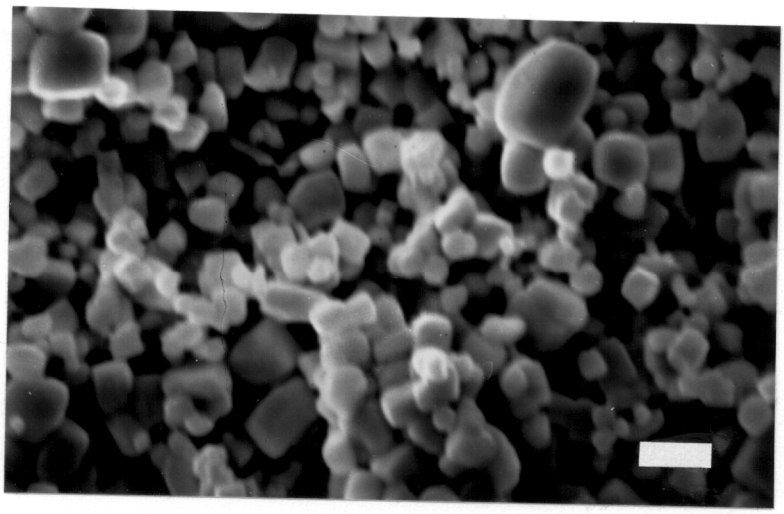

(C)

Figure 4.9 (Continued)

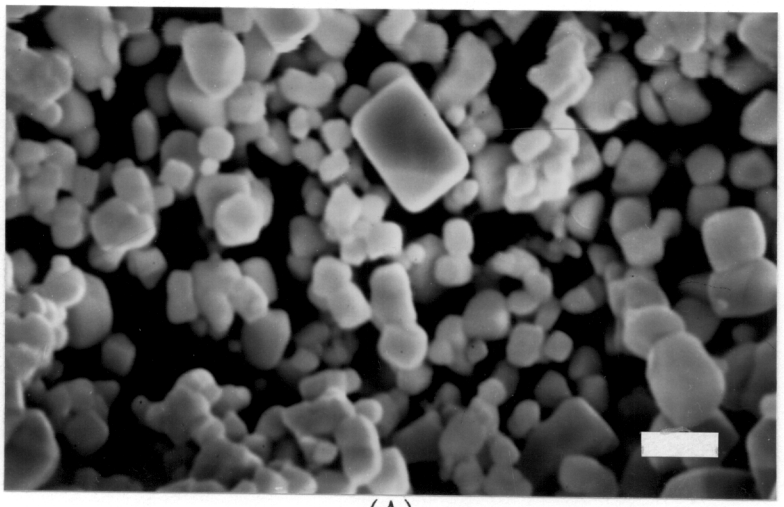

(A)

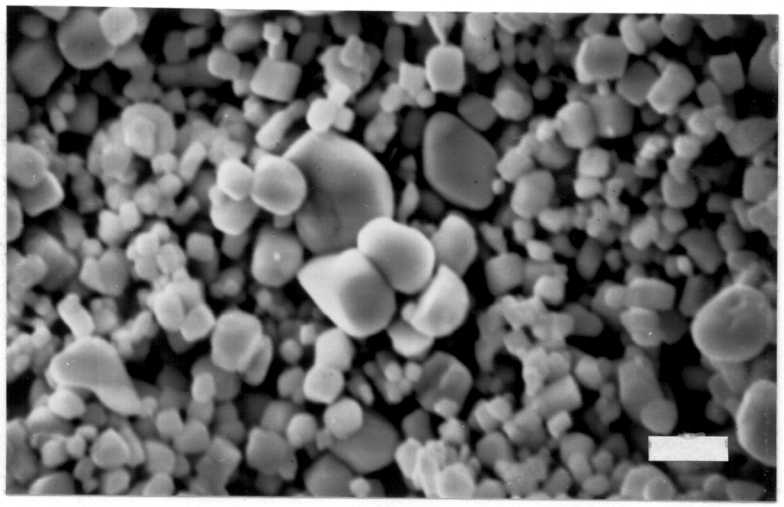

(B)

Figure 4.10 The SEM micrographs of PFN powders with different flux composition; NaCl (A)= 16.5% (B)= 33.5% (C) 67.5% (D) 83.5%. The fabrication condition is the same as Fig. 4.9. (Bar = 2μm)

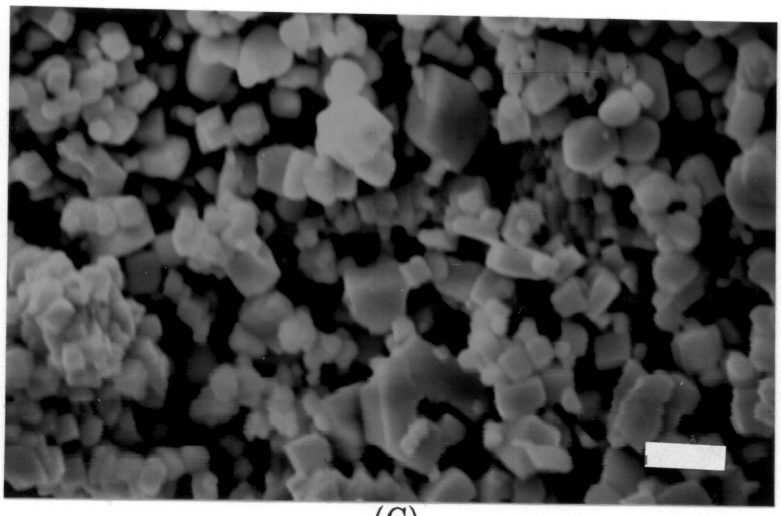

(C)

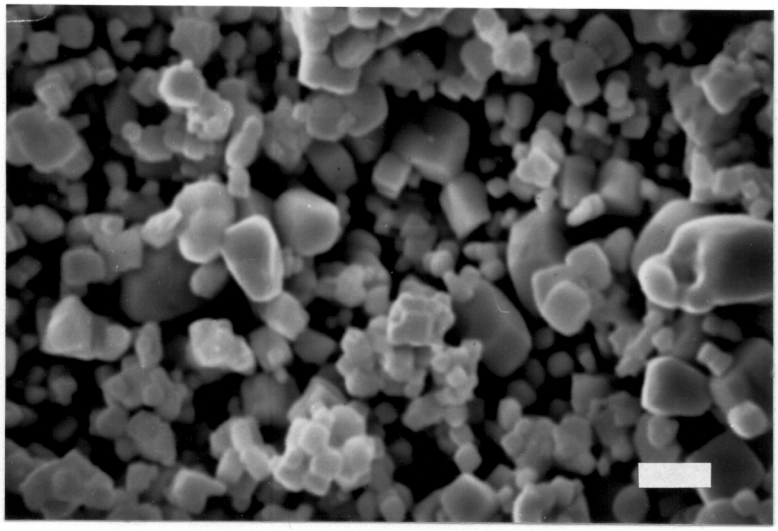

(D)

Figure 4.10 (continued)

4.2 Sintering and Microstructure Characterization of the PFN Powders

It has been demonstrated that pure PFN powders can be prepared at lower temperatures and shorter times in molten salts in comparison to the solid–state methods. However, as shown in Figure 4.5, the morphology and particle sizes of PFN powders prepared by molten salt synthesis are different from those of the powders prepared from solid–state methods. Since these two factors can have significant effect on the sinterability, grain growth as well as the dielectric properties, the following sections are going to discuss these characteristics. The effects of additives such as PbO and Li_2CO_3 on these characteristics will also be discussed.

4.2.1 Sinterability of pure PFN powders

Figure 4.11 shows the density, in terms of percentage of theoretical density (8.456 g/cm^3), of the sintered PFN pellets as a function of sintering time at various temperatures. PFN powders with an average particle size of 1.3μm, prepared at 800^{0}C for 1 hour using 10 mole% excess lead oxide were used in the starting composition. For the investigated sintering temperatures, it was seen that the densities seemed to be independent of the sintering times. However, increasing the sintering temperature resulted in a increase of the density of the pellets except for the higher sintering temperatures (*e.g.* 1050^{0}C and 1100^{0}C).

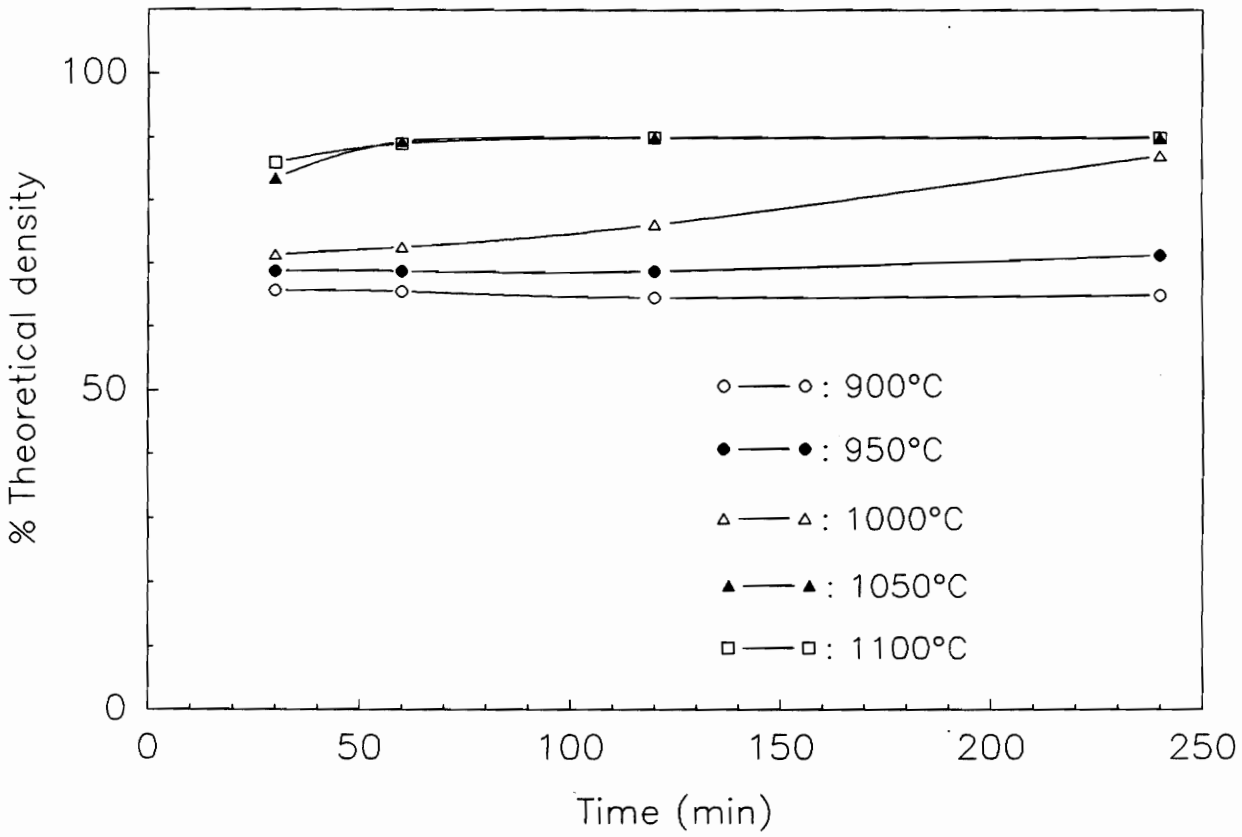

Figure 4.11 The densities of sintered pure PFN pellets as a function of time for various temperatures.

4.2.2 PFN powders with lead oxide additive

Owing to the volatile nature of lead oxide, it is not advisable to sinter $Pb(B'_xB''_{1-x})O_3$ ceramics at high temperatures (e.g. 1000^0C), unless measures are taken for minimizing the loss PbO. In addition the loss of lead oxide, this may lead to an increase in the amount of the pyrochlore phase in as–sintered pellets because of the reverse reaction of Reaction 4.5. In order to increase the as–sintered densities, excess lead oxide was added to serve as a densification aid and to displace Reaction 4.5 towards the right [60,61]. Figure 4.12 shows the effect of lead oxide additive on the densification of PFN powders in the range 900^0C to 1000^0C for 4 hours. From Figure 4.12, it is evident that for a given sintering temperature the density of PFN increased, as expected, with increasing the amount of PbO additive. It can also be observed from Figure 4.12 that the rate of density increase with the amount of PbO additive is higher for temperatures 900^0C to 950^0C as compared to 1000^0C. The phase diagram for PbO and PFN was presented in Figure 4.13, which clearly shows the absence any compound formation [62]. Based on this, one can neglect reactive liquid sintering process for accounting the affects of PbO additive on PFN density. The higher densification rate of PFN in presence of PbO additive can be clearly attributed to capillary forces exerted by liquid PbO. It should be noted that the melting point of lead oxide is 889^0C. SEM micrographs, corresponding to the sintering condition of 1000^0C for 4 hours with the excess lead oxide varying from 0 to 2.0 wt%, are shown in Figure 4.14. It can be clearly seen that the grain size increased and the pores were eliminated with increasing amount of lead oxide. When the sintering temperature and time were increased to 1100^0C and 12 hours, respectively, the densities were almost independent of the amount of

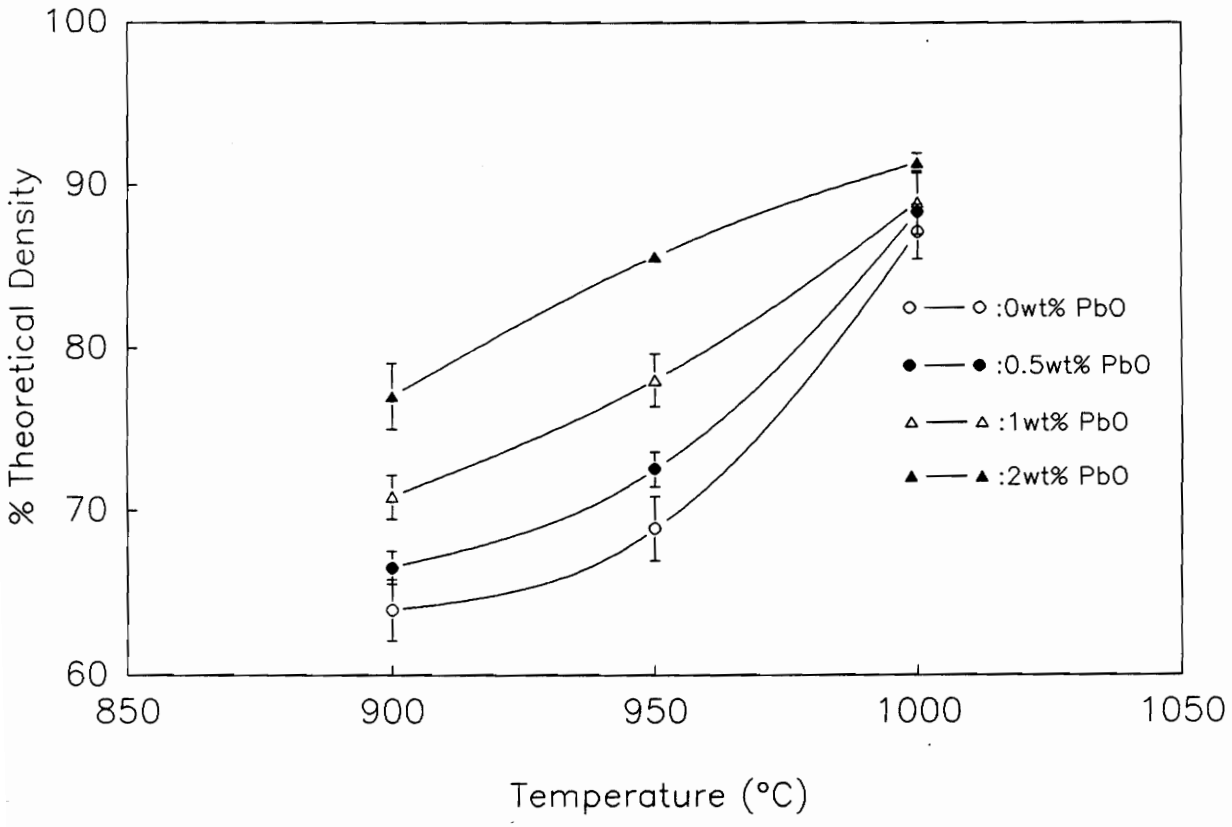

Figure 4.12 The effect of PbO additions on the densification of PFN sintered for 4 hours at the temperature range from 900°C to 1000°C.

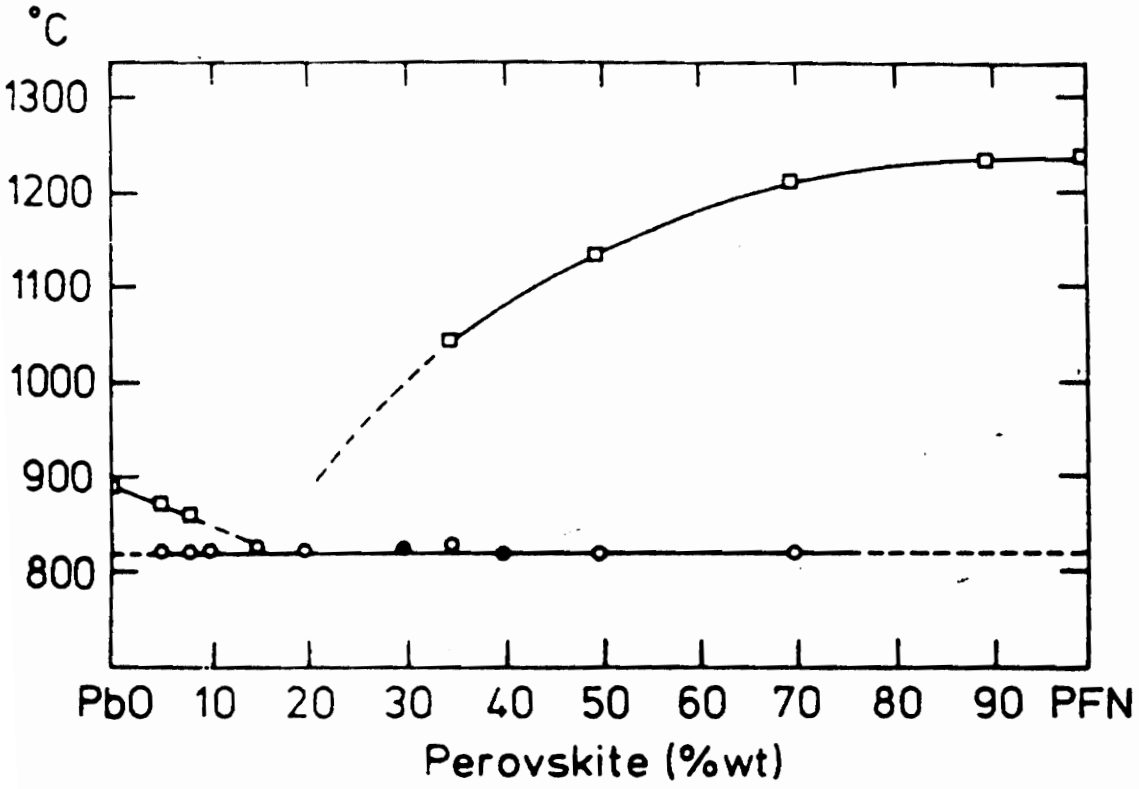

Figure 4.13 The PbO–PFN pseduobinary phase diagram[62].

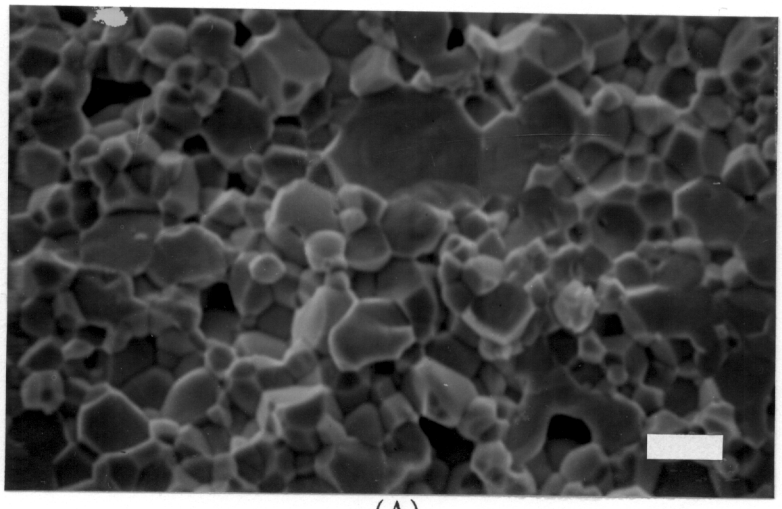

(A)

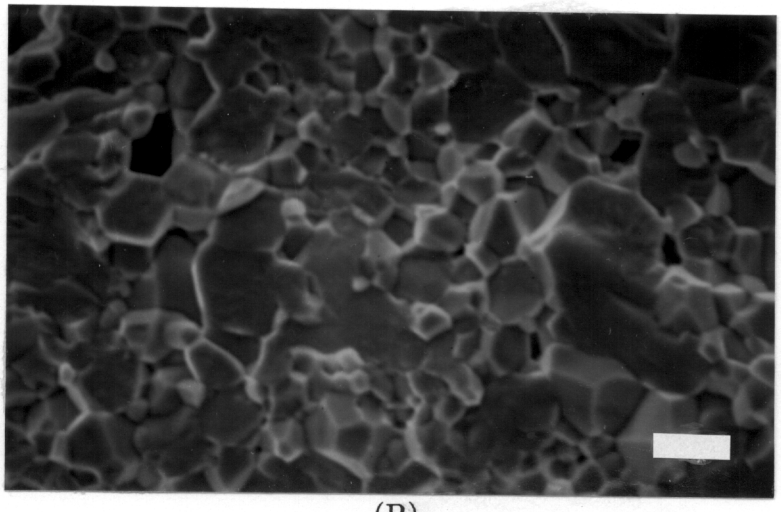

(B)

Figure 4.14 Microstructure of PFN sintered at 1000^{0}C for 4 hr. with various amount of PbO addition: (A) 0wt%, (B) 0.5wt% (C) 1.0wt% (D) 2.0wt%. (Bar = 2μm)

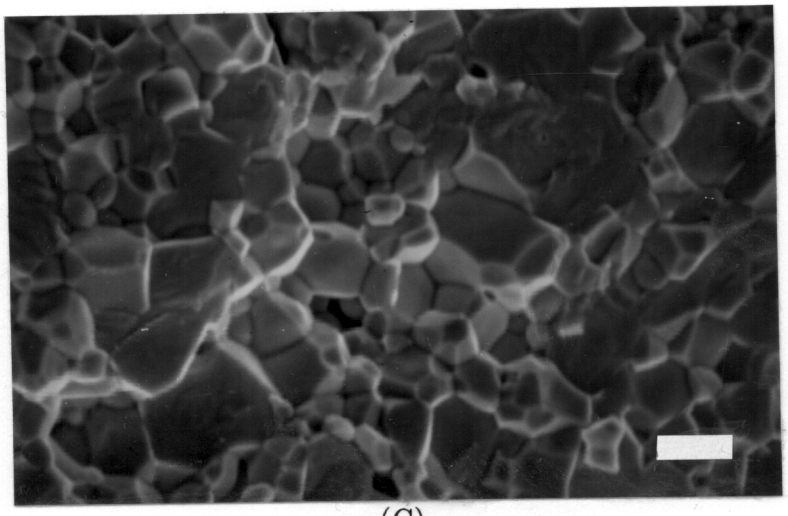

(C)

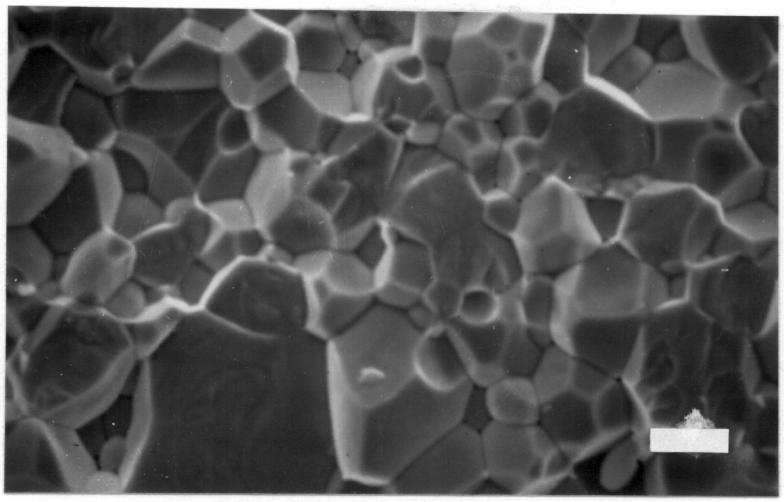

(D)

Figure 4.14 (Continued)

lead oxide addition (Figure 4.15). Microstructures, shown in Figure 4.16, depict that the grain size did not increase with increasing amount of lead oxide addition. This indicated that the liquid phase sintering is less probable at higher sintering temperatures due to the volatile nature of lead oxide.

4.2.3 PFN powders with Li_2CO_3 additive

Figure 4.17 depicts the effect of Li_2CO_3 addition on the densification nature of PFN. In contrast to the results for the addition of lead oxide, as–sintered PFN densities decreased with increasing the amount of Li_2CO_3 addition. It can also be noted that in the case of Li_2CO_3 addition, sintering temperature had very small effect on the PFN sintered density.

The average grain size for PFN samples for various sintering temperatures is plotted as a function of the amount of Li_2CO_3 additive in Figure 4.18. The grain size increased with increasing sintering temperature for a fixed amount of Li_2CO_3 additive (Figure 4.18). In contrast to the effect of sintering temperature, the grain size increased very rapidly with small amounts Li_2CO_3 addition, but later decreased with further increase in the amount of Li_2CO_3. The grain size was largest for 0.5 wt% Li_2CO_3 addition. For a given sintering temperature and time, the grain sizes of PFN with Li_2CO_3 additions are significantly larger than those of pure PFN and PFN with lead oxide addition (Table 4.2).

In general, in oxides like PFN the grain growth is controlled by the diffusion coefficient of oxygen. One way to increase the diffusion constant of oxygen is to

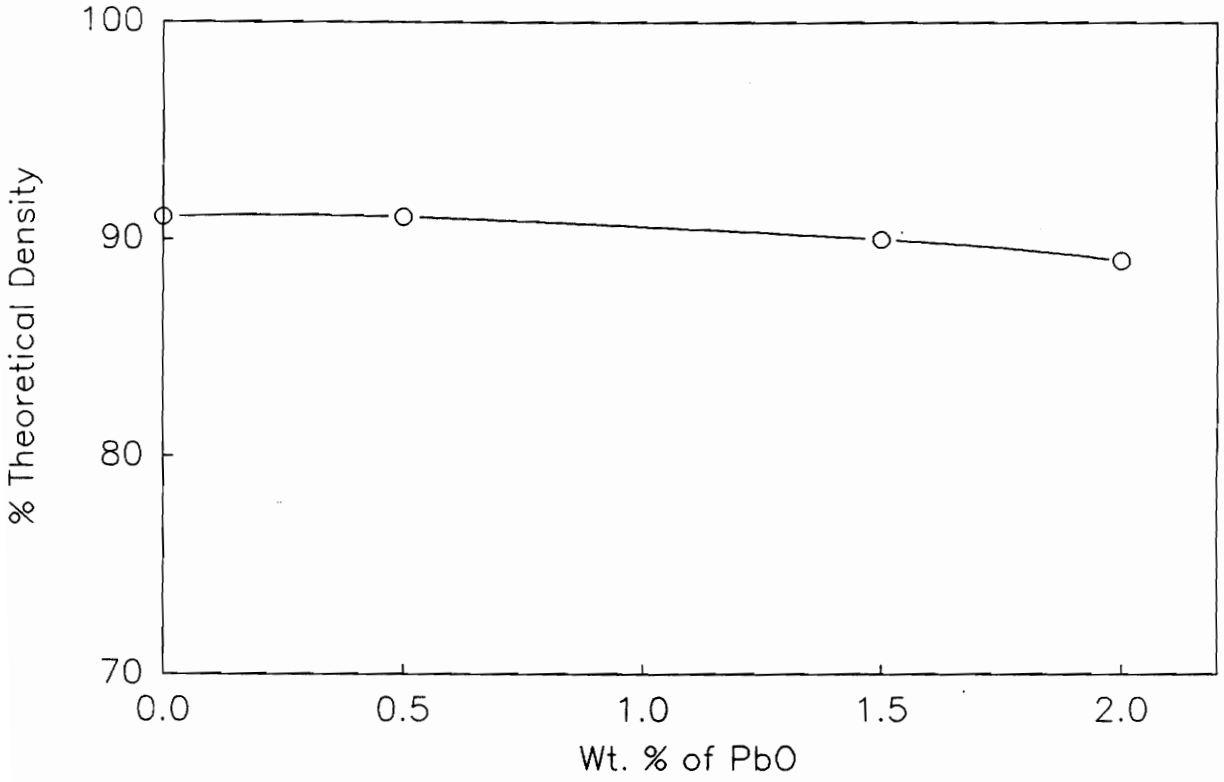

Figure 4.15 The densities of PFN sintered at 1100°C for 12 hrs. with various amount of PbO.

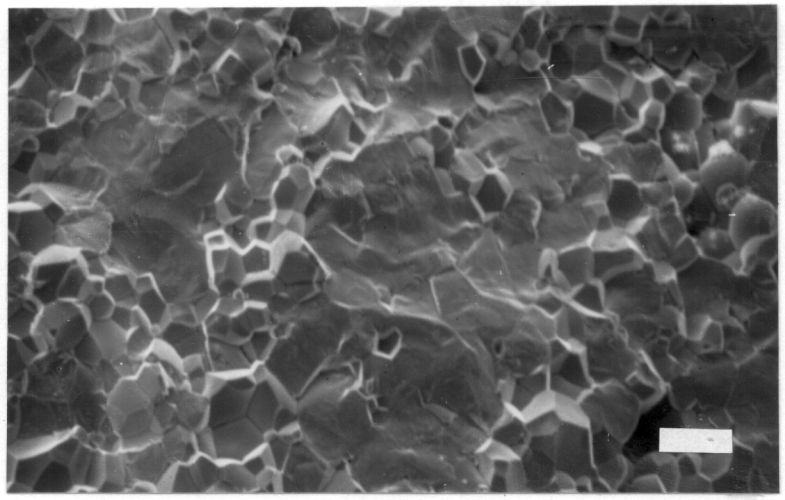

(A)

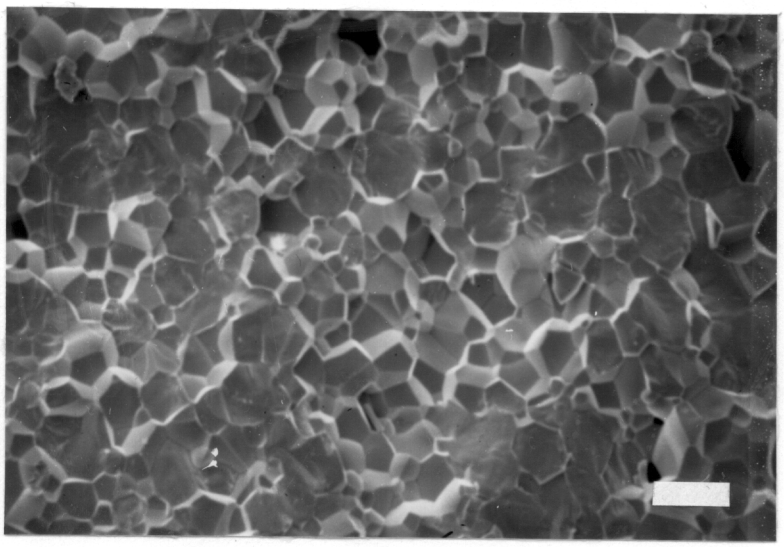

(B)

Figure 4.16 Microstructure of PFN sintered at 1100^{0}C for 12 hrs. with various amount of PbO: (A) 0wt% (B) 0.5wt% (C) 1.0wt%. (Bar = 10μm)

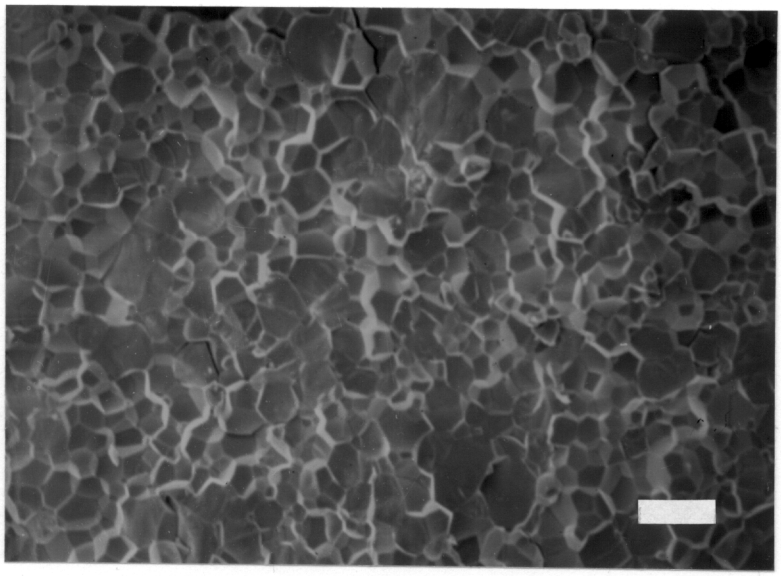

(C)

Figure 4.16 (Continued)

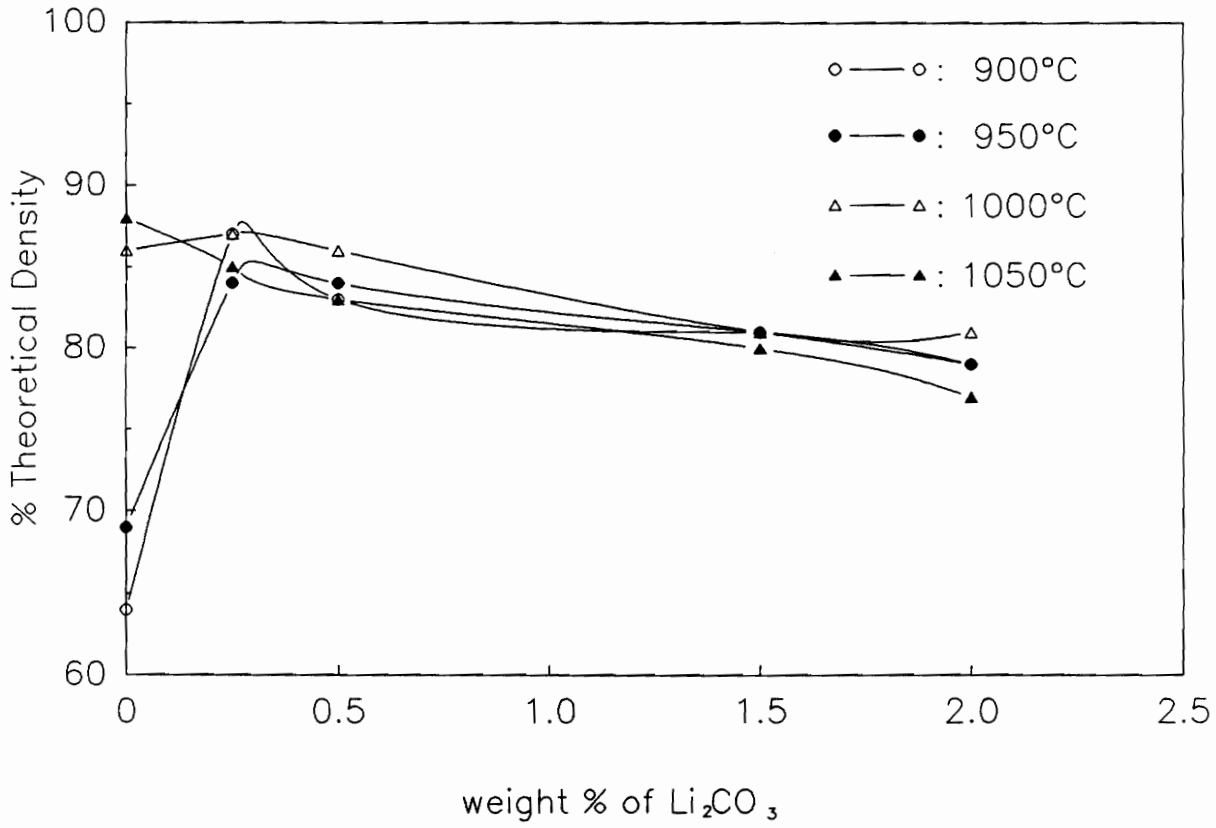

Figure 4.17 The effect of Li_2CO_3 on the densities of PFN sintered at various temperatures for 4 hrs.

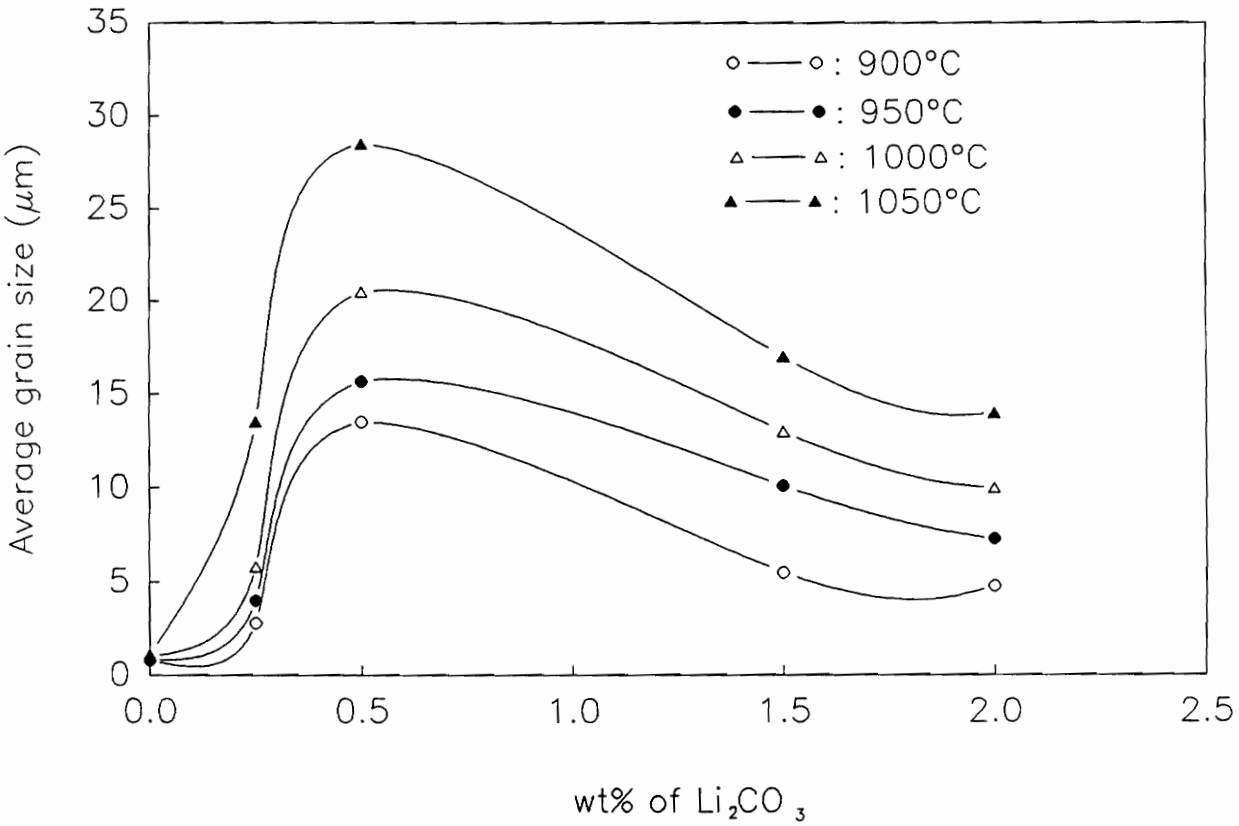

Figure 4.18 The effect of Li_2CO_3 on the grain sizes of PFN sintered for 4 hrs.

Table 4.2 Average grain size for different PFN composition sintered at 1000°C for 4 hours

composition	grain size
PFN	1.0μm
PFN + 2.0 wt% PbO	2.0μm
PFN + 0.5 wt% Li_2CO_3	20μm

increase the oxygen vacancy concentration (Equation 4.8).

$$D_0 = D_k [V_{\ddot{O}}] \exp(-E_a/kT) \quad (4.8)$$

Lattice parameter studies and compositional analysis (Section 4.3.3) indicated that Li^+ ions ($\simeq$ 2 wt% Li_2CO_3) substitute for Fe^{3+} in PFN. In other words, for every two substituted Li^+ ions one oxygen vacancy is generated (Equation 4.9).

$$Li_2O \xrightarrow{Fe_2O_3} 2Li_{Fe}'' + V_{\ddot{O}} + \frac{1}{2} O_2 + 2h^{\cdot} \quad (4.9)$$

Thus, the addition of Li_2CO_3 increases the oxygen vacancy concentration, which in turn increases the oxygen diffusion constant and enhances the grain growth rate.

As seen from the SEM micrographs of PFN with Li_2CO_3 additions (Figure 4.19), the second phase started to appear when the amount of Li_2CO_3 additive was 0.5 wt%. This indicates that the solubility of Li_2O in PFN is lower than 0.5 wt% Li_2CO_3. For Li_2CO_3 amounts greater than or equal to 0.5wt%, liquid phase sintering can also contribute to the densification of PFN (the melting point of Li_2CO_3 is 723^{0}C) . The contribution of liquid phase sintering coupled with the solubility limit of Li^+ can account for the decrease in the grain size for Li_2CO_3 additions greater than 0.5wt%. Loss of Li_2CO_3 by evaporation from the liquid at grain boundaries is also possible. This Li_2CO_3 loss can leave pores behind and thus, can reduce the density (Figure 4.17).

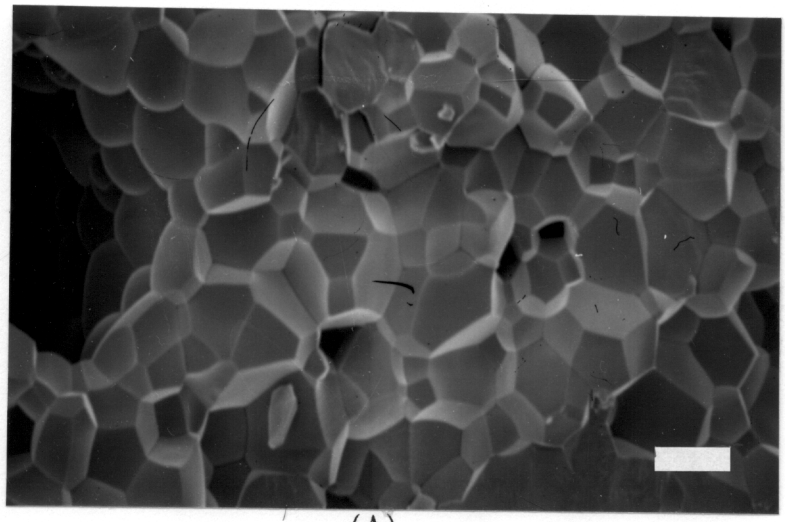

(A)

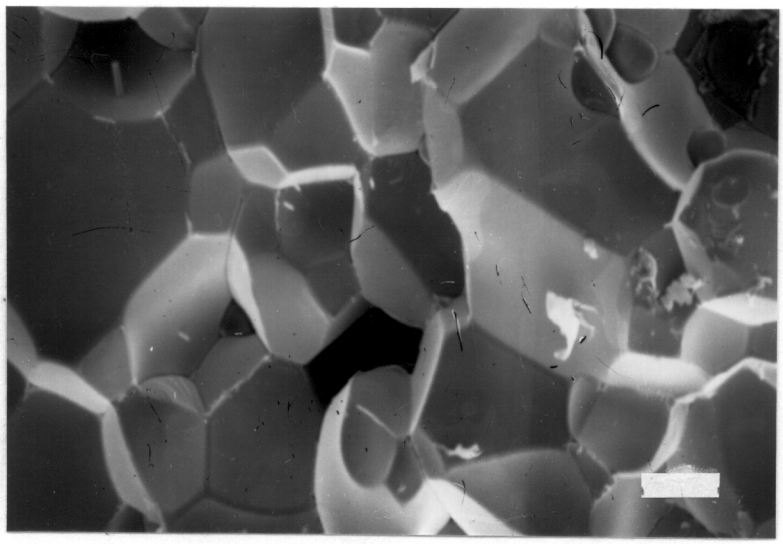

(B)

Figure 4.19 Microstructure of PFN with (A) 0.25wt% (b) 0.5wt% (C) 1.5wt% (D) 2.0wt% of Li_2CO_3. (Bar = 10μm)

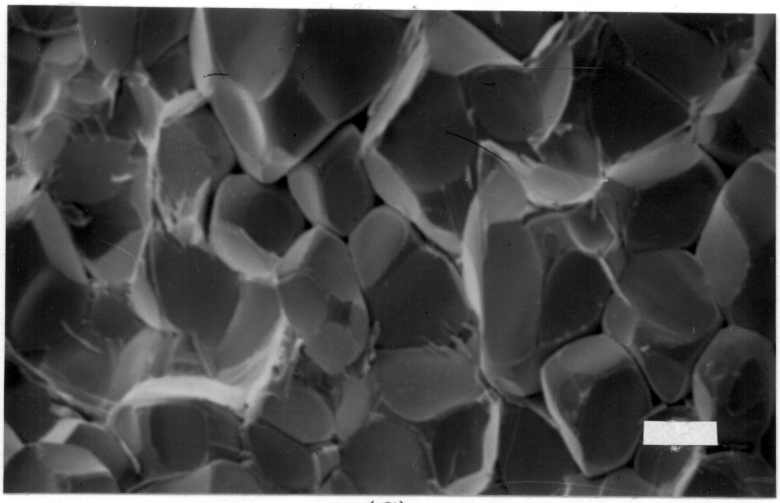

(C)

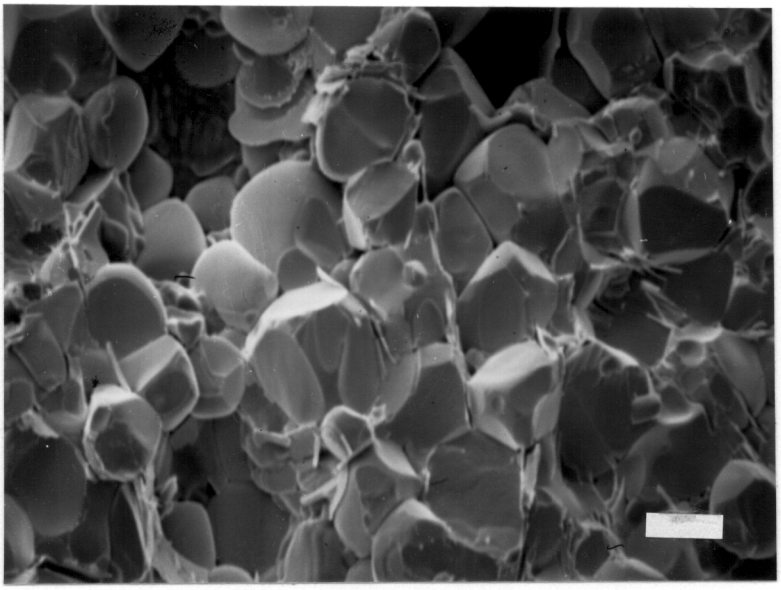

(D)

Figure 4.19 (Continued)

4.3 Dielectric properties

4.3.1 Dielectric properties of pure PFN powders

Table 4.3 shows the dielectric properties and the densities as a function of the firing conditions for pure PFN and PFN with PbO addition. As can be seen from Table 4.3 the dielectric constants were dependent upon the sintering conditions. In this study, for pure PFN the dielectric constant at 1 MHz varied from 1980 to 12270 when the sintering conditions are changed from 950^{0}C/4 hours to 1100^{0}C/13 hours. Further increase in the sintering time (e.g., 15 hours) at higher temperatures (1100^{0}C) led to the formation of $Pb_3Nb_4O_{13}$ and lowered the value of dielectric constant (3000). The sintered density of pure PFN varied from 60% to 92% of the theoretical density when the sintering conditions are changed from 950^{0}C/4 hours to 1100^{0}C/13 hours. Since the sintered density is not 100% of theoretical density, the effect of porosity need to be included in interpreting the properties of PFN. This requires the consideration of dielectric properties of mixtures. A general empirical relationship, mixture rule [46, 63], was applied:

$$k^n = \Sigma\, v_i k_i^n \qquad (4.10)$$

where n is a constant, and v_i and k_i are the volume fraction and dielectric constant of phase i, respectively. When n = –1, the structure of the mixture corresponds to the capacitive elements in series, and their inverse capacitances are additive. Then for phase 1 and 2, the effective dielectric constant ",K'," is given by:

Table 4.3 Dielectric Properties as a Function of Firing Condition for Pure PFN and PFN with lead oxide addition

Composition	Firing Condition	Density* (%theor)	T_c(°C)	Dielectric properties #	
				$K_{(max)}$	tanδ(%)
PFN	950°C/4h	68	100	1980	–
PFN	1000°C/4h	86	104	4280	3.2
PFN	1100°C/30m	85.5	95	3771	3.2
PFN	1100°C/1h	89	100	6009	3.4
PFN	1100°C/2h	89.5	100	6464	4.0
PFN	1100°C/4h	90	97	8260	4.8
PFN	1100°C/9h	90	100	7500	10.2
PFN	1100°C/12h	91	100	10000	13.1
PFN	1100°C/13h	92	96	12270	7.8
PFN**	1100°C/15h	87	108	3000	23.2
0.5wt%PbO	1000°C/4h	88	104	3910	6.6
1.0wt%PbO	1000°C/4h	89	110	4100	5.6
2.0wt%PbO	1000°C/4h	91	110	4630	8.4
0.5wt%PbO	1100°C/12h	91	101	7500	7.9
1.0wt%PbO	1100°C/12h	90	105	5600	7.1
2.0wt%PbO	1100°C/12h	89	110	3750	8.1

*Theo. Density of PFN = 8.456 g/cm^3

** Two–phase mixture: PFN + $Pb_3Nb_4O_{13}$

Measured at the frequency of 1MHz

$$1/k' = (v_1/k_1') + (v_2/k_2') \tag{4.11}$$

In contrast, when n=1, the structure corresponds to capacitive elements parallel to each other and therefore the applied field is similar for each element making the capacitances additive:

$$k' = v_1k_1' + v_2k_2' \tag{4.12}$$

As n approaches zero, k^n equals 1 + n*log*k, and we have the so called logarithmic mixture rule:

$$log k = \Sigma v_i log k_i \tag{4.13}$$

This rule gives a valve intermediate between the two extremes n = 1 and n = −1.

Figure 4.20 depicts the comparison between the experimental data and the prediction from the empirical mixture rule for pure PFN sintered at different conditions. Since the permittivity of air (or pore) can be treated as unity, Equation 4.10 becomes

$$k^n = V_{pfn}k_{pfn}^n + V_{air} \tag{4.14}$$

A reasonable empirical fitting was obtained for the n value of 0.2, and the k_{pfn} value of 14,900 was obtained, which agrees very closely with the dielectric constant of well sintered PFN [22,27,49]. For comparison, the predicted curves for n = 0.4

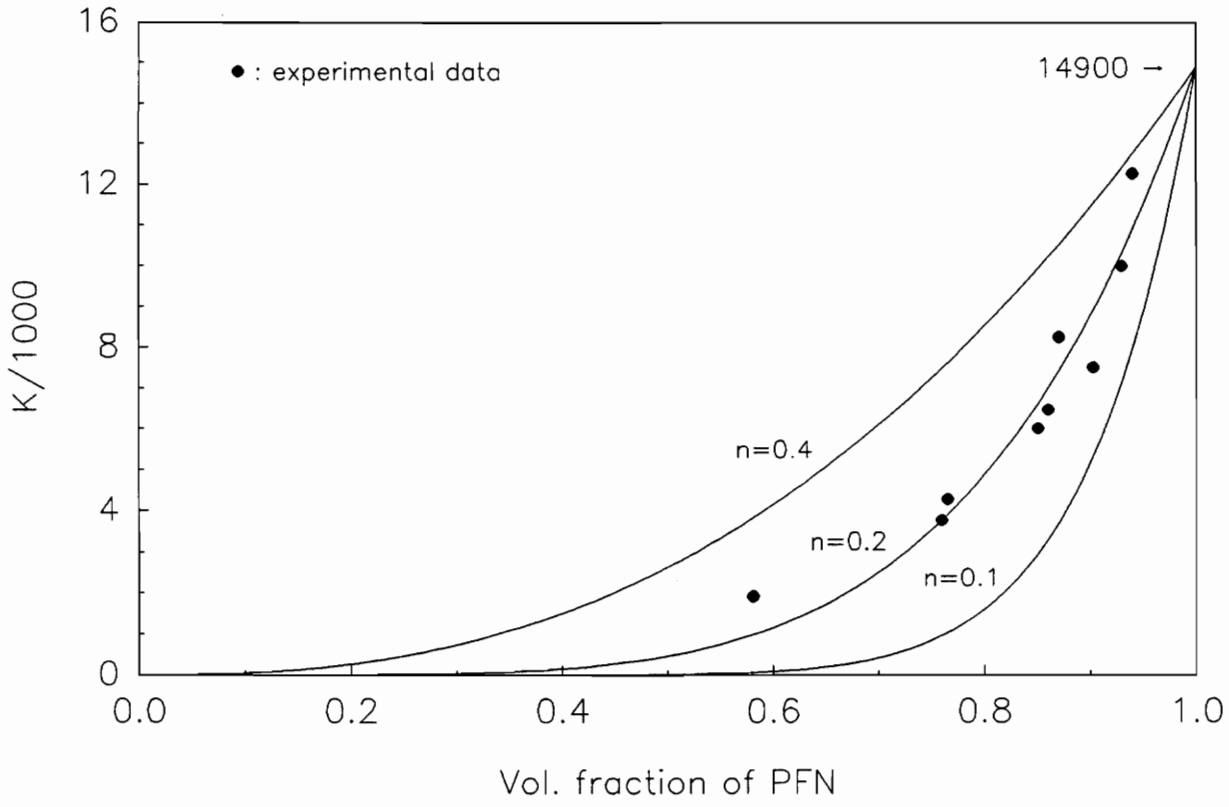

Figure 4.20 Comparison of experimental data with theoretical expressions of Mixture rule for permittivity of PFN–Air diphasic mixtures.

and n = 0.1 are also included in the Figure 4.20.

For pure PFN powders, sintered at 1100^{0}C for 13 hours, the variation of the relative dielectric constant (k) and dielectric loss factor (tanδ) as a function of temperature and frequency, are shown in Figure 4.21. It is evident from Figure 4.21 that the dielectric constant increased with decreasing frequency. In contrast, the dielectric loss did not show any systematic frequency dependence. At Curie point, the dielectric constant increased significantly with decreasing frequency. For low frequencies (0.1 kHz), the dielectric loss in the paraelectric region increased very rapidly with increasing temperature. The temperature at which the maximum dielectric constant is observed (Curie point) moved to higher temperatures with increasing the applied field frequency. The curve in Figure 4.21(A), which exhibits broad ferroelectric–paraelectric phase transition is a characteristic of "relaxor" ferroelectrics. The broad peak transition can be explained by the existence of fluctuations in composition throughout the material, which are attributed to a statistical inhomogeneity in the distribution of Fe^{+3} and Nb^{+5} ions in octahedral sites [64]. The microregions within a grain having different chemical compositions can have different Curie temperatures. Thus, the observed broad peaks can be viewed as the superposition of many individual peak associated with these regions having different Curie temperatures.

Figure 4.22 depicts the specific heat of sintered PFN powders as a function of temperature, and shows an endothermic reaction with small amount of latent heat around the Curie temperature region. This endothermic reaction was also reported by Brunskill et al for single crystal PFN [30]. The small amount of latent heat is

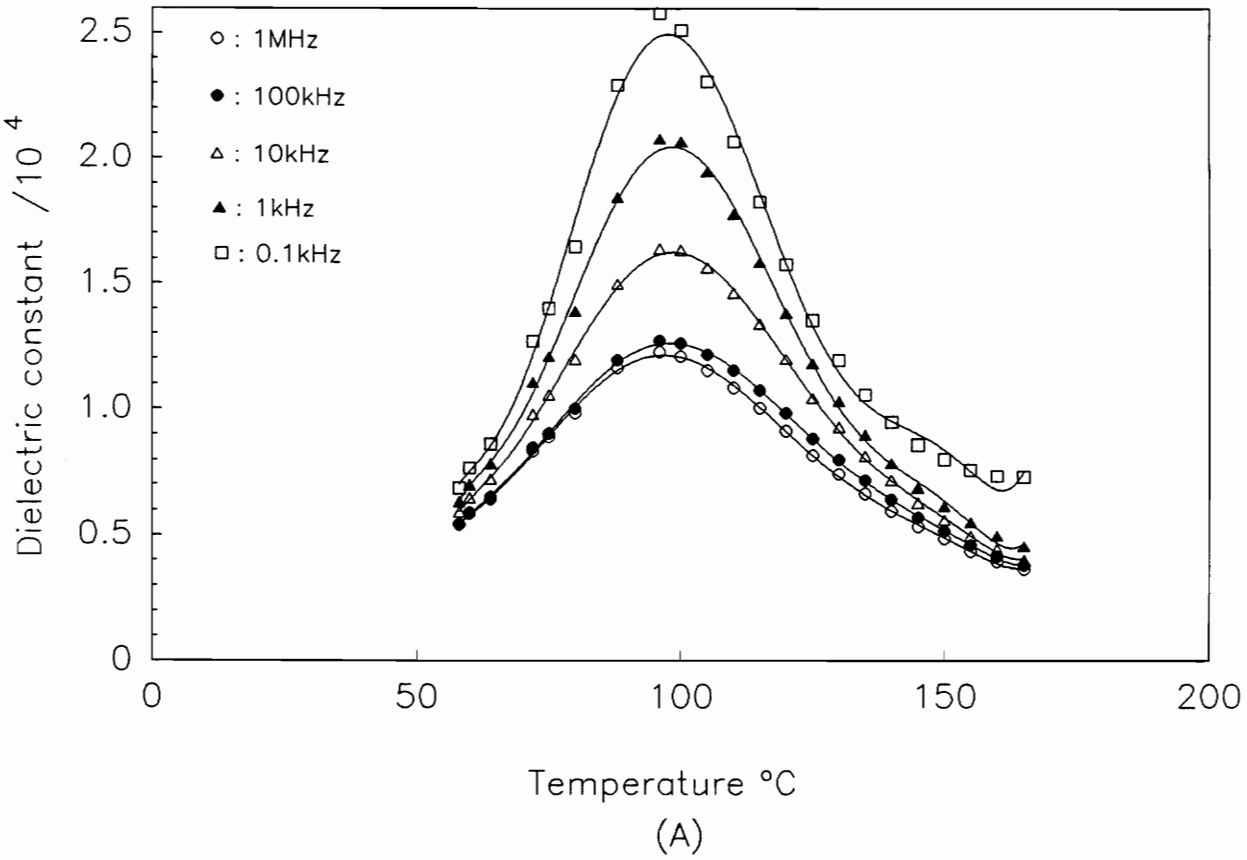

Figure 4.21 Dielectric constant (A), and dielectric loss (B) as a function of temperature for pure PFN sintered at 1100°C for 13 hours.

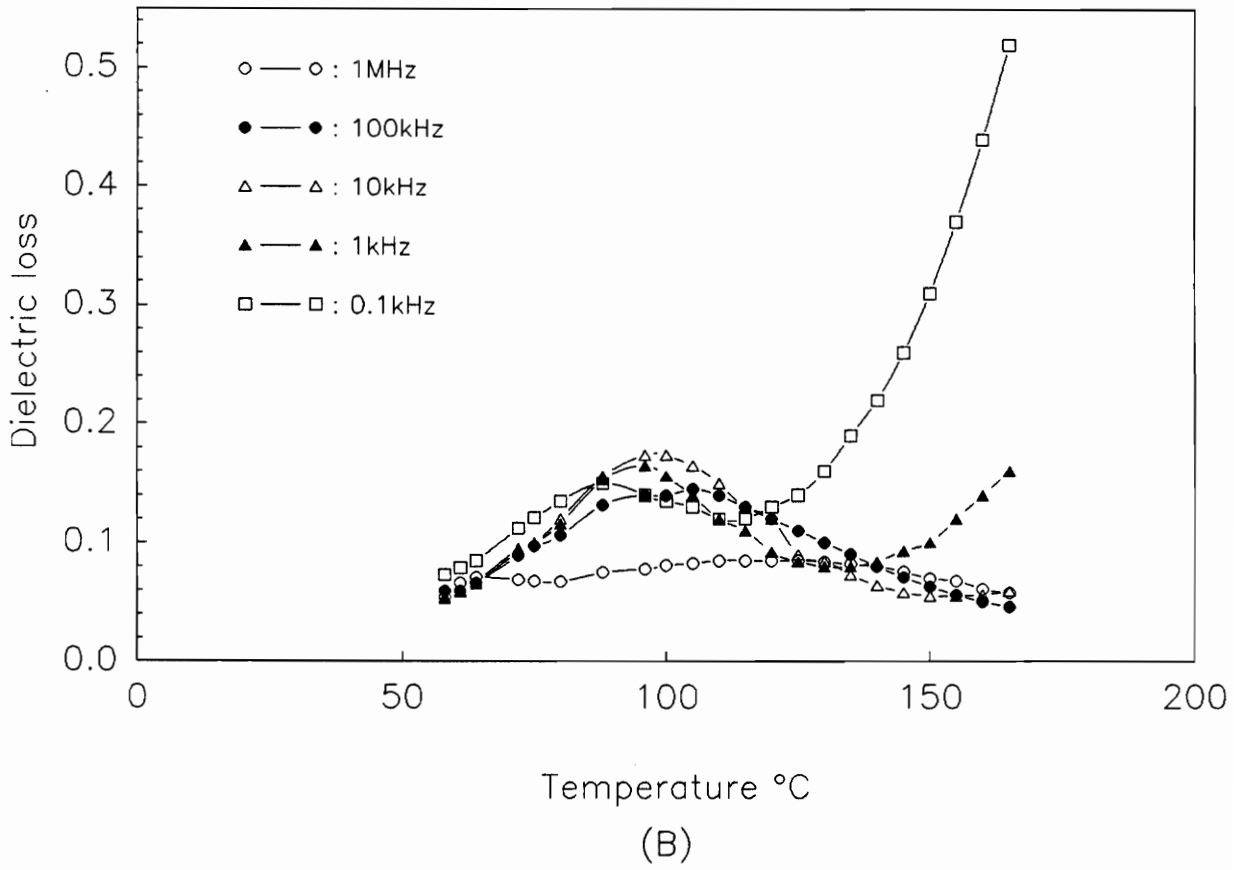

Figure 4.21 (Continued)

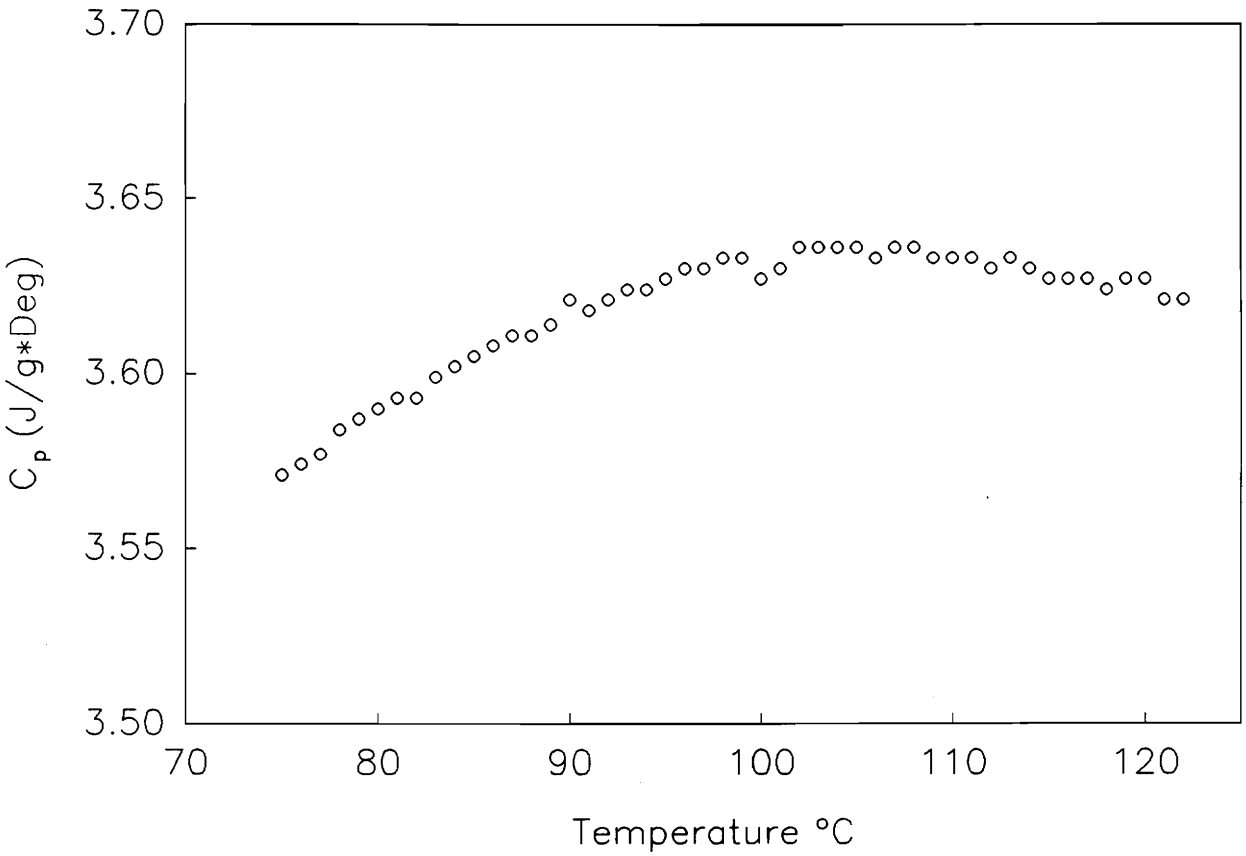

Figure 4.22 Specific heat (C_P) as a function of temperature.

believed to originate from the slow change in spontaneous polarization over the Curie temperature region. This broad transition peak was also reported by Strenger for the disordered $Pb(Sc_{0.5}Ta_{0.5})O_3$ ceramics [51].

4.3.2 Dielectric properties of PFN with PbO additive

As mentioned above, lead oxide served as a densification aid in sintering PFN and increased the as–sintered densities by reducing the volume fraction of porosity. Because of this and according to Equation 4.7, the dielectric constant of the as–sintered pellets should increase as a result of the addition of lead oxide. This expected increase in dielectric constant due to the reduction in porosity was seen for pure PFN (Section 4.3.1) and also was reported for $Pb(Mg_{0.33}Nb_{0.67})O_3$ ceramics [61]. However, for PFN, as shown in Figure 4.23, the dielectric constant depending on the sintering conditions either decreased (1100^{0}C/12 h) or stayed almost constant (1000^{0}C/4 h) with increasing amount lead oxide addition.

The decrease in the value of dielectric constant with increasing excess amount of lead oxide, for samples sintered at 1100^{0}C/12 h, can be attributed to the presence of a low dielectric constant ($k \simeq 20$) amorphous or partially amorphous PbO–rich grain boundary phase. Such phases, in fact, have been identified in $Pb(Mg_{0.33}Nb_{0.67})O_3$ (PMN) [65,66] and $Pb(Sc_{0.5}Ta_{0.5})O_3$ (PST) [67] ceramics by using transmission electron microscopy (TEM). Barber et al [68] proposed a mechanism for the early entrapment of lead oxide at grain boundaries and within pores during the early stage sintering. Such phases, which are believed to be mechanically weak, give rise to intergranular fracture [1], which was in fact

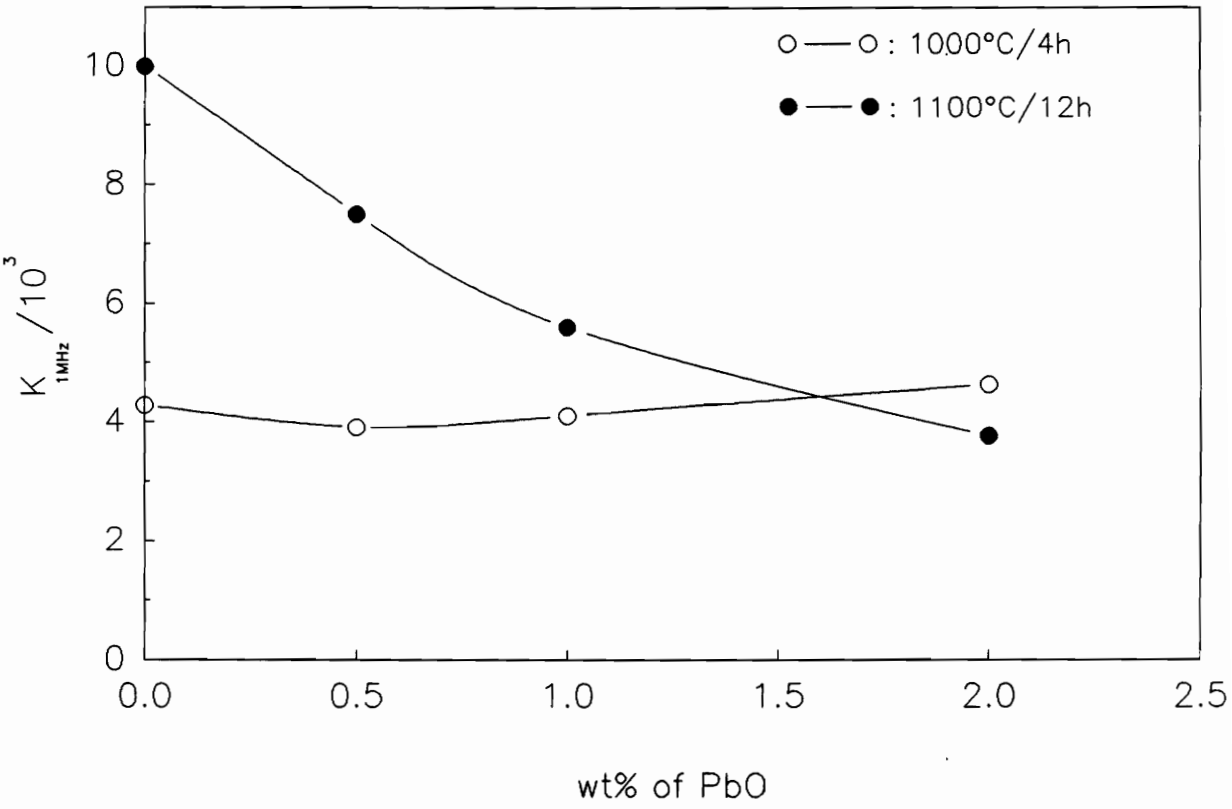

Figure 4.23 The effect of PbO additions on dielectric constant of PFN.

observed for our samples (Figure 4.16). The pure PFN showed partial intergranular fracture ($\simeq$ 50%) as compared to the PFN with 1 wt% PbO additive, where in the intergranular fracture ($\simeq$ 94%) dominated. Although the grain boundary phase was present in relatively small volume fraction, because of its very low dielectric constant it prevented the achievement of optimum dielectric properties [65].

For samples sintered at 1000^{0}C for 4 hours (Figure 4.23), the two factors increased density and the formation of PbO–rich grain boundary phase might have compensated each other. Since the additions of lead oxide had little effect on the density of the as–sintered samples for sintering conditions of 1100^{0}C for 12 hours, the dielectric constants was governed by the grain boundary phase.

4.3.3 Dielectric properties of PFN with Li_2CO_3 additives

The dielectric properties of sintered PFN with Li_2CO_3 additions are summarized in Table 4.4. For the specimens sintered for four hours at various temperatures, the dielectric constant values, measured at 1 MHz, were plotted in Figure 4.24 as a function of the amount of Li_2CO_3 additive. In general, as shown in Figure 4.24, the dielectric constant increased with increasing sintering temperature, and an optimum dielectric constant (14,000) is achieved for specimens sintered at 1000^{0}C with 1.5 wt% Li_2CO_3 additive. It is interesting to note that for pure PFN specimens 12,270 is the highest dielectric constant that was obtained, which required sintering conditions of 1100^{0}C/13 h. In contrast, a dielectric constant value of 14,000 was obtained at sintering conditions of 1000^{0}C/4 h for PFN specimens with 1.5 wt% Li_2CO_3. The smaller values of the dielectric constant for

Table 4.4 Dielectric Properties of PFN as a Function of Firing Condition with Li_2CO_3 Addition

Composition x wt% Li_2CO_3	Firing Condition	Density (%Theor)	T_c(°C)	Dielectric Properties# $K_{(max)}$	tanδ(%)
0.25	900°C/4h	87	103	3760	5.3
0.5	900°C/4h	83	97	4910	5.5
1.5	900°C/4h	81	95	6960	5.4
2.0	900°C/4h	79	95	3800	4.9
0.25	950°C/4h	84	104	5450	7.5
0.5	950°C/4h	84	105	6330	4.8
1.5	950°C/4h	81	104	7300	8.4
2.0	950°C/4h	79	104	6970	8.1
0.25	1000°C/4h	87	104	10250	3.5
0.5	1000°C/4h	86	105	11000	1.9
1.5	1000°C/4h	81	96	14000	4.1
2.0	1000°C/4h	81	93	10150	4.4
0.25	1050°C/4h	85	106	10600	5.9
0.5	1050°C/4h	83	107	11900	5.7
1.5	1050°C/4h	80	106	11220	3.0
2.0	1050°C/4h	77	98	10020	3.0

: Measured at the Frequency of 1MHz

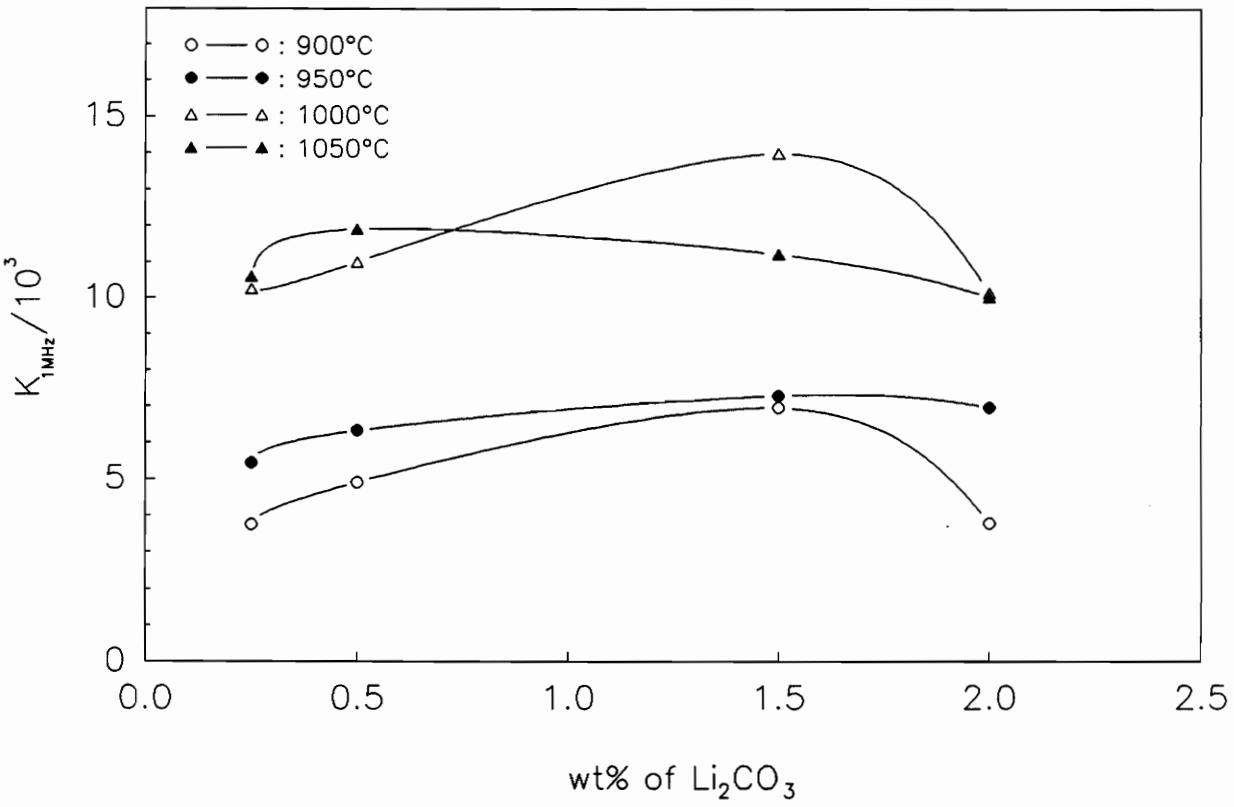

Figure 4.24 The effect of Li_2CO_3 on the dielectric constant of PFN.

the 0.25wt% Li_2CO_3 than those for 0.5wt% Li_2CO_3 might have been caused by the significant difference in grain sizes (Figure 4.18). A second phase formation was observed around each grain for the compositions $\geq$ 1.5 wt% Li_2CO_3 (Figure 4.19). Therefore, the dielectric constants for these compositions should be interpreted by two phase mixture rule. From the investigation of DC conductivities of these samples it was found that the conductivities of PFN specimens with Li_2CO_3 additives are much smaller than those of pure PFN samples, which indicated that grain–boundary phase might be a higher resistivity phase than the grain bulk. For such materials, the dielectric properties can be described in terms of an effective permittivity ",K_{ef},". According to Mauczok et al [69], K_{ef} can be expressed as:

$$K_{ef} = K_{ri}(d_a/d_i) \tag{4.15}$$

where K_{ri} is the relative permittivity of the insulating layer, d_a the average grain size, and d_i the thickness of the insulating layer. Thus, including the contributions from all the phases, the dielectric constant K of a sample can be expressed as:

$$K^n = V_{air} + V_{pfn}K_{ef}^n \tag{4.16}$$

by applying the mixture rule (Equation 4.10).

For the case of 1.5wt% Li_2CO_3 addition sintered at 1000^{0}C, the values of d_a and d_i might be optimum, and thus, resulted in the highest value of K_{ef}. The additions of Li_2CO_3 in excess of 1.5wt% resulted in a decrease in the dielectric constants, as shown in Figure 4.24, mainly due to the small grain sizes (d_a), small

densities as well as probably large thickness (d_i).

Table 4.5 shows the D.C. conductivity for PFN specimens with different compositions and and for different sintering conditions. Because of the insulating grain–boundary layers, the samples with Li_2CO_3 addition showed lower D.C. conductivities at 100^{0}C and 150^{0}C than those for PFN. However, the conductivity value was higher at room temperature due to the decreased as–sintered density. It can also be seen from Table 4.5 that PFN with lead oxide additions or for cases with lower density (PFN 1000^{0}C for 4 hours) exhibited much higher conductivity values.

The second phase observed on the surface of the samples of PFN with Li_2CO_3 as observed on the free surfaces of sintered samples is shown in Figure 4.25. The nature of this second phase could not be identified because its X–ray pattern did not closely match with any known phase. Energy dispersive X–ray analysis (Figure 4.25) showed that the second phase is highly enriched with iron. However, the presence of lithium in this second phase cannot be excluded. This indicated that the Li^+ cations tend to substitute the Fe^{+3} cations in the octahedral sites of perovskite. This substitution can also be confirmed by the increased lattice parameter of PFN from 4.011Å to 4.021Å due to the larger radius of Li^+ (0.78Å) comparing to that of Fe^{+3} (0.67Å). The reduced conductivities can also be explained by considering the defect equilibrium for the introduction of lithium cations.

Table 4.5 D.C Conductivity as a Function of Firing Condition and Composition

Composition & Firing Condition	Temperature(^{0}C)	Conductivity(Ω–cm)$^{-1}$
PFN 1100^{0}C/12h	RT	2.95×10^{-12}
	100	3.05×10^{-10}
	150	2.90×10^{-8}
PFN+1.5 wt% Li_2CO_3 1000^{0}C/4h	RT	5.17×10^{-12}
	100	1.42×10^{-10}
	150	2.33×10^{-9}
PFN+2 wt% PbO 1100^{0}C/12h	RT	7.42×10^{-9}
	100	1.20×10^{-6}
	150	7.59×10^{-6}
PFN 1000^{0}C/4h	RT	1.22×10^{-8}
	100	1.01×10^{-6}
	150	5.31×10^{-6}

RT : Room Temperature

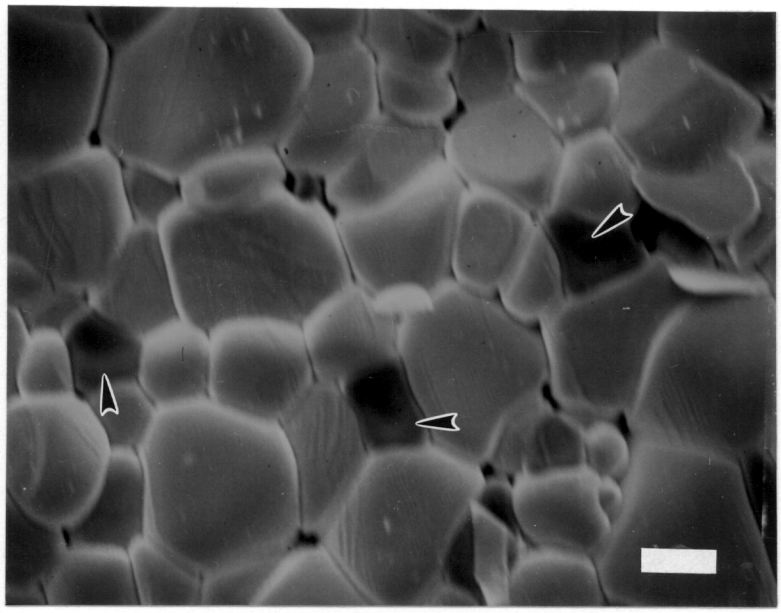

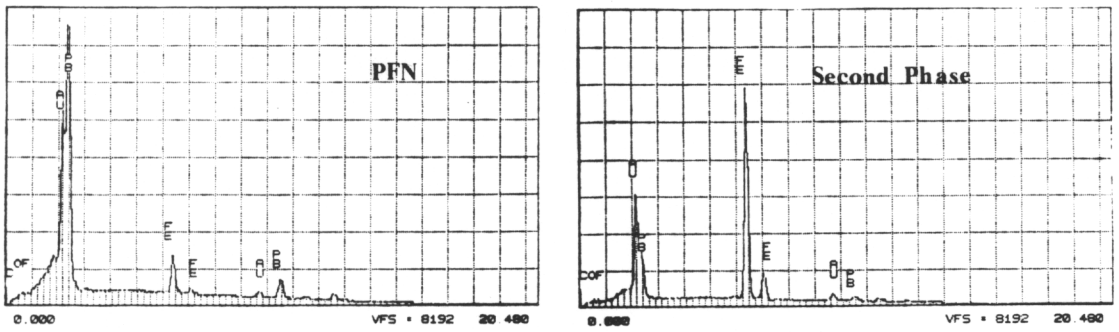

Figure 4.25 SEM micrograph and energy dispersive X–ray analyses of PFN with Li_2CO_3 addition show the second phase grains and their iron–rich content. (Bar = 5μm)

The incorporation of Li_2O can be expressed by the following equations:

$$Li_2O \xrightarrow[K_x]{Fe_2O_3} 2Li_{Fe}'' + O_o + 4h^{\cdot} \quad (4.17)$$

$$O_o \xrightarrow{K_1} V_o^{\cdot\cdot} + 2e' + \frac{1}{2} O_2 \quad (4.18)$$

$$e' + Fe_{Fe} \xrightarrow{K_2} Fe_{Fe}' \quad (4.19)$$

$$e' + h^{\cdot} \xrightarrow{K_e} \text{Null} \quad (4.20)$$

To maintain the charge neutrality, $2[Li_{Fe}''] + [Fe_{Fe}'] + [e'] = [h^{\cdot}] + 2[V_o^{\cdot\cdot}]_f$. Considering a limited charge neutrality condition of $[Li_{Fe}''] = [V_o^{\cdot\cdot}]_f$, the following equation can be derived:

$$[Fe_{Fe}']_f = K_1K_2K_e[h^{\cdot}]^5[Li_{Fe}'']/K_x[Li_2O]P_{O_2}^{0.5} \quad (4.21)$$

where $[Fe_{Fe}']_f$ and $[V_o^{\cdot\cdot}]_f$ are the concentrations after the addition of Li_2CO_3.

The $[Fe_{Fe}']_i$, which is the concentration without the addition of Li_2CO_3, can be calculated from Equations 4.18, 4.19, and 4.20. This concentration is given by the following equation:

$$[Fe_{Fe}']_i = [h^{\cdot}]K_1K_2K_e/[V_o^{\cdot\cdot}]_i P_{O_2}^{0.5} \quad (4.22)$$

where $[V_o^{\cdot\cdot}]_i$ represents the concentration of oxygen vacancy without the addition of Li_2CO_3. Then

$$\frac{[Fe_{Fe}{}']_f}{[Fe_{Fe}{}']_i} = \frac{[h^{\cdot}]^4 [Li_{Fe}{}''] [V_O^{\cdot\cdot}]_i}{K_x [Li_2O]} \tag{4.23}$$

Substitute $K_x = [Li_{Fe}]^2[h^{\cdot}]^4/[Li_2O]$ into Equation 4.23. Then

$$\frac{[Fe_{Fe}{}']_f}{[Fe_{Fe}{}']_i} = \frac{[V_O^{\cdot\cdot}]_i}{[Li_{Fe}{}'']} \tag{4.24}$$

Therefore, the D.C. conductivities and dielectric losses, which are attributed to electron hopping by the formation of $[Fe_{Fe}{}']$, can be reduced as a result of the introduction of Li_2CO_3 according to Equation 4.24.

Chapter 5: SUMMERY

Pure, single phase $Pb(Fe_{0.5}Nb_{0.5})O_3$ powders were successfully prepared by molten salt synthesis using equimolar mixture of NaCl and KCl at formation temperatures as low as 800^{0}C and for times as short as 1/2 hour. Optimum results were obtained for the weight ratio of flux/oxide less than or equal to 1, and with addition of 10 mol.% excess lead oxide to the starting powders. Carrying out the reaction in closed crucibles minimized the loss of lead oxide.

For all the investigated temperatures and times of powder formation, the resultant particles were cuboidal and without any facets. The particle size showed an Arrhenius dependence on the formation temperature. The apparent activation energy for particle growth was found to be at least an order of magnitude higher at high temperatures (1000^{0}C) than at lower temperatures (800^{0}C). Furthermore, the PFN powders were free of agglomerates.

These ceramics have the characteristic of relaxor with broad peak around the Curie temperature and frequency–dependent dielectric constants, which are attributed to a statistical inhomogeneity in the distribution of B–site cations. The dielectric properties are a function of the sintering conditions, type of additive and additive concentration. Optimum dielectric constants for pure PFN specimens were obtained at the sintering conditions of 1100^{0}C/ 13 hours.

The addition of lead oxide, which assisted densification and promoted grain growth through liquid phase sintering, adversely affected the dielectric properties.

The adverse effects were attributed to the formation of low dielectric constant grain boundary phases which are enriched with lead oxide.

The sintering temperatures and times could be considerably reduced and the dielectric properties were improved by the introduction of small amounts of Li_2CO_3 despite the poor densification of the specimens. These improvements were attributed to either the formation of a higher insulating second layer around each grain or to the reduction in concentration of Fe'_{Fe}. The resultant large grain size was explained by the enhancement of oxygen diffusion constant by the substitution of the Li^{+} ions for Fe^{+3} ions.

Chapter 6: REFERENCES

1. T.R. Shrout and A. Halliyal, "Preparation of Lead–Based Ferroelectric Relaxors for Capacitors," Am. Ceram. Soc. Bull., **66**[4], 704–711 (1987)
2. G. Smolenskii, "Ferroelectrics with Diffuse Phase Transition," Ferroelectrics, **53**, 129–135, (1984)
3. T.R. Shrout, S.L. Swartz, and M.J. Haun, "Dielectric Properties in the $Pb(Fe_{0.5}Nb_{0.5})O_3$–$Pb(Ni_{0.33}Nb_{0.67})O_3$ Solid–Solution System," Am. Ceram. Soc. Bull., **63**[6], 808–810 (1984)
4. W.Y. Pan, T.R. Shrout, and L.E. Cross, "Modelling the Ageing Phenomena in 0.9PMN–0.1PT Relaxor Ferroelectric Ceramics," J of Mater. Sci. Lett., **8**, 771–776 (1989)
5. A. Morell, "Synthesis, Sintering and Dielectric Measurements of PMN–PT Ceramic Materials," EURO–CERAMICS, Vol:**2** "Properties of Ceramics" Edited by G. de With, R.A. Terpstra, and R. Metselaar, 2.355–2.359 (1989)
9. M. Halmi, G. Desgardin, and B. Raveau, "Low–Temperatures Sintered Lead Tantalate–Based Ceramics of High Dielectric Constants," Mater. Lett., **5**[3], 103–110 (1987)
7. S.R. Winzer, A.E. Bailey, A.P. Ritter, and I. Jawed, "Synthesis and Characterization of PZN–PT Materials," IEEE 6th Int'l. Symp. on Appl. of Ferroelectrics, 432–436 (1986)
8. M.Lejeune and J.P. Boilot, "Low Firing Dielectrics Based on Lead Magnesium Niobate," Mater. Res. Bull., **20**, 493–499 (1985)

9 K. Uchino and S. Nomura, "Cyrstallographic and Dielectric Properties in the Solid Solution System $Pb(Fe_{0.67}W_{0.33})O_3$–$Pb(Mg_{0.33}W_{0.67})O_3$ and $Pb(MgW)_{0.5}O_3$–$Pb(FeTa)_{0.5}O_3$," J. Phys. Soc. Jpn., **41**[2], 542–547 (1976)

10 A. Tawfik, M.I.A. El–Ati, and M.M. Abou–Sekkina, "Dielectric Properties of Pseudobinary $Pb(Fe_{0.5}Nb_{0.5})O_3$–$Pb(Mg_{0.5}W_{0.5})O_3$ Solid Solution," J. Phys. Soc. Jpn., **54**[7], 2730–2734 (1985)

11 M.L. Baumler, A. Halliyal, and R.E. Newnham, "Dielectric and Piezoelectric Properties of $Pb(Zn_{0.33}Nb_{0.67})O_3$–$PbTiO_3$–$BaTiO_3$ Ceramics," IEEE 6th Int'l. Symp on Appl. of Ferroelectrics, 418–421 (1986)

12 M. Yonezawa,"Low–Firing Multilayer Capacitor Materials", Am. Ceram. Soc. Bull., 62, 1375–1383 (1983)

13 M. Yonezawa, K. Utsumi, and T. Ohno, "Properties of the Multilayer Capacitor $Pb(Zn_{0.33}Nb_{0.67})O_3$–$Pb(Fe_{0.5}Nb_{0.5})O_3$–$Pb(Fe_{0.67}W_{0.33})O_3$ Ternary System," Proc. 2nd Meet. on Ferroelectric Mater. and Appl., 215–220, Kyoto, Japan (1979)

14 H. Takamizawa, K. Utaumi, M. Yanezawa, and T. Ohno, "Large Capacitance Multilayer Ceramic Capacitor," IEEE Tran. Comp. Hyb. Manu. Technol., CHMT–4, **4**, 345–349 (1981)

15. Y. Shimada, K. Utsumi, M. Yonezawa, and H. Takamizawa, "Properties of the Large Capacitance Multilayer Ceramic Capacitor," Jpn. J. of Appl. Phys., **20**, supplement, 20–4, 143–146 (1981)

16 M.P. Kassarjian, R.E. Newnham, and J.V. Biggers, "Sequence of Reactions During Calcining of a Lead–Iron Niobate Dielectric Ceramic," Am. Ceram. Soc. Bull., **64**[8], 1108–1111 (1985)

17 T.C. Reiley, J.V. Badding, D.A. Payne, and D.A. Chance, "A low–Temperature Firing Thick Film Capacitor Material Based on Lead Iron Niobate/Tungstate," Mat. Res. Bull., **19**, 1543–1549 (1984)

18 M. Lejeune and J.P. Boilot, "Formation Mechanism and Ceramic Process of Ferroelectric Perovskite: $Pb(Mg_{0,33}Nb_{0.67})O_3$ and $Pb(Fe_{0.5}Nb_{0.5})O_3$," Ceram. Int'l., **8**[3], 99–104 (1982)

19 A.I. Agranovskaya, "Physical–Chemical Investigation of the Formation of Complex Ferroelectrics with the Perovskite Structure," Akad. Nauk., Phys. Serie., 1271–1277 (1966)

20 V.M. Frinkin, Ferroelectric Semiconductors, N.Y. (1975)

21 S. Nomura and K. Doi, "PTC Effect in $Pb(FeNb)_{0.5}O_3$," Jpn. J. Appl. Phys., **9**, 716 (1970)

22 G.A. Smolenskii, A.I. Agranovskaia, S.N. Popov, and V.A. Isupov, "New Ferroelectrics of Complex Composition," Sov. Phys. – Tech. Phys., **3**, 1981–1982 (1958)

23 V.A. Bokov, I.E. Myl'nikova, and G.A. Smolenskii, "Ferroelectrics and Antiferromagnetics," Sov. Phys–JETP, **15**,447–450 (1962)

24 D.N. Astrov, B.I. Al'shin, R.V. Zorin, and L.A. Drobyshev, "Spontaneous Magnetoelectric Effect" Sov. Phys. – JETP, **28**[6], 1123–1125 (1969)

25 J. Pietrzak, A. Maryanowska, and J. Leciejewicz, "Magnetic Ordering in $Pb(Fe_{0.5}Nb_{0.5})O_3$ at 4.2°K," Phys. Stat. Sol.(A), **65**, K79–K82 (1981)

26 G.L. Platonov, L.A. Drobyshev, Y.Y. Tamashpol'skii, and Y.N. Venevtesv, "Microelectron Diffraction and X–ray Study of Atom Displacement in $Pb(Fe_{0.5}Nb_{0.5})O_3$ Ferromagnetic," Kristallografiya, **14**(5), 800–803 (1969)

27 S.A. Mabud, "X–ray and Neutron Diffraction Studies of Lead Iron Niobate Ceramics and Single Crystals," Phase Transitions, **4**, 183–200 (1984)

28 H.H. Lee and W.K. Choo, "A Phase Analysis in Pesudobinary $Pb(Fe_{0.5}Nb_{0.5})O_3$–$Pb(Mg_{0.5}W_{0.5})O_3$ Solid Solution," J. Appl. Phys., **52**[9], 5767–5773 (1981)

29 V.A. Isupov, A.I. Agranovskaya, and N.P. Khuchua, "Physical Properties of Ferroelectric Lead Ferroniobate and Ferrotantalate," Izvest. Akad. Nauk S.S.S.R., Ser. Fiz., **24**, 1271–1274 (1960)

30 I.H. Burnskill, H. Schmid, and P. Tissot, "The Characterization of High Temperature Solution–Grown Single Crystals of $Pb(Fe_{0.5}Nb_{0.5})O_3$," Ferroelectrics, **37**, 547–550 (1981)

31 M. Granahan, M. Holmes, W.A. Schulze, and R.E. Newnham, " Grain–Oriented $PbNb_2O_6$ Ceramics," J. Am. Ceram. Soc., **64**[4], C–68–C–69 (1981)

32 R.H. Arendt, J.H. Rosolowski, and J.W. Szymaszek, "Lead Zirconate Titanate Ceramics from Molten Salt Solvent Synthesized Powders," Mater. Res. Bull., **14**, 703–709 (1979)

33 R.H. Arendt, " The Molten Salt Synthesis of Single Magnetic Domain $BaFe_{12}O_{19}$ and $SrFe_{12}O_{19}$ Crystals," J. of Solid State Chem., **8**, 339–347 (1973)

34 T. Kimura and T. Yamaguchi, "Morphology Control of Electronic Ceramic Powders by Molten salt Synthesis," Adv. in Ceram., **21**: Ceram. Powder Science, 169–177 (1987)

35 C. Li, C. Chiu, and S.B. Desu, "Formation of Lead Niobates in Molten Salt System," Submitted to J. Am. Ceram. Soc.

36 Y. Hayashi, T. Kimura, and T. Yamaguchi, "Preparation of Acicular NiZn–Ferrite Powders," J. of Mater. Sci., **21**, 2876–2880 (1986)

37 T. Kimura, T. Kanazawa, and T. Yamaguchi, "Preparation of $Ba_4Ti_3O_{12}$ Powders in the Presence of Molten Salt Containing LiCl," J. Am. Ceram. Soc., **66**[8], 597–600 (1987)

38 S.S. Lopatin, T.G. Lupeiko, and T.I. Ivleva, "The preparation of Lead Ferroniobate in the Presence of Molten Sodium and Potassium Chlorides," Zh. Neorg. Khim. (Russ. J. of Inorganic Chem.), **32**[4], 865–868 (1987)

39 F. Galasso and W. Darby, "Preparation of Single Crystals of Complex Perovskite Ferroelectric and Semiconducting Compounds," Inorganic Chem., **4**[1], 71–73 (1965)

40 I.H. Brunskill, R. Boutellier, W. Depmeier, and H. Schmid, " High–Temperature Solution Growth of $Pb(Fe_{0.5}Nb_{0.5})O_3$ and $Pb(Mn_{0.5}Nb_{0.5})O_3$ Crystals," J. of Crystal Growth, **56**, 541–546 (1982)

41 S–L Fu and G–F Chen, "Fabrication of Perovskite $Pb(Fe_{0.5}Nb_{0.5})O_3$ and Reaction Mechanism," Ferroelectrics, **82**, 119–126 (1988)

42 P. Groves, "Fabrication and Characterization of Ferroelectric Perovskite Lead Indium Niobate," Ferroelectrics, **65**, 67–77 (1985)

43 Y. Hayashi, T. Kimura, and T. Yamaguchi, "Preparation of Rod–Shaped $BaTiO_3$ Powder," J. of Mater. Sci., **21**, 757–762 (1986)

44 T. Kimura and T. Yamaguchi, "Morphology of Bi_2WO_6 Powders Obtained in the Presence of Fused Salts," J. of Mater. Sci., **17**, 1863–1870 (1982)

45 A. Halliyal, T.R. Gururaja, U. Kumar, and A. Safari, "Stability of Perovskite Phase in $Pb(Zn_{0.33}Nb_{0.67})O_3$ and Other $A(B'B'')O_3$ Perovskite," IEEE 6th Int'l. Symp. on Appl. of Ferroelectrics, 437–441 (1986)

46 W.D. Kingery, H.K. Bowen, and D.R. Uhlmann, "Introduction to Ceramics," 2nd edition, John Wiley & Son Co., 1976

47 T. Zhang, "Electrical Conduction Transport Mechanisms of Barium Titanate–Based Multilayer Ceramic Capacitors," M.S. Thesis, VPI&SU, 1988

48 R. Coelho, "Physics of Dielectrics for the Engineer," Sci. Pub. Co., 1979

49 C.F. Buhrer, "Some Properties of Bismuth Perovskites," J. of Chem. Phys., **36**[3], 798–803 (1962)

50 A. Maryanowska and J. Pietrzak, "Critical–Point Anomalies in EPR Linewidth of $Pb(Fe_{0.5}Nb_{0.5})O_3$," Phys. Stat. Sol., **68**(a), K185–K188 (1981)

51 C.G.F. Stenger, F.L. Scholten, and A.J. Burggraaf, "Ordering and Diffuse Phase Transitions in $Pb(Sc_{0.5}Ta_{0.5})O_3$ Ceramics," Solid State Comm., **32**, 989–992 (1979)

52 H–C Wang and W.A. Schulze, "Order–Disorder Phenomenon in Lead Scandium Tantalate," J. Am. Ceram. Soc., **73**[5], 1228–1234 (1990)

53 C.A. Randall, D.J. Barber, and R.W. Whatmore, "*In Situ* TEM Experiments on Perovskite–Structured Ferroelectric Relaxor Materials," J. of Microscopy, **145**, 275–291 (1987)

54 A. Bloom, "The Chemistry of Molten Salts," W.A. Benjamin Co., 1967

55 M. Lejeune and J.P. Boilot, "Optimization of Dielectric Properties of Lead–Magnesium Niobate Ceramics," Am. Ceram. Soc. Bull., **64**[4], 697–682 (1985)

56 B.D. Cullity, "Elements of X–ray Diffraction," 2nd Edition, Addison–Wesley Co. Inc., 1978

57 ASTM, "Standard Test Methods for Apparent Porosity, Water Absorption, Apparent Specific Gravity, and Bulk Density of Burned Refractory Brick and Shapes by Boiling Water," Annual Book of ASTM Standards, C20–87 (1987)

58 F.W. Sears, M.W. Zemansky, and H.D. Young, "University Physics," 5th Edition, Addison–Wesley Co. Inc., 1976

59 JCPDS Diffraction File, Card #: 32–522, Joint Committee on Powder Diffraction Standards, Swarthmore, Pa

60 S.L. Swartz, G.O. Dayton, and D.K. Laubscher, "Low–Temperature Fired Lead Magnesium Niobate," IEEE 6th Int'l. Symp. on Appl. of Ferroelectrics, 1986

61 J.P. Guha, D.J. Hong, and H.U. Anderson, "Effect of Excess PbO on the Sintering Characteristics and Dielectric Properties of $Pb(Mg_{0.33}Nb_{0.67})O_3$ –$PbTiO_3$–Based Ceramics," J. Am Ceram. Soc., **71**[3], C–152–C–154 (1988)

62 I.H. Brunskill, P. Tissot, and H. Schmid, "Determination of the Phase Diagram, PbO–$Pb(Fe_{0.5}Nb_{0.5})O_3$ and PbO–$Pb(Mn_{0.5}Nb_{0.5})O_3$," Thermochimica Acta, **49**, 351–355 (1981)

63 J. Chen, and M.P. Harmer, "Microstructure and Dielectric Properties of Lead Magnesium Niobate–Pyrochlore Diphase Mixture," J. Am. Ceram. Soc., **73**[1], 68–73 (1990)

64 Y. Yokornizo, T. Takahashi, and S. Nomura, "Ferroelectric Properties of $Pb(Zn_{0.33}Nb_{0.67})O_3$," J. of Phys. Soc. Jpn., **28**[5], 1278–1284 (1970)

65 J. Chen, A. Gorton, H.M. Chan, and M.P. Harmer, "Effect of Powder Purity and Second Phases on the Dielectric Properties of Lead Magnesium Niobate Ceramics," J. Am. Ceram. Soc., **69**[12], C–303–C–305 (1986)

66 E. Goo, T. Yamamoto, and K. Okazaki, "Microstructure of Lead–Magnesium Niobate Ceramics," J. Am. Ceram. Soc., **69**[8], C–188–C–190 (1986)

67 K. Z. Baba–Kishi, I.M. Reaney, and D.J. Barber, "Transmission Electron Microscopy of Second–Phase Particles in $Pb(Sc_{0.5}Ta_{0.5})O_3$ Ferroelectric Ceramics," J. of Mater. Sci., **25**, 1645–1655 (1990)

68 D.J. Barber, A.D. Hilton, and K.Z. Baba–Kishi, "Some Microstructural Characteristics of Relaxor Ferroelectrics," IEEE Int'l. Conf. on Prop. and Appl. of Dielectric Mater., Vol 1, 217–220 (1988)

69 R. Mauczok and R. Wernicke, " Ceramic Boundary–Layer Capacitors," Philips Tech. Rev., **41**, No. 11/12, 338–346 1983/84

Vita

The author was born on March 30, 1963 in Keelung, Taiwan. Upon graduating from the High School of Nation Taiwan Normal University, he entered National Cheng Kung University, Tainan, Taiwan, in 1981. He received his Bachelor of Science degree in Metallurgy and Materials Engineering in June 1985. After graduation from college, he was enlisted as a second lieutenant in the ROC Army for about two years. Thereafter, he joined HCG Inc. as an assistant engineer. He has been a graduate student at Virginia Polytechnic Institute and State University, Blacksburg, Virginia since January 1989.

He is a member of the American Ceramic Society.